CHAPTER 8

AMSLER and LEROS WEAR RESULTS

8.1 Introduction

Most of the test conditions were determined within the context of the research contract with British Rail and are representative of conditions on their rail network. As will be seen this has resulted in many results falling in a transitional zone of wear behaviour, between mild and severe wear. During some tests a change of wear regime occurred, marked by a sudden jump from one steady state wear curve to another. Previous British Rail work[Bolton et al, 1982; Bolton and Clayton, 1984] has examined wear with respect to the product of test conditions, $p_o\gamma$, where p_o is maximum contact stress and γ is circumferential creepage. This relationship is further examined in the Discussion (Chapter 10). For convenience, results in the present work have been grouped in $p_o\gamma$ order, however variations of stress or creepage within one value of $p_o\gamma$ gave quite different wear characteristics.

The test programmes for the modified Amsler and LEROS are given in Tables 6.1 and 7.1, respectively. Not all test conditions were duplicated on both machines, as test requirements changed as the research contract progressed and a requirement of LEROS was for tests under conditions which were beyond the capabilities of the Amsler machine. Where tests on both machines were at, or near, the same nominal levels of maximum contact stress and creepage, wear curves are presented in adjacent figures. Tabulated wear rate data are based on the least squares analyses of the linear parts of wear curves. Where a distinct change of wear regime has occurred during a test, two wear rates are presented ("Slopes A and B"). The effects of machine variables on wear rates, such as changes in the hydraulic loading system of the LEROS machine, are presented in these tabulated results.

8.2 Wear rate analysis

Initially, changes in air blast direction, the torque measuring system and disc grainflow orientations, plus the effects of differently spaced weighing intervals, were

separately assessed on the Amsler machine using a fixed set of test conditions. There were distinct, but minor effects as described in Chapter 6 (cf. Figures 6.9 and 6.10). For the remainder of the Amsler test programme, both the air blast condition shown for Tests 5 and 7 and the rigid torque arm measuring system were maintained, also weighing intervals were spaced in a more standardised manner and all further rail test discs, on both wear machines, were machined from rails and rolled barstock with their grainflow parallel to the axis of the disc. Bottom discs, for both wear machines, were machined out of "cheeses" cut transversely from wheel tyres. This gave as even a grainflow as circumferentially possible, however grainflow direction and intensity were more variable in these forgings than in rail discs.

The formula used here for maximum contact stress, p_o (MPa), was determined from Hertzian elastic deformation criteria for alloy steels[Timoshenko and Goodier, 1933], where Poisson's Ratio (υ) has been taken as 0.3. This gives:

$$p_o = 0.418\sqrt{(LE/R)} \qquad (8.1)$$

where L is the normal load per unit contact width (N/mm), R is given by $1/R = 1/R_t + 1/R_b$, where R_t and R_b are the top and bottom disc radii (mm), respectively, and E is Young's Modulus (MPa). A value for E of 210 GPa has been used throughout, for all rail and wheel steels.

Although there was plastic deformation of the disc track edges during testing, the width of the track under direct normal loading remained essentially unchanged and this initial value has been used in the calculations.

Bolton and Clayton's[1984] definition of creepage has been used where creepage, γ, is defined as the difference in circumferential speeds divided by the average of the two speeds.

Wear rates were calculated from weight loss values determined by least squares analysis of the steady state part, or parts, of the wear curves. These values have

been divided by the Hertzian contact area, A, given by:

$$A = 4Lb/\pi p_o \tag{8.2}$$

where b (mm) is the contact length, i.e. Lb is the total load. This facilitates comparisons of results for different test conditions and contact geometries (eg, on other wear machines, or on railway track).

Calculations of p_o, γ and $T\gamma/A$, where "T " (N) is tangential force, have been based on measured disc diameters and coefficients of friction at the mid-point of the steady part, or parts, of the wear curves. This is referred to in the tabulated results (Tables 8.1 and 8.2) as the "measuring point".

Previous Amsler results[Bolton and Clayton, 1984] have been expressed as weight loss per unit contact area per unit distance rolled. However, there has not been pure rolling, but rolling-sliding. The sliding distance has been positive for the bottom driving discs and negative for the top driven (or "braking") discs, so that just using the distance rolled, by one, or by each disc, does not accurately reflect their wear resistance. In this work, rolling distance, R, has been defined as the "mean distance rolled by the two discs":

$$R = (\pi/2)(D_bN_b + D_tN_t) \tag{8.3}$$

where D_b and D_t are bottom and top disc diameters and N_b and N_t are their revolution counts, respectively. (In a similar manner, creepage represents the average of the slip rates of each disc.) To take account of the different creepages used in the tests, the distance slid, S, has been defined as:

$$S = \pi(D_bN_b - D_tN_t) \tag{8.4}$$

These two distances are related through the creepage:

$$\gamma = S/R \tag{8.5}$$

Wear data are presented in two versions. Firstly, as weight loss per unit contact area per unit mean distance rolled, Y_r:

$$Y_r = W/AR \tag{8.6}$$

where W is the weight loss. Secondly, as weight loss per unit contact area per unit mean distance slid, Y_s:

$$Y_s = W/AS \tag{8.7}$$

For both definitions of wear rate, the units used are g/m^3: a rationalization of μg weight loss per mm^2 contact area per metre rolled or slid. This approach is discussed further in Chapter 10.

8.3 Wear Test Procedure

Disc manufacture.

"Braking" top discs were machined from transverse sections cut from pearlitic rail head and from 60 - 80mm diameter hot rolled bainitic bar stock. Care was taken that LEROS 47mm diameter discs were centrally sectioned from rail head slices, so that any inhomogenous rail surface layers were machined off. All disc dimensions, track width, track diameter and shoulder width, were measured by micrometer, and eccentricity and surface finish by Talysurf and Talyrond profilometry equipment. Individual top and bottom discs were paired so that variations in shoulder and track widths balanced to thus give the maximum degree of transverse alignment between the two tracks. All discs were stored in dessicators prior to testing.

Test Procedure.

All electronic equipment was stabilised for at least one hour prior to use. Wear machines were run empty to equalise bearing temperatures. Discs were cleaned with isopropanol and weighed to an accuracy of ±0.1mg on a balance (Sartorius R300S),

capable of weighing up to 300g at this accuracy. (The LEROS discs weighed around 180g.) Wear tracks were again cleaned with isopropanol just prior to testing. Amsler discs were set between paper washers and tightened to the same torque setting for each test; no disc slippage, with subsequent abrasive wear of disc sides, was observed. Environment chamber conditions were stabilised prior to starting a test period. Amsler discs had to be pre-loaded prior to the start or ending their rotation; disc stoppage with this loaded condition often generated a line of small abrasions across wear tracks. LEROS discs could be loaded and unloaded whilst rotating; these discs were always slightly separated before and after application of the hydraulic load.

Environment conditions (air temperature and humidity) were logged during each test period and disc surface temperatures were measured as soon as the discs were accessed at the end of a test period. During testing, the environment chamber air extraction filter was regularly checked, as excessive debris build-up could affect the air flow. For most tests, debris was removed at weighing interval, however during some severe tests it was necessary to quickly remove debris during test runs, between weighing intervals.

At each weighing interval, discs were removed from the machine and all their surfaces, except the wear tracks, were cleaned prior to weighing. After weighing, the wear surfaces were examined on a low power microscope and features of interest photographed. Some discs were roundness profiled on a Talyrond at an intermediate weighing stage.

At the test end, after weighing and wear surface examination, all discs were Talyrond profiled. Changes in the width and diameter of wear tracks were measured by micrometer. Diameter loss was assumed to be linear for the steady state period of the wear curve, hence the disc diameters at the mid-point of this period were used for calculating representative values of creepage, maximum contact stress and coefficient of (tractive) friction.

Some discs were sectioned for microexamination, usually circumferentially along the track centre. Transverse sections were taken on a few discs. The cut sections were nickel plated to give edge-retention on polishing, encapsulated in mounting compound and examined on an optical microscope. Some were further examined on a scanning electron microscope (SEM). Several worn disc surfaces were also directly examined on the SEM. Carbon replicas were taken from a few microsections for examination on a transmission electron microscope (TEM). Microhardness profiles were taken of some of the sections and the respective wear track surfaces. The results of all these examinations are reported in Chapter 9.

8.4 Wear rate results

Exploratory Amsler tests.

Some exploratory tests under moderate wear conditions were carried out at the start of experimentation so as to establish a standard testing technique on the Amsler machine. These variables are discussed in Chapter 6.

Comparative results, all materials, both machines.

Wear rate patterns for mean distance rolled and slid (Y_r and Y_s respectively) are given in Figures 8.1 to 8.5 with respect to material, test condition and wear machine. *(Note that the scale of the wear rate axis varies by at least one order of magnitude between each figure.)* The results are in ascending order of $p_o\gamma$. Wear rates and further test details are given in Tables 8.1 and 8.2.

The results show that top disc material ranking with respect to wear resistance has been dependent upon test conditions, although in most cases B04 was clearly inferior to the others and B20 was rarely superior to R52. Although B52 had the lowest wear rates, it induced heavy wear of the bottom W64 "driving" discs. This was also the case with the other bainitic steels, B04 and B20, except under the mildest conditions. Only under conditions of high contact stress and low creepage (Tests 46 to 49, Figures 8.2 and 8.3) did top disc material ranking match the respective bulk hardness values (Table 2.3).

Track width spread was far more pronounced with the pearlitic steels than with the bainitic steels (see Tables 6.3 and 7.2). This is further illustrated in Figure 8.6 where wear rates, measured by the standard weight loss method, are compared with rates estimated from diameter loss. It should be noted that railway companies usually measure railway track wear by the loss of metal from the contact profile; i.e. a measure of both metal removal as loose debris and by plastic flow out of the contact zone. During field surveys, it has been observed that the gauge corner lip formed by plastic flow is far less pronounced on bainitic rails than pearlitic rails, even though the bainitic rails have higher gauge face wear rates[Allery, 1987].

8.5 Disc surface features

There were no worn surface features uniquely applicable to a particular bainitic or pearlitic steel. Specific surface features were associated with certain wear rates, so that their occurrence varied with test conditions for each of the rail steels. Even where B04 disc wear tracks were comparatively smooth whilst the others were a mass of adhered flakes, debris analysis showed that B04 had been generating flakes in a similar manner, however these had been removed within one, or a few, revolutions.

Flakes

A prominent feature was the progressive ratchetting of surface and near-surface material resulting in the generation of surface flakes. These tended to be retained on the top "driven" discs with wear occurring by fracture of thinned flake tips. On bottom "driving" discs, flakes fractured further from the tip thus leaving shallow "flake" pits. This difference in behaviour can be accounted for by the opposite location of compressive and tensile circumferential forces in, and around, the contact zone (Figure 8.7). Flake widths could vary in size from sub-micron to complete track widths, as shown in Figure 8.8, with the size of largest flake generally increasing with the severity of test condition, but not always. In all but the severest conditions, at least *90%* of all wear debris passed through the 0.4mm square grid in the "exit air" filter chamber, as determined by weight analysis, even though coarse wear features on the disc surfaces, and the constant generation of large flake debris,

made it appear that these large flakes were the primary form of debris.

Amsler corrugations

The formation of fine surface corrugations on Amsler test discs, which were all about 0.3mm in wavelength with an amplitude of a few microns (Figure 8.9a), was not found to affect wear rates significantly. These formed immediately or very early during a test. As discussed in Chapter 6, these corrugations formed with the same wavelength at the two operating speeds (193 and 386 rpm), suggesting a "stick-slip" mechanism of formation connected to the Amsler fixed gear disc speed differential. This explanation is supported by the fact that no fine wave length corrugations formed on LEROS discs, where the disc drive systems are not directly connected.

Amsler and LEROS facets

Tayrond profilometry revealed that coarse, and often severe, undulations (termed "facets") had formed on the Amsler discs, their appearance obscured by the fine 0.3mm wavelength corrugations. Facets also formed, in a more dramatic manner, on LEROS test discs (Figure 8.9b). Detailed observations on disc plastic deformations, including periodic surface undulations, were tabulated earlier (Tables 6.3 and 7.2). As shown in these Chapters, facets sometimes developed late on in a test and were always associated with an increase in machine noise and vibration. Their appearance, or disappearance, was usually accompanied by a small change in wear rate as shown in Figure 8.10. In this figure, the more pronounced wear rate change of Test 38 was due to a change from a mild to a more severe wear regime in which facets formed, rather than being due to facet formation. It is worth noting that all the materials tested faceted under some conditions, though within different test condition boundaries for each wear machine, as shown in Tables 6.4 and 7.3.

Some faceting, of one or both discs, occurred in all LEROS tests at 900 MPa maximum contact stress (p_o) and 3% creepage (γ) and in all but one test at 1300 MPa p_o and 3% γ. Surface features of facets, irrespective of material, were oxidised flaking peaks and partially oxidised troughs containing very fine pits and abrasive scrape marks, as shown in Figure 8.11. Such features were not affected by test

speed. Trough features were similar to those found on non-faceting discs tested under milder conditions (500 MPa p_o and 10% γ).

The shallower facets on the Amsler discs were normally obscured by 0.3mm wavelength corrugations, therefore differences in appearance between facet peaks and troughs could not be clearly distinguished.

Ripples

Under test conditions which generated a severe form of wear, gross plastic deformation of the wear surfaces could occur in the form of regular, or semi-regular, ripples (Figures 7.17 and 7.18). These would often clear for a period and then re-establish themselves. They are described and discussed in the "severe wear tests" part of the following section.

8.6 Wear Regimes

Mild wear tests at 500 MPa p_o and 3% γ.

Top and bottom disc wear curves, and "combined" wear curves showing the sum of the top and bottom wear rates, are shown for Amsler tests in Figures 8.12 and 8.13, respectively, and for LEROS tests in Figures 8.14 and 8.15, respectively. (With respect to the Test 34 results shown in Figure 8.13, although an initial creepage control problem reduced the running-in period, from the linear nature of the steady state part of the wear curves, and from the surface appearance of the discs, it was felt that the steady state wear rate was a valid result.) Comparative rolling and sliding wear rates are schematically shown in Figure 8.1 and presented, along with test details in Table 8.1. In both sets of tests, pearlitic R52 had a lower wear rate than the carbide free bainitic steels and it was near to that of B52. If combined wear rates are considered, it can be seen that the harder bainitic top discs generated more wear of the pearlitic W64 bottom discs such that the pearlitic R52/W64 pair had equivalent (Amsler), or lower (LEROS) wear rates to the best bainite/W64 combination. B04 had a particularly high wear rate.

The pearlitic R52, B52 and B20 top discs, and respective W64 discs, had oxidised wear tracks with minimal flaking and pitting; features typical of mild wear. These

features were also seen on B04 discs which had the far higher wear rates (Figure 8.16). During the Amsler B04/W64 test, angled "stick-slip" marks sporadically formed on the top disc surface but these cleared by the test end. In the equivalent LEROS B04 test there was faceting delineated on either side by dark oxide bands; this was observed to develop between 70000 and 140000 (top disc) revolutions. The LEROS B52 disc also exhibited slight faceting under these conditions, although it had a far lower wear rate.

Oxidised wear debris.

At the end of the last measuring period of the Amsler tests, a 1μm cellulose nitrate filter was inserted into the air flow drawn from the environment chamber. This collected fine debris that had passed through the in-built 0.4mm square grid filter. As this practice drastically reduced the flow of cooling air across the discs, and thus affected steady state wear rates, it was only carried out at the end of each test. Although absolute quantitative results could not be obtained, X-ray diffraction techniques carried out by British Rail Research (Derby, UK) gave an indication of the debris make-up. For Test 8 (R52/W64) and Test 18 (B52/W64), the debris was an approximate equal mix of Fe and Fe_3O_4. For Test 19 (B04/W64) there was a large amount of Fe, a small amount of Fe_3O_4 and a trace of Fe_2O_3. (Some debris analysed from R52/W64 tests at 1100 MPa p_o and 3% γ contained a large volume of Fe, a medium volume of Fe_2O_3 and a small amount of Fe_3O_4.)

From these results it seemed that B04/W64 tests showed some of the characteristics of a severer wear regime.

Mild/severe transitional wear tests.

Tests at 900 MPa p_o and 3% γ.

This arbitary test condition was chosen for initial experimentation when test methods were being first determined on the Amsler machine, as it was representative of worn rail contact. In hindsight, it can be seen that the features of many of these tests fall between those described as "mild" and "severe" by Bolton and Clayton[1984].

Comparative rolling and sliding wear rates are schematically shown in Figures 8.2 and 8.3, respectively, and detailed results are given in Tables 8.1. The disc wear curves, individual and combined, are given in Figures 8.17 and 8.18, respectively, for Amsler tests and Figures 8.10 and 8.19, respectively, for LEROS tests. (The effect of faceting on wear curves, as shown in Figure 8.10, are discussed in Section 8.5.) The sudden mid-test change to a lower wear rate during (Amsler) Test 14 (B52/W64) was associated with a change in the appearance of the wear tracks from corrugated, semi-metallic to smoother, more oxidative, i.e. from a transitional wear mode to a mild wear mode. Consequently, two steady state wear rates have been given in the results (Figures 8.2 and 8.3; Table 8.1).

Amsler Tests 7 (R52/W64) and 16 (B04/W64) both had corrugated semi-metallic surfaces with moderate flaking. Two of the bainites were run against themselves under these conditions (Amsler Tests 15 and 17). Both eventually had similar corrugated surfaces to those seen in Tests 7 and 16. Although during running-in some fine ripples were formed on the (Test 17) B04 disc surface, its wear rate was still less than when run against pearlite (Test 16). In contrast, when run against itself, B52 remained in the transitional wear regime with a higher wear rate than that seen when run against pearlite and a higher combined wear rate than the two pearlitic steels. Although these bainite - bainite tests were of great interest, the time constraint on the test programme did not allow for any further tests.

The transitional nature of these test conditions was further illustrated by the LEROS tests, although in this case it was facets, rather than corrugations, that appeared or disappeared as steady state wear rates changed mid-test (Figures 8.10, 8.19). The Test 30 R52 top disc was typically faceted, i.e. oxidised, flaking peaks and smooth semi-metallic, semi-oxidised troughs. The Test 30 W64 bottom disc wear track had similar surface features, over the complate wear surface, to the troughs of the top disc. Both Test 36 discs (B04/W64) were faceted for half the test and then facets gradually cleared from the B04 disc, accompanied by slight decreases in both wear rates. The Test 37 B20 disc was faceted for most of the test whilst facets on the bottom W64 disc partially cleared to leave a mixed oxidative-metallic surface with

some moderate flaking. In contrast to the Amsler test, the wear mode of the LEROS B52/W64 test (Test 38) changed in the opposite direction; from fully mild to transitional. Both discs were fully faceted by the test end, as revealed by profilometry, although this was only visually apparent on the top R52 disc. Flaking was fine on these discs. All these results reflect the transitional nature of these test conditions, in both wear mode, and in bordering the test condition / material envelope for facet formation (cf. Tables 6.4 and 7.3).

Comparative Amsler machine tests at 1100 MPa p_o and 3%γ.

These test conditions were chosen for some comparative tests on two Amsler machines. Test 10B was a standard R52/W64 test. (The results of another test, Test 10A are not presented as the environment chamber malfunctioned during running-in. Test 10A was repeated as Test 10B.) Test 10C was a further repeat test where the machine speed was halved after 60,000 cycles. Test 11A was a repeat of Test 10B, but on an alternative Amsler machine situated at British Rail Research, Derby. Although this was a standard Amsler (i.e. not modified for yawing) standard size Amsler discs were not used. The larger size discs used on the modified "yawing" Amsler machine at Leicester were used, together with the Leicester environment chamber and rigid loading arm (with attached strain gauge) for measuring torque.

The comparative wear rolling and sliding wear rates are shown in Figures 8.2 and 8.3, respectively, with detailed results given in Table 8.1. Disc wear curves, individual and combined, are given in Figures 8.20 and 8.21, respectively. In all of these tests, bottom driving disc wear was slightly higher than top braking disc wear. The speed change during Test 10C did not appear to affect wear rates, perhaps reflecting the efficiency of disc cooling. The wear rates of each test differed. Test 10B disc surfaces were oxidised with fine flaking, whereas Test 10C disc surfaces were oxidised and partially corrugated, with moderate to heavy flaking. Test 11A discs (on the standard Amsler) were fully corrugated with heavy flaking; this corrugation pattern was seen to vary during the test. Surface profiles revealed that Test 10B discs were partially faceted, Test 10C discs partially faceted and corrugated and Test 11A (Derby) discs were far more clearly, and more fully, corrugated and

faceted. Again, the variability of these wear curves and the changing surface features reflect the transitional nature of the tests under these conditions.

At the end of Tests 10A and 10B, a 1μm cellulose nitrate filter was fitted to the air flow exit of the environment chamber. A large amount of dark, powdery debris was collected. This was analysed on the X-ray diffraction unit at British Rail Research, Derby, together with coarse debris collected from the 0.4mm grid filter during both tests. Both coarse and fine debris of Test 10A and the fine debris of Test 10B were found to consist of large amounts of Fe, medium amounts of Fe_2O_3 and small amounts of Fe_3O_4. The coarse debris of Test 10B was found to consist of large amounts of Fe, small amounts of Fe_3O_4 and only a trace of Fe_2O_3.

Tests at 1300 MPa p_o and 3% γ.

The load required to generate this contact stress on standard 5mm wide cylindrical Amsler discs was thought to be a limiting condition on that machine. The disc edges rapidly distorted and the loading spring was set to maximum. Only one test was carried out. However on LEROS these conditions were easily accommodated. Track edge distortion was less relevant on the 10mm wide LEROS discs. Comparative rolling and sliding wear rate results for both machines are summarised in Figures 8.2 and 8.3 respectively, with detailed results in Tables 8.2. Amsler disc wear curves, both individual and combined, are shown in Figure 8.22; LEROS individual and combined wear curves in Figures 8.23 and 8.24, respectively. As seen with previous results for R52/W64 (pearlitic) tests on the Amsler, bottom disc wear clearly exceeds top disc wear, whereas on LEROS wear rates are similar.

Under these higher contact stress and moderate creepage conditions the wear rates of R52, B04 and B20 top discs were similar, with B52 lower. However, all combined wear rates were similar (Figure 8.24), as again the B52 top disc induced heavier wear in the W64 bottom disc.

The transitional nature of these tests was reflected more by disc surface features. Amsler R52/W64 disc wear tracks were oxidised with surface features of moderate

flaking, pitting and partial corrugations; the degree of each feature varied throughout the test. Bottom disc pitting was particularly marked with some large and thick pieces of debris fracturing off by a short cycle fatigue mechanism, rather than normal flake thinning. For example, the size of one large piece of flake debris was 2 x 0.8 x 0.05mm. These mechanisms were indicative of severe wear. Neither disc was faceted by the test end. The comparable R52/W64 LEROS worn test discs had similar surface features, except that bottom disc pitting was not as severe. The top disc profile revealed semi-periodic undulations but there were no clear facets on either disc.

The LEROS B04/W64 test (Test 39) also reflected the transitional nature of wear under these test conditions. Up to 25000 top disc cycles, both discs were fully faceted with surface features typical of those described for tests at 900 MPa p_o and 3%γ. But after this point disc appearances changed, though not wear rates. The bottom disc became similar to that seen in the R52/W64 tests, but with much finer pitting. The top disc surface remained relatively smooth, semi-oxidised and semi-metallic, but the facets had disappeared around part of the circumference.

The discs in the LEROS B20/W64 test (Test40) also changed appearance during the test. The top disc became progressively more faceted and its wear rate slightly diminished. The bottom disc rapidly changed around 25000 cycles from faceted to heavily pitted (as described above), with a sudden increase in wear rate (Figure 8.23), therefore two sets of wear rate data are presented (Figures 8.2, 8.3). The disc surfaces at 25000 top disc revolutions are shown in Figure 8.25; it can be seen that the bottom disc had both faceted and pitted features. The disc surfaces and the resultant debris at 40000 top disc revolutions are shown in Figure 8.26. This bottom disc had begun to pit severely and coarse debris was generated (although this coarse debris, collected by the 0.4mm square grid filter, was only 6% of the total weight loss). During the LEROS B52/W64 test (Test 41) the top B52 disc remained irregularly faceted throughout the test whilst the bottom W64 disc moderately pitted in the manner described above.

Tests at low maximum contact stress (around 500 MPa) and high creepage (10%). R52/W64 discs, tested on the Amsler under these conditions (at 491 MPa p_o), developed distinct undulations, both facets and corrugations, consequently these conditions were chosen for vibration analyses on of the Amsler and LEROS (given in Chapters 6 and 7, respectively).

Wear rate results for rolling and sliding are shown in Figures 8.4 and 8.5, respectively, and detailed results are given in Table 8.2. Amsler individual and combined wear curves are shown in Figures 8.27 and 8.28, respectively, and LEROS individual and combined wear curves are shown in Figures 8.29 and 8.30, respectively.

The change of test speed between the two R52/W64 Amsler tests did *not* have any effect on wear rates; the wear curves are nearly identical (Figure 8.27). Both discs faceted at the higher speed and just the bottom disc at the lower speed (at the same frequency, i.e. double the wavelength). Respective Talyrond disc profiles, and the corrugated surface appearance of the lower speed discs, are shown in Figure 8.31. On the profiles, the fine wavelength corrugations can be seen superimposed on the coarser facet patterns. Wear surfaces were oxidative-metallic with clear corrugations (Figure 8.31c) of equal wavelength at both machine speeds.

The B52/W64 discs were similar, also with clear corrugations and facets. The surfaces of the B04/W64 test discs (Test 21) showed some signs of severe wear, indicating that these conditions were at the limit of the transitional grouping for this material combination. As above, the surfaces were oxidative-metallic but there were also some "scooped" depressions, indicative of a severer, adhesive wear mechanism (Figure 8.32). These discs were not clearly faceted or corrugated.

The R52/W64 LEROS discs used for the vibration analysis of the wear machine, Tests 51 and 52 (see Chapter 8), both had oxidative-metallic surfaces. The higher speed discs had clear visual facets with the surface features described earlier (see Figures 7.19). The lower speed discs had no visual facets; their surfaces had a

network of micro-pits. These discs had slightly lower wear rates (Figures 8.29). The Talyrond profile of the lower speed top disc revealed that it had faceted at a frequency close to that of the higher speed top disc (Table 7.2).

A test at moderate maximum contact stress (900 MPa) and creepage (7%).
This R52/W64 test (Test 30A) was carried out whilst developing the control system for the LEROS machine. The comparative rolling and sliding wear rates are shown in Figures 8.4 and 8.5, respectively. The wear curves, individual and combined, are shown in Figure 8.33 with detailed results are given in Table 8.2. Wear rates and wear features (shown in Figure 7.13) were similar to those of other pearlite discs in this transitional group.

Severe wear tests

Tests at high maximum contact stress (1800 MPa) and low creepage (1.5%).
The Amsler machine cannot apply such a contact stress to standard width discs, however this was well within the capabilities of the LEROS machine. A maximum contact stress of around 1800 MPa is not uncommon on railway systems, particularly where new track has yet to run-in. A creepage of 1.5% was chosen so that the results could be compared to tests at 900 MPa p_o and 3%γ; i.e. with the same value of $p_o\gamma$. These high p_o conditions produced a marked difference in the wear behaviour of the bottom "driving" discs, as some of the tests at 1300 MPa p_o had begun to indicate. Wear rate results are shown in Figures 8.2 and 8.3, respectively, with detailed results in Table 8.1. The individual and combined wear curves are shown in Figures 8.34 and 8.35, respectively.

Only under these test conditions did top disc wear rate ranking match that of the bulk material hardness values (Table 2.3); i.e. all bainitic steels had slightly better wear resistance than the pearlitic steel. The wear rates of all the top discs were at the lower end of those seen for mild/severe transitional wear, whereas all the bottom disc wear rates were well within the severe wear regime.

Wear surfaces of the R52, B20 and B52 top discs were heavily flaked, whereas the

B04 disc surface appeared smooth. The R52 surface is shown in Figure 8.8, B04 in Figures 8.36a and b, B20 in Figure 8.37a and B52 in Figure 8.37b. Figure 8.36b indicates that B04 wear was still primarily due to flake formation, but either on far smaller scale than seen on the other top discs, or because any large flakes were cleared in one wear cycle. All the surfaces were finely oxidised, as were those of the bottom discs.

The bottom W64 disc wear surfaces from Tests 47 (B04/W64) and 48 (B20/W64) are shown in Figures 8.38 and 8.39, respectively. The surfaces of the bottom discs from the other two tests were similar in appearance. Wear mechanisms included the low cycle fatigue and eventually fracture of thick flakes, or platelets. The cyclic movement of such plates prior to fracture is clearly shown in these two figures. The spalling of plates left deep pits.

The difference in wear rates, and wear regimes, of the top and bottom discs is further illustrated by the worn disc profiles. Despite the heavy flaking, the top "braking" discs retained their shape, whereas the bottom "driving" discs were heavily deformed. The profiles of the Test 48 (B20/W64) discs are shown in Figure 8.40. Profiles for the other tests were similar.

Amsler tests at very high creepage ($\geq$ 15%).

An early R52/W64 test (Test 9) was carried out at a low maximum contact stress (474 MPa) and 25% creepage, with the machine at the higher speed setting. The wear curves are shown in Figure 8.41. Comparative rolling and sliding wear rates are given in Figures 8.4 and 8.5, respectively, with detailed results in Table 8.2. The disc surfaces were a metallic/oxide mix, with deep abrasions and micro- and macro-pits. Adhesive wear was such that sizeable lumps of material were scooped from the surfaces (Figure 8.42). Despite this heavy wear, the forced air cooling kept bulk disc temperatures to below 40°C. The test was terminated due to the imminent impingment of the plastically deformed wear track edges on the disc shoulders, plus excessive machine vibrations. Profilometry revealed that the top disc had faceted; there was no visual indication.

It was decided that further tests would be carried out at the slower machine speed and at a lower creepage. The conditions of Tests 13A (a B52/W64 test) and Test 13B (a B04/W64 test), 833 MPa p_o and 15% γ, were chosen to give the same $p_{o\gamma}$ product as the test described above (Test 9). The comparative rolling and sliding wear rates are shown in Figures 8.4 and 8.5 respectively with detailed results in Table 8.2. The wear curves are shown in Figure 8.43. There are significant differences between the comparative rolling and sliding wear rates for these high creepage tests (Figures 8.4 and 8.5); the sliding results show far more clearly the poor wear resistance of the B04/W64 combination under high creepage conditions.

The appearance of the disc wear surfaces from the B04/W64 test (Test 13B) was similar to that described above for Test 13 above, except that debris was in the form of coarse flakes and there were no "scooped pits". This top disc had also formed periodic surface undulations; these were more in the form of ripples than facets. Its profile is shown in Figure 8.44.

The appearance of the disc wear surfaces from the B52/W64 test (Test 13A) was also similar, highly undulating with numerous abrasions, however no coarse debris was generated during this test. Disc profiles reflected this surface roughening, although there were no regular undulations.

Amsler tests at moderate maximum contact stress (884 MPa) and high creepage (10%).

These tests were performed with the machine again at the higher speed setting. The comparative rolling and sliding wear rates of Tests 22, 23 and 25 are shown in Figures 8.4 and 8.5, respectively, with detailed results given in Table 8.2. Individual disc wear curves are given in Figure 8.45 and combined wear curves in Figure 8.46. The B04 disc appeared to have had particularly poor wear resistance under these conditions; it also induced high wear in the W64 "driving" disc. As a consequence, the test was terminated after a short period. The other bainitic disc, B52, had good wear resistance, but again high wear was induced in the W64 disc.

The pearlitic discs of Test 25 showed clear "severe" wear patterns up to 20,000 cycles with both developing semi-periodic, short wavelength ripples (Figure 8.47a). During the remainder of the test, the wear surfaces slowly smoothed as the ripples dispersed. By the test end, the top disc was visually clearly faceted (8.48b) and profilometry revealed that the bottom disc was also distinctly faceted (Figure 8.48); i.e. there had been a slow change, from "severe", to a "transitional" form of wear, even though there was only a slight change in the wear rates.

Both discs from the B04/W64 test were rippled throughout the test. A large volume of gross debris was generated, consisting of large flakes plus compacted and "scooped" globular debris. Profilometry revealed a degree of regularity to the top disc rippling and that bottom disc ripples were super-imposed upon a facet pattern (Figure 8.49).

Wear patterns on both discs from the B52/W64 tests appeared to be a mix of low amplitude rippling and corrugations; profilometry revealed that the top B52 disc had small regular ripples and that the bottom W64 disc was faceted. This was not visually apparent as the facets were obscured by severer wear surface features (Figure 8.50).

The higher degree of surface abrasion under these high creepage test conditions, for all three top discs, can be compared by viewing the SEM micrographs shown in Figures 8.51a, b and c, respectively; the degree of surface disruption matched wear rate ranking. To summarise, under these conditions, only the B04 disc was well within a regime of "severe" wear. Although the other discs showed some characteristics of severe wear, the clear faceting showed that a form of "stick-slip" wear had also occurred, typical of that seen in the transitional wear regime.

LEROS tests at high maximum contact stress (1300 MPa) and high creepage (10%). These tests were carried out at the slower LEROS machine speed. The conditions were judged to be beyond the stable working range of the Amsler machine using full width discs, even at its lower speed setting. The comparative rolling and sliding wear

rates are shown in Figures 8.4 and 8.5, respectively, with detailed results given in Table 8.2. Individual disc wear curves are shown in Figure 8.52 and combined wear curves in Figure 8.53. Only the Test 43 discs (B04/W64) appeared to have worn at a steady rate. There was some variability with the Test 44 (B20/W64) curves and with the Test 45 (B52/W64) curves. There was also a more pronounced change for both disc wear rates during Test 42 (R52/W64). Two wear rates have been given for Test 42 (for 2500 - 7500 and 7500 - 12500 top disc cycles, respectively; see Table 8.2). Note that the combined wear rate for this pearlitic test equalled that of the high carbon bainite test and was less than the rates for both tests involving carbide free bainites; a similar pattern to the Amsler 10% creepage results at lower contact stresses (Figures 8.28 and 8.46).

In all of these tests, the discs formed features which match the description of "severe wear" given by Bolton and Clayton[1984]; the formation and clearance of sizeable disc surface undulations during testing. Examples of these undulations for the top discs can be seen in Figures 7.17 and 7.18 in the previous chapter. The exceptionally large undulations present on both pearlite Test 42 discs, up to 650μm in amplitude (Figure 7.17a), cleared suddenly at 6100 top disc cycles. Subsequent ripple formation was at a far finer scale (hence the change in the wear curves). The features on these discs could be described as "track wide ripples, i.e. a form of gross corrugations. The bainite discs formed regular patterns of ripples that were not track-wide (Figures 7.17b, 7.17c and 7.18b). These regularly formed and cleared, with corresponding undulations in the friction curves. Talyrond profiles clearly show the regularity of these features (Figures 7.54 and 7.55), even on the heavily worn bottom W64 discs.

In the tests involving the harder bainites (Test 44 - B20 and Test 45 - B52), as seen with other high contact stress LEROS tests, there was a clear difference between the behaviour of top driven discs and bottom driving discs. The high contact stresses generated by top disc ripple peaks resulted in the formation of zones of short cycle fatigue on the bottom disc surfaces, with the consequent generation of thick debris and high wear rates. The matching bottom disc, to the rippled top disc is shown in

Figure 7.17c, is shown in Figure 8.56. Note the degree of track width spread (quantified in Table 7.2). The debris from the B04/W64 test (Test 43) was more "conglomorate" (adhered debris particles including scooped debris), an indication that the adhesive wear mechanism had been of more significance during this test.

A mass of coarse debris was generated during all of these tests and the (400μm square grid) coarse filter required frequent clearance during test periods. However, the total weight of such debris did not exceed 50%of the total weight loss; eg. 15% of the weight loss during Test 44 (B20/W64) and 30% during Test 45 (B52/W64). Therefore, even under these severe conditions, most of the debris was on a fine scale. On a micro-scale, the undulating disc surfaces visually appeared to be a mix of metal and oxide. Hardly any massive flakes (as picked up by the filters) were found adhering to the wear surfaces, i.e. they had been sheared off within a few cycles. Large flakes were found to have one metallic shear face, usually tempered coloured, and an oxidised "outer" face often with adhering "conglomorate" debris. However, a flaking wear mechanism clearly existed on both top and bottom discs; a bottom disc surface has been shown in Figure 8.56 and closer views of the B20 top disc surface (also shown in Figure 7.17c) reveal a mass of flakes on the ripples (Figure 8.57).

8.7 Summary

These results have shown that:

* The bulk mechanical properties of the steels do not give a clear guide to their wear behaviour.
* The ranking of the materials varies with test conditions, although it is generally consistent on both wear machines for a given set of conditions.
* The behaviour of the driving and driven discs did conform to a set pattern under certain test conditions, irrespective of the material combinations used.
* Disc pairs with similar wear curves, for a given set of test conditions, can have different wear surface features and profiles.
* Discs under test near the transformation between one wear regime and another can change from one steady state curve to another. Similarly, wear

surface features can change from those of one wear regime to another and/or change from, or to, a pattern of periodic wear surface undulations.

The sub-surface features associated with such behaviour are described and discussed in the Chapter 9 and the relationships between wear rates, friction and test conditions are given and discussed in Chapter 10. This chapter has illustrated the complexity of wear testing and how any change to the numerous wear system inputs, outlined in Chapter 4, can change wear characteristics.

8.8 References.

Allery, M. B. P., British Rail Research, Derby (1987). Personal communication.

Bolton, P.J., Clayton, P. and McEwen, I.J. (1980). "Wear of rail and tyre steels under rolling-sliding conditions." *Proc. ASME/ASLE Lubrication Conf., San Francisco, USA, 18-21/08/80.* Pub. *ASLE Trans.* 25 (1), pp. 17-24.

Bolton, P.J. and Clayton, P. (1984). "Rolling-sliding wear damage in rail and tyre steels." *WEAR* 93, pp. 145-165.

Timoshenko, H. P. and Goodier, J. N. (1970). Theory of Elasticity, 3rd. edn., McGraw-Hill, New York, pp. 403-420.

Table 8.1 Wear results from the Amsler (A) and LEROS (L) for $p_{o\gamma}$ values between 15 and 33 MPa. [Note: In this table, "friction coefficient" represents tractive friction.]

Test Number		8	19	18	29	33	34	35	7	16	14		17	15
Wear Machine (Amsler or LEROS)		A	A	A	L	L	L	L	A	A	A		A	A
Top braking disc		R52	B04	B52	R52	B04	B20	B52	R52	B04	B52		B04	B52
Bottom driving disc		W64	W64	W64	W64	W64	W64	W64	W64	W64	W64		B04	B52
Initial max. contact stress (MPa)		500	500	500	500	500	500	500	900	900	900		900	900
Initial creepage (%)		3	3	3	3	3	3	3	3	3	3		3	3
Test speed (top disc Hz)		5.83	5.83	5.83	6.72	6.72	6.72	6.72	5.83	5.83	5.83		5.83	5.83
Test length (X 10^3 cycles)	[a]	200	160	160	160	160	160	160	50	90	95		60	100
Measuring point (X 10^3 cycles)	[b]	115	100	100	100	90	90	100	35	35	20	65	40	60
(At the measuring point *)	[c]										sA	sB		
* Maximum contact stress, p_o, (MPa)		505	505	505	505	500	500	500	910	923	914	916	913	913
* Creepage, γ, (%)		3.0	3.2	2.9	3.4	3.0	3.1	3.0	3.2	3.4	2.7	2.1	3.2	2.9
* Friction coefficient		0.73	0.70	0.83	0.58	0.60	0.61	0.65	0.62	0.70	0.62	0.66	0.66	0.60
* $p_{o\gamma}$ (MPa)		15.1	16.1	14.8	17.3	15.0	15.3	15.0	28.9	31.3	25.0	19.2	29.0	26.4
* Tγ/A (MPa)	[d]	8.6	8.9	9.6	6.8	7.1	7.2	7.6	14.0	17.1	12.2	10.0	15.1	12.4
Rolling wear, top disc V_r (g/m^3)		4.27	18.53	3.55	3.67	29.63	5.17	2.26	61.1	241.3	27.6	3.9	154.6	77.8
Rolling wear, bottom disc V_r (g/m^3)		10.35	2.76	11.14	3.49	3.50	4.12	9.58	68.8	155.4	129.2	31.3	104.9	73.7
Sliding wear, top disc V_s (g/m^3)		142.8	583.1	120.9	107.1	990.4	169.4	75.4	1921	7123	1009	186	4868	2688
Sliding wear, bottom disc V_s (g/m^3)		346.6	86.9	379.5	101.9	117.1	135.0	318.9	2165	4589	4684	1497	3304	2544

Test Number		30	30B	36		37		38		46	47	48	49	10B	10C	11A
Wear Machine (Amsler or LEROS)		L	L	L		L		L		L	L	L	L	A	A	[f]
Top braking disc		R52	R52	B04		B20		B52		R52	B04	B20	B52	R52	R52	R52
Bottom driving disc		W64	W64	W64		W64		W64		W63	W64	W64	W64	W64	W64	W64
Initial max. contact stress (MPa)		900	900	900		900		900		1800	1800	1800	1800	1100	1100	1100
Initial creepage (%)		3	3	3		3		3		1.5	1.5	1.5	1.5	3	3	3
Test speed (top disc Hz)		6.72	1.47	6.72		6.72		6.72		1.47	1.47	1.47	1.47	5.83	[e]	5.83
Test length (X 10^3 cycles)	[a]	100	50	100		100		100		40	40	40	40	70	80	70
Measuring point (X 10^3 cycles)	[b]	60	40	30	80	40	80	30	80	25	25	30	25	30	40	35
(At the measuring point *)	[c]			sA	sB	sA	sB	sA	sB							
* Maximum contact stress, p_o, (MPa)		901	900	900	900	900	900	900	900	1803	1802	1802	1803	1106	1106	1107
* Creepage, γ, (%)		3.0	3.0	3.0	3.0	3.0	3.0	3.0	3.0	1.5	1.5	1.5	1.5	2.7	2.7	2.8
* Friction coefficient		0.46	0.48	0.49	0.38	0.38	0.32	0.48	0.47	0.37	0.34	0.33	0.39	0.68	0.66	0.59
* $p_{o\gamma}$ (MPa)		27.0	27.0	27.0	27.0	27.0	27.0	27.0	27.0	27.0	27.0	27.0	27.0	30.2	30.0	30.4
* Tγ/A (MPa)	[d]	9.7	10.3	10.4	8.0	8.0	6.8	10.2	10.0	7.8	7.3	7.0	8.3	16.0	15.4	14.1
Rolling wear, top disc V_r (g/m^3)		57.87	48.48	111.60	71.09	65.16	37.95	3.70	32.85	37.03	27.42	23.40	23.83	72.28	45.18	92.77
Rolling wear, bottom disc V_r (g/m^3)		54.01	43.02	71.25	37.70	68.98	78.08	13.19	60.21	142.63	140.53	161.64	140.59	81.22	78.87	112.64
Sliding wear, top disc V_s (g/m^3)		1940	1599	3674	2345	2169	1265	123	1098	2471	1828	1560	1587	2649	1686	3375
Sliding wear, bottom disc V_s (g/m^3)		1810	1419	2345	1244	2296	2602	439	2012	9517	9367	10779	9366	2976	2943	4098

[a] : Bottom disc cycles on the Amsler machine and top disc cycles on the LEROS machine.
[b] : The mid-point of the steady state, linear part of the wear curve.
[c] : During some tests there was a distinct change of wear regime during the test resulting in two steady wear rates; Slope A ("sA") and Slope B ("sB").
[d] : T = tangential force (N) and A = contact area (mm^2).
[e] : Change of speed during test; no significant change in wear curve. (0 → 60,000 cycles; 5.83 Hz; 60,000 → 80,000 cycles, 2.92 Hz.)
[f] : Test carried out (with smaller test discs) on a conventional Amsler machine at British Rail Research, Derby, UK.

Table 8.2 Wear results from the Amsler (A) and LEROS (L) for p_{oT} values between 39 and 130 MPa. [Note: In this table, "friction coefficient" represents tractive friction.]

Test Number		[a] 28	33	34	35	30		30B	36		37		38		46	47
Top braking disc		R52	B04	B20	B52	R52		R52	B04		B20		B52		R52	B04
Bottom driving disc		W64	W64	W64	W64	W64		W64	W64		W64		W64		W64	W64
Initial max. contact stress, p_o, (MPa)		500	500	500	500	900		900	900		900		900		1800	1800
Initial creepage, γ, (%)		3	3	3	3	3		3	3		3		3		1.5	1.5
Nominal p_{oT} (MPa)		15	15	15	15	27		27	27		27		27		27	27
Test speed (top disc Hz)		6.72	6.72	6.72	6.72	6.72	6.72	1.47	6.72	6.72	6.72	6.72	6.72	6.72	1.47	1.47
Profiled at (bottom disc cycles X 10^3) (ie, at the test end unless indicated⁻)		160	160	160	160	50⁻	100	50	50⁻	100	50⁻	100	50⁻	100	40	40
Track width spread (%)	Top	0.8	1.4	0.6	0.2	-	6.4	4.3	-	5.9	-	3.6	-	1.5	20.8	12.3
	Bottom	1.9	1.5	1.3	0.6	-	6.9	3.7	-	6.6	-	15.7	-	7.1	23.0	20.0
Disc eccentricity (μm) [b]	Top	2	15	2	1	24	50	18	38	50	42	90	3	43	17	5
	Bottom	5	4	7	4	5	16	14	15	30	26	37	9	20	180e	153e
Max. amplitude of long wave-length undulations (±μm) [c]	Top	3F	13F	-	-	30F	65F	26F	3.5F	4.5F	50F	80F	-	76F	-	-
	Bottom	2.5i	-	-	-	7F	14F	-	48F	86F	6.5F	-	-	16F	-	-
Facets (or Ripples) per circumference [d]	Top	37p	34	-	-	33	31	33	~~16p~~ 37	15p	38	38	-	36p	-	-
	Bottom	-	-	-	-	34p	35	-	36	36	15p	-	-	30p	-	-
Facet "double peaks" [e]	Top	-	-	-	-	-	11	-	-	-	-	9	-	4p	-	-
	Bottom	-	-	-	-	-	-	-	1	14	-	-	-	16p	-	-
Facet (or Ripple) frequency	Top	249	228	-	-	222	208	48.5	~~108~~ 252	101	255	255	-	242	-	-
	Bottom	-	-	-	-	235	242	-	249⁻	249	104	-	-	202	-	-
Max. amplitude of short wave-length undulations (±μm) [f]	Top	0.5	nm	<0.5	0.5	nm	nm	nm	1	1	nm	nm	<0.5	nm	70	1
	Bottom	4	2	3.5	2.5	nm	nm	4.5	nm	nm	3	7	4	14	23	20

Test Number		48	49	32	39	40	41	51		52		30A	42	43	44	45
Top braking disc		B20	B52	R52	B04	B20	B52	R52		R52		R52	R52	B04	B20	B52
Bottom driving disc		W64	W64	W64	W64	W64	W64	W64		W64		W64	W64	W64	W64	W64
Initial max. contact stress, p_o, (MPa)		1800	1800	1300	1300	1300	1300	500		500		900	1300	1300	1300	1300
Initial creepage, γ, (%)		1.5	1.5	3	3	3	3	10		10		7	10	10	10	10
Nominal p_{oT} (MPa)		27	27	39	39	39	39	50		50		63	130	130	130	130
Test speed (top disc Hz)		1.47	1.47	1.47	1.47	1.47	1.47	6.72	6.72	1.47	1.47	1.47	1.47	1.47	1.47	1.47
Profiled at (bottom disc cycles X 10^3) (ie, at the test end unless indicated⁻)		40	40	40	40	40	40	60⁻	100	60⁻	100	50	12.5	7.5	10	10
Track width spread (%)	Top	7.5	8.3	10.9	8.3	5.8	3.6	-	6.1	-	3.7	5.4	22.6	14.9	10.5	5.5
	Bottom	28.7	31.7	10.0	12.7	10.1	16.9	-	4.4	-	2.4	4.3	18.6	31.3	47.2	34.8
Disc eccentricity (μm) [b]	Top	13	21	45	70	37	68	28	150	16	18	23	46	22	2	26
	Bottom	170e	270e	42	52	48	75	24	31	10	11	20	32	90	106	80
Max. amplitude of long wave-length undulations (±μm) [c]	Top	-	-	14i	15F	40F	71F	170F	190F	4.5F	4.5F	16F	13.5Ri	70R	53R	40R
	Bottom	-	-	-	-	-	-	2.5F	4.5F	-	-	-	-	76R	58i	-
Facets (or Ripples) per circumference [d]	Top	-	-	-	31p	36	38p	27	26	48p	42p	43	-	29	36	38
	Bottom	-	-	-	-	-	-	12p	12p	-	-	-	-	26	-	-
Facet "double peaks" [e]	Top	-	-	-	-	1	8p	7	8	-	-	-	-	-	-	-
	Bottom	-	-	-	-	-	-	-	-	-	-	-	-	-	-	-
Facet (or Ripple) frequency	Top	-	-	-	45.6	52.9	55.9	181	175	70.6	61.8	63.2	-	42.6	52.9	55.9
	Bottom	-	-	-	-	-	-	89	89	-	-	-	-	42.2	-	-
Max. amplitude of short wave-length undulations (±μm) [f]	Top	34	26	nm	nm	nm	nm	nm	nm	1	2	nm	3	nm	nm	nm
	Bottom	15	35	8	8.5	12	21	1	6	2	2.5	3	5	nm	nm	49

[a] : The Test 29 discs were damaged and not profiled. The results for a similar test are given, Test 28. The tests differed in that the Test 28 bottom disc had a direct drive, not a geared drive.

[b] : "e" - reading larger than profilometer scale; an estimate has been given based upon profile extrapolation and micrometer measurements.

[c] : "F" - long wavelength, track-wide corrugations formed, termed "facets".
"R" - long wavelength, regular ripples formed ("sand-dune" effect).
"i" - irregular undulation wavelengths.

[d] : Although initially regularly spaced, some facet peaks migrated during testing and "double peaks" formed.

[e] : "p" - only part of the circumference has a clear pattern of regular undulations; the data given has been extrapolated to represent the full circumference.

[f] : On the LEROS machine this represents maximum surface roughness; no short wavelength corrugations formed on any LEROS discs. On some discs, where steep undulations had formed, surface roughness could not be measured ("nm").

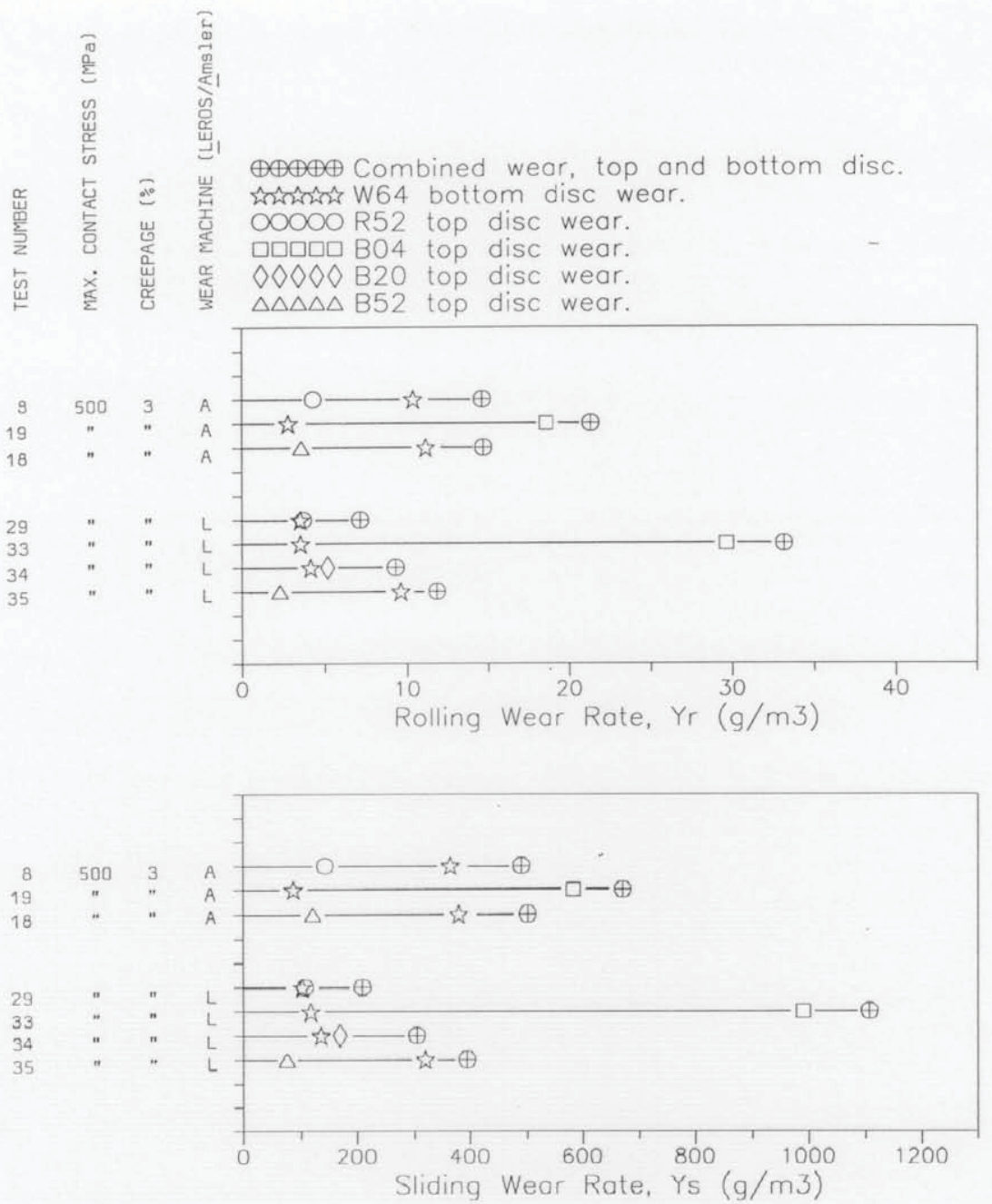

Figure 8.1 "Mild wear" rolling and sliding wear rate patterns, for the Amsler (A) and LEROS (L), for values of $p_o\gamma$ of 15 MPa.

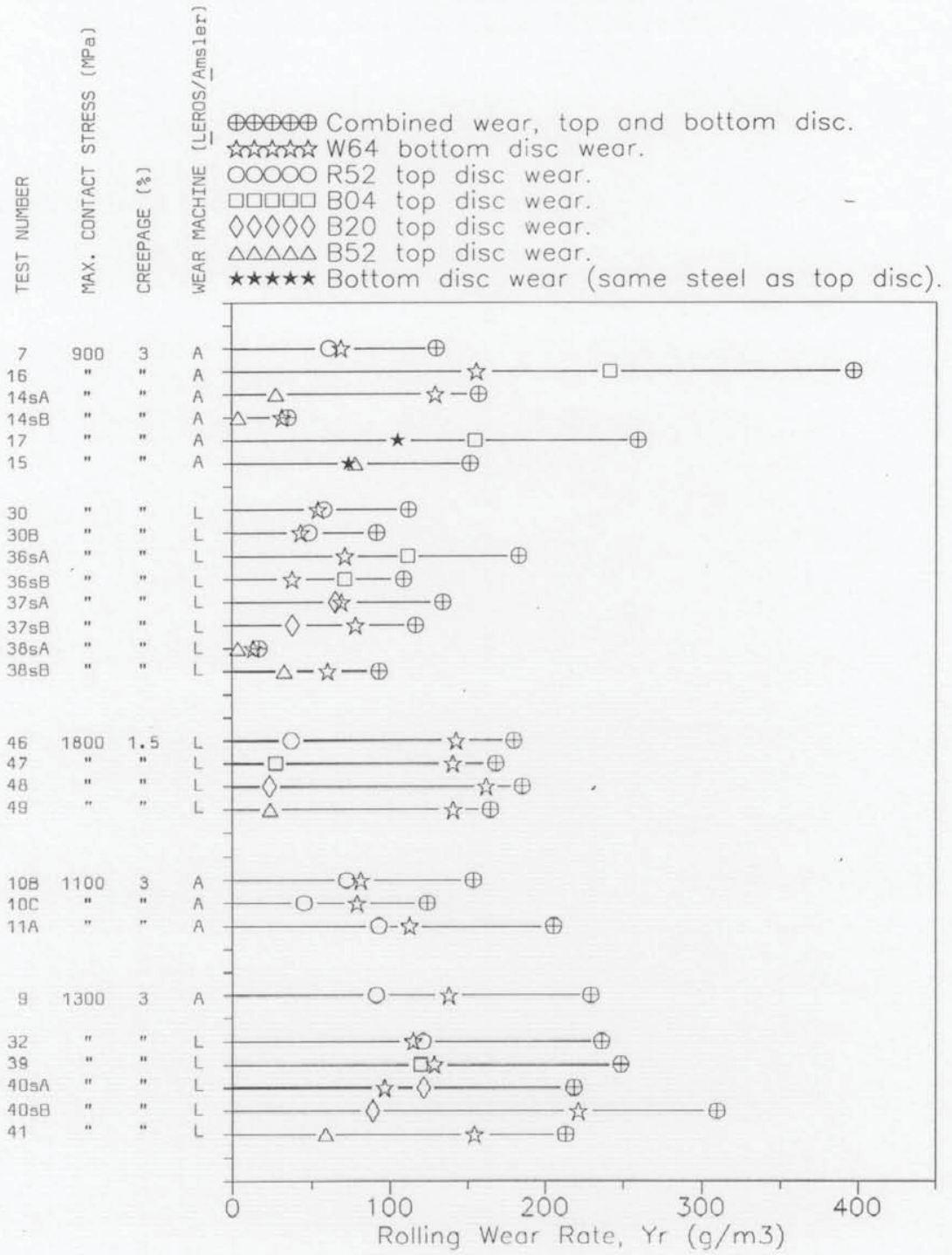

Figure 8.2 "Transitional wear" rolling wear rate patterns, for the Amsler (A) and LEROS (L), for values of $p_o\gamma$ between 27 and 39 MPa.

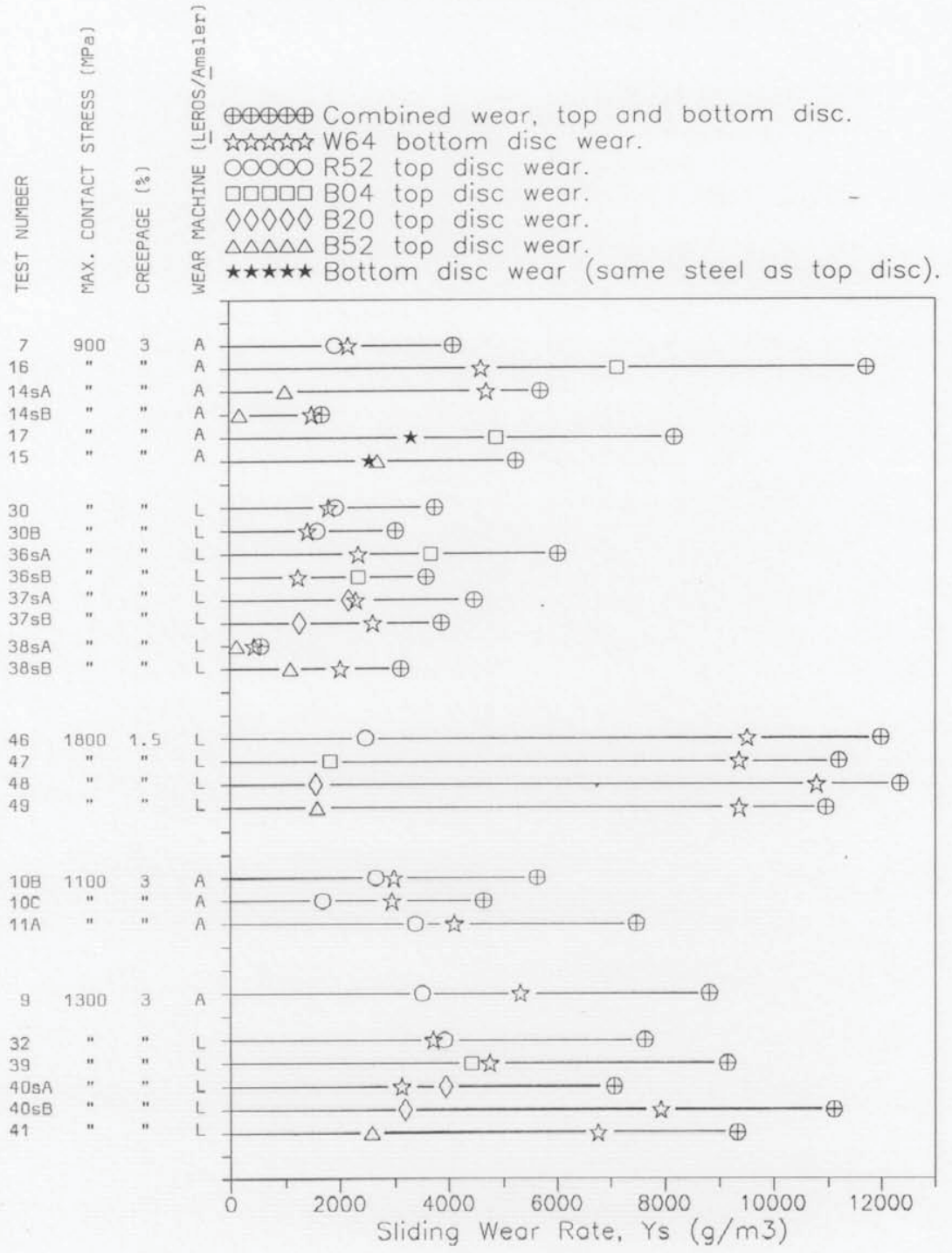

Figure 8.3 "Transitional wear" sliding wear rate patterns, for the Amsler (A) and LEROS (L), for values of $p_o\gamma$ between 27 and 39 MPa.

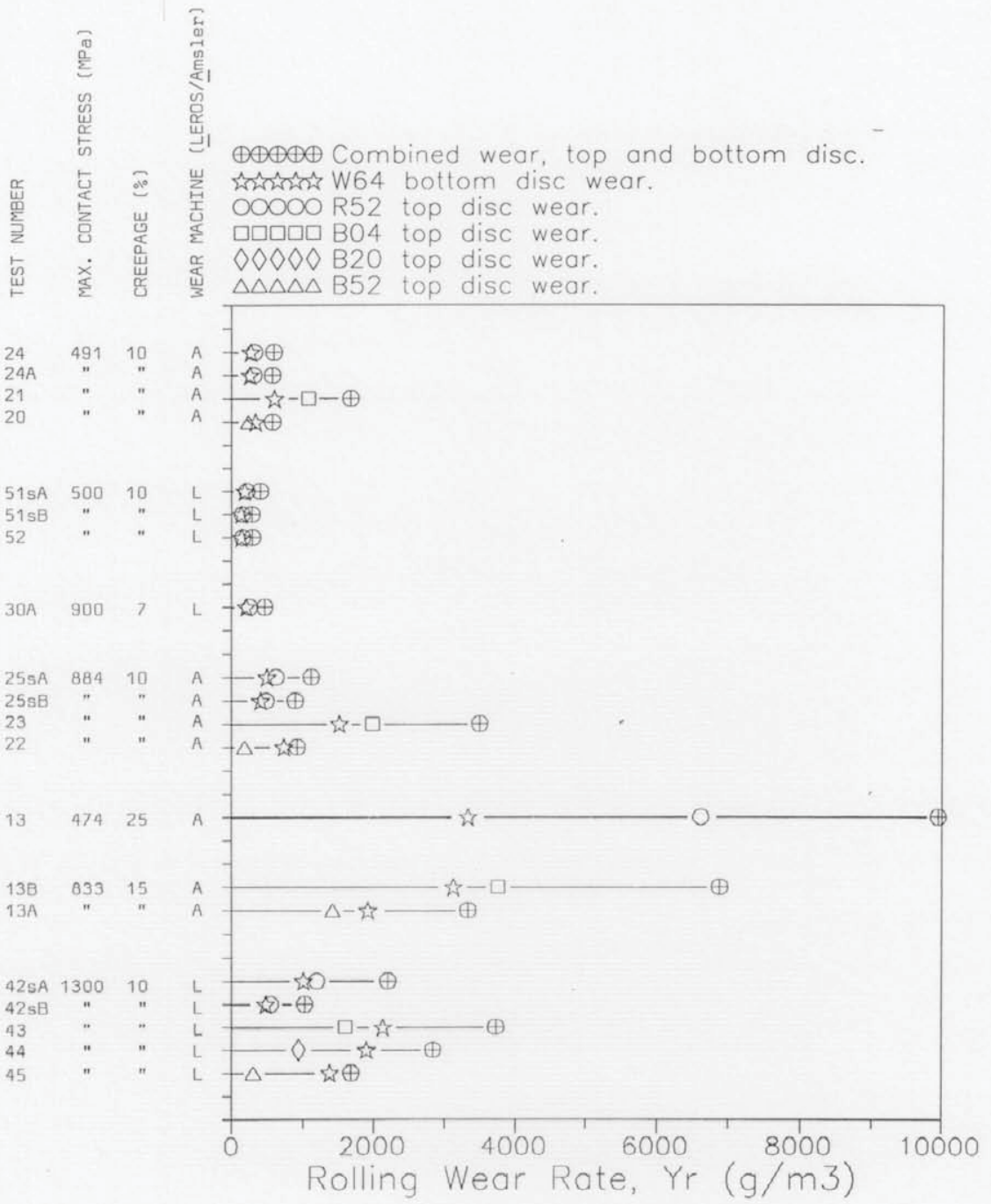

Figure 8.4 Higher creepage rolling wear rate patterns, for the Amsler (A) and LEROS (L), for values of $p_o\gamma$ between 49 and 130 MPa.

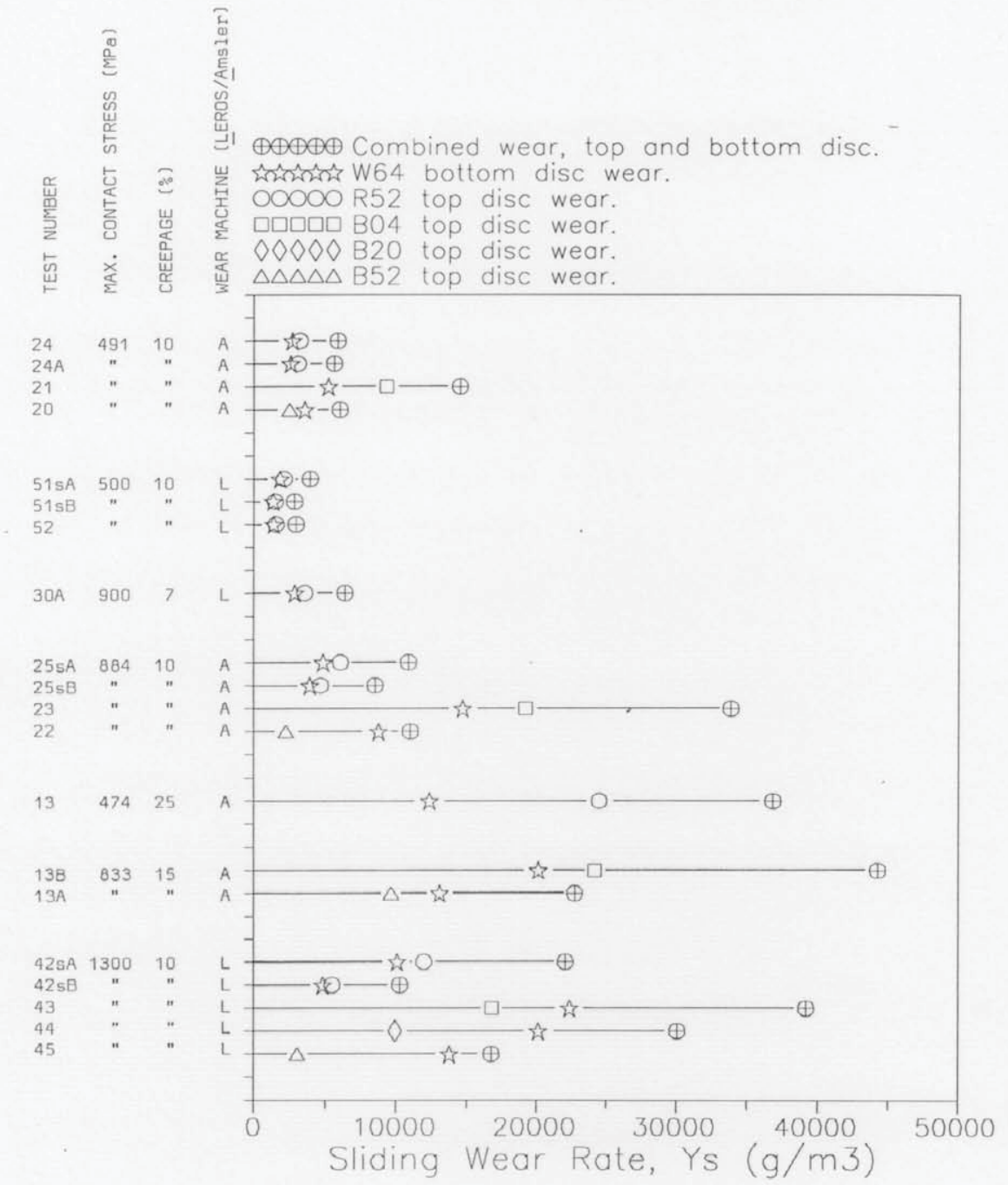

Figure 8.5 Higher creepage sliding wear rate patterns, for the Amsler (A) and LEROS (L), for values of $p_o\gamma$ between 49 and 130 MPa.

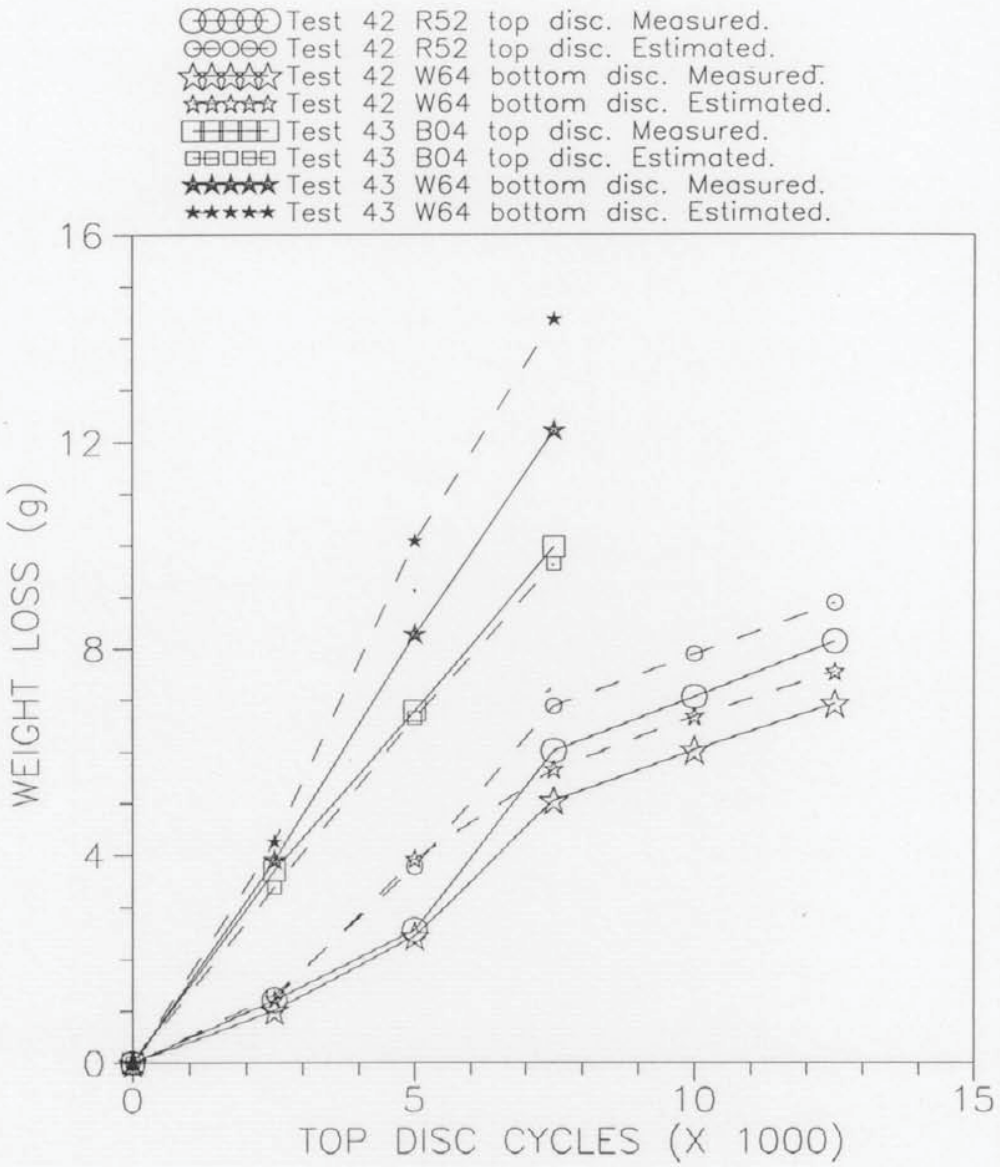

Figure 8.6 A comparison between wear rates determined by weight loss and wear rates estimated by disc diameter reduction, for R52/W64 and B04/W64 disc pairs, tested under severe conditions (1300 MPa p_o, 10% γ).

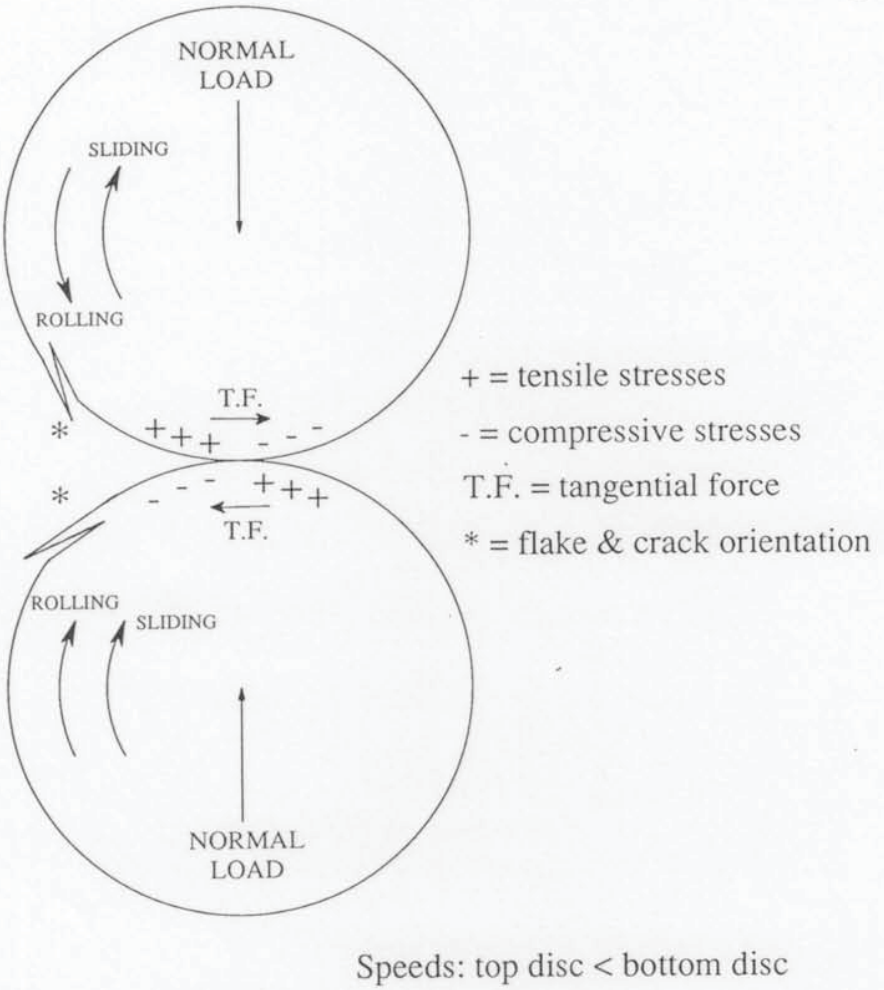

Figure 8.7 Schematic representation of the circumferential stress distribution near the contact of rolling-sliding cylindrical discs. The direction of surface ratchetting and flaking is indicated for each disc (not to scale).

a (x8 mag.)

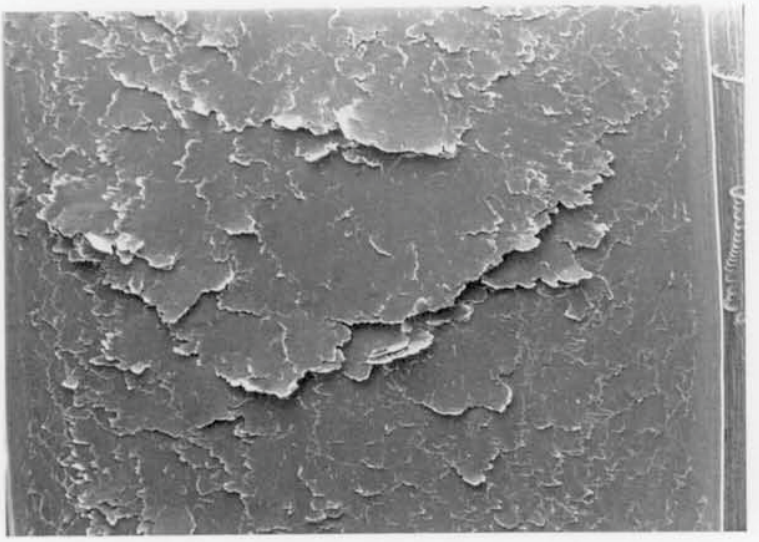

b (x1800 mag.)

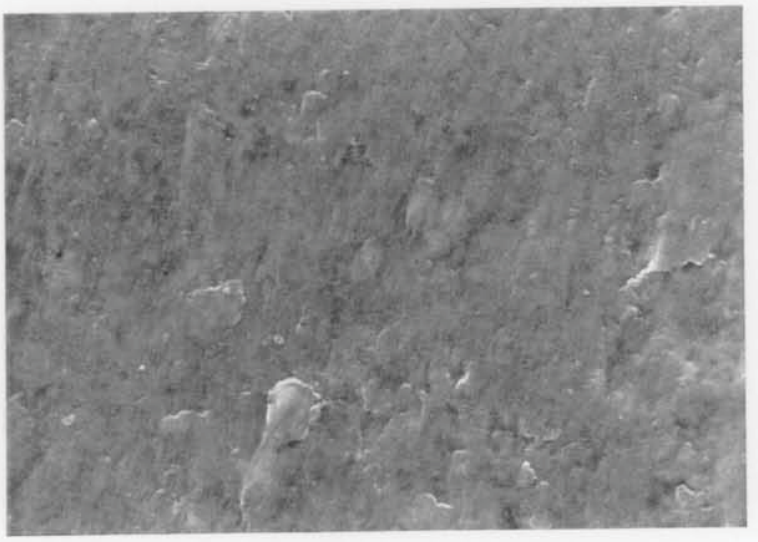

Figure 8.8 SEM photographs showing that the flaking mechanism could vary in size from (a) the complete track width, to (b) sub-micron. [Both views of the Test 46 R52 top disc, tested at 1800 MPa p_o, 1.5% γ.]

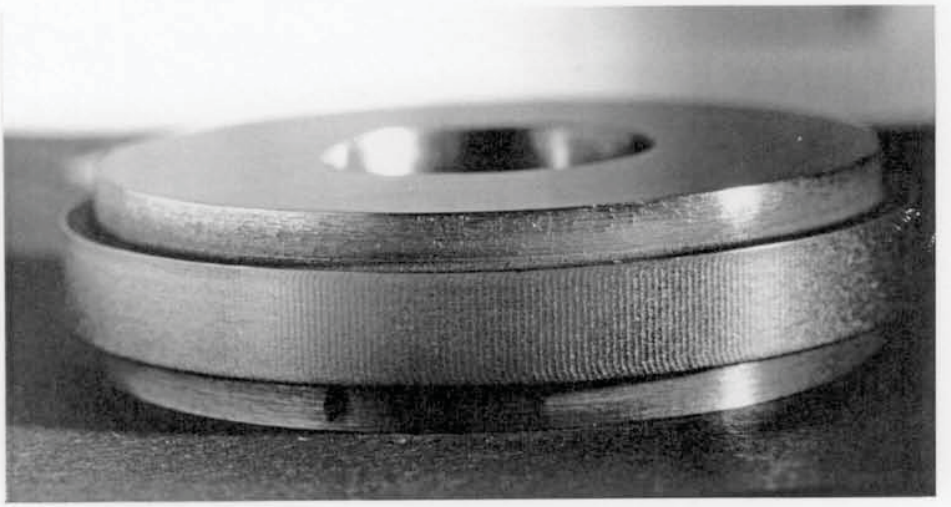

a (x3.1 mag.)

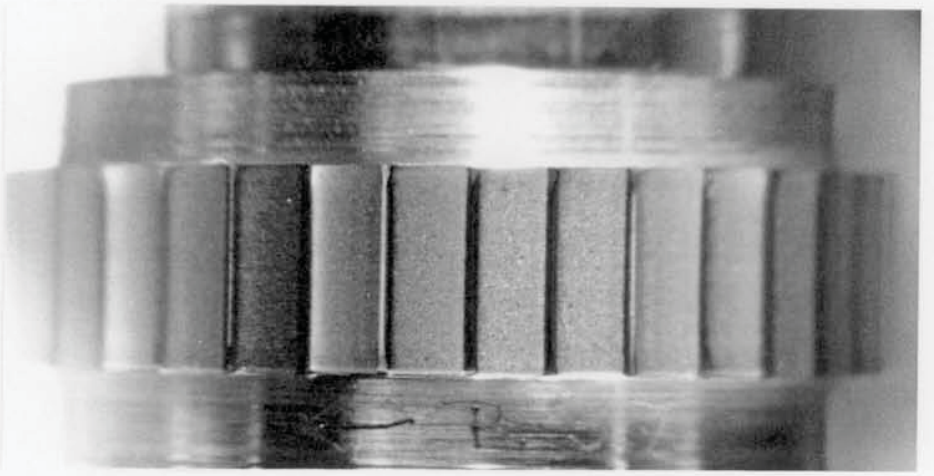

b (x2.8 mag.)

Figure 8.9 Complete disc views showing the two forms of track wide, periodic undulations. (a) Amsler disc fine wavelength corrugations and (b) LEROS disc long wavelength facets.

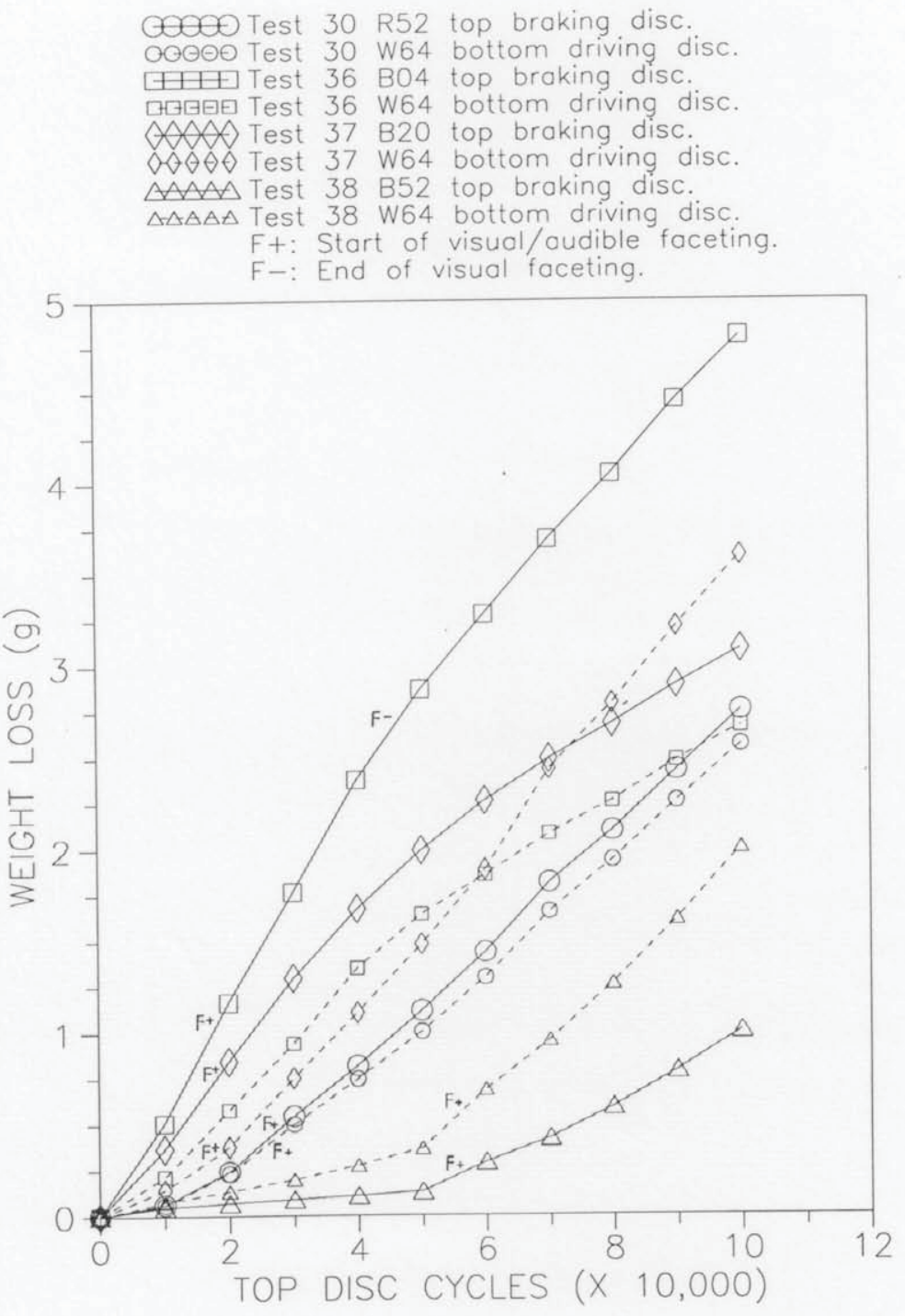

Figure 8.10 The effect on wear rate of facet formation. LEROS wear curves where facets were observed to develop during testing, and one one curve, disappear later during the test. [Test conditions, 900 MPa p_o, 3% γ.]

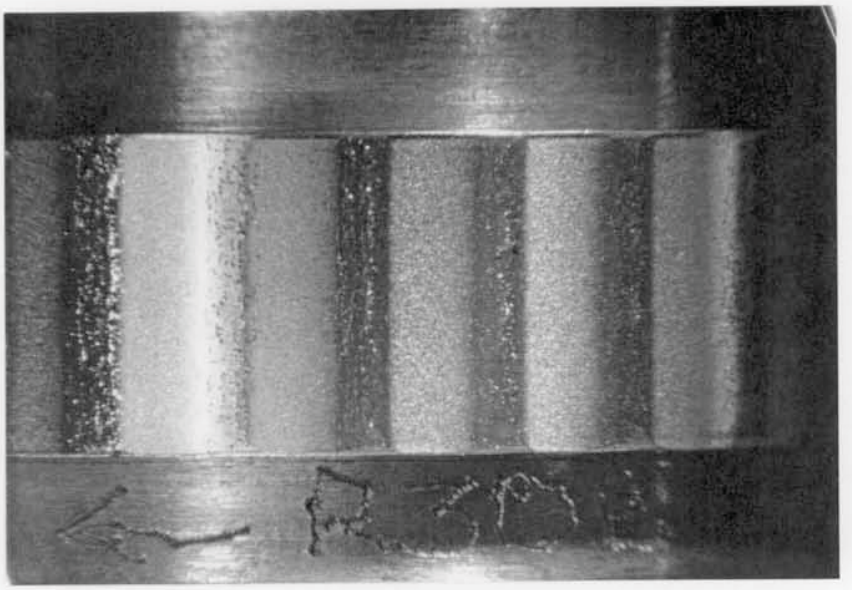

a (x4.3 mag.)

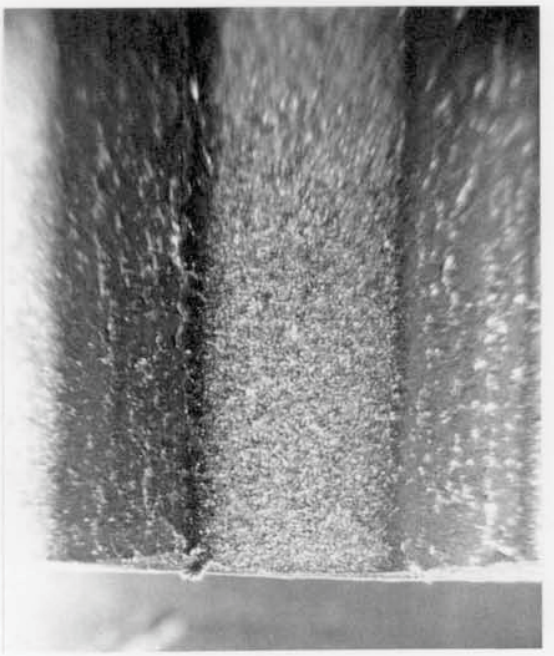

b (x11 mag.)

Figure 8.11 Typical surface features of most LEROS disc facets - heavily oxidised, flaking peaks and partially oxidised troughs with far finer flaking. (a) Overview of faceted wear track. (b) Detail. [Test 30B R52 top disc, tested at 900 MPa p_o, 3% γ.]

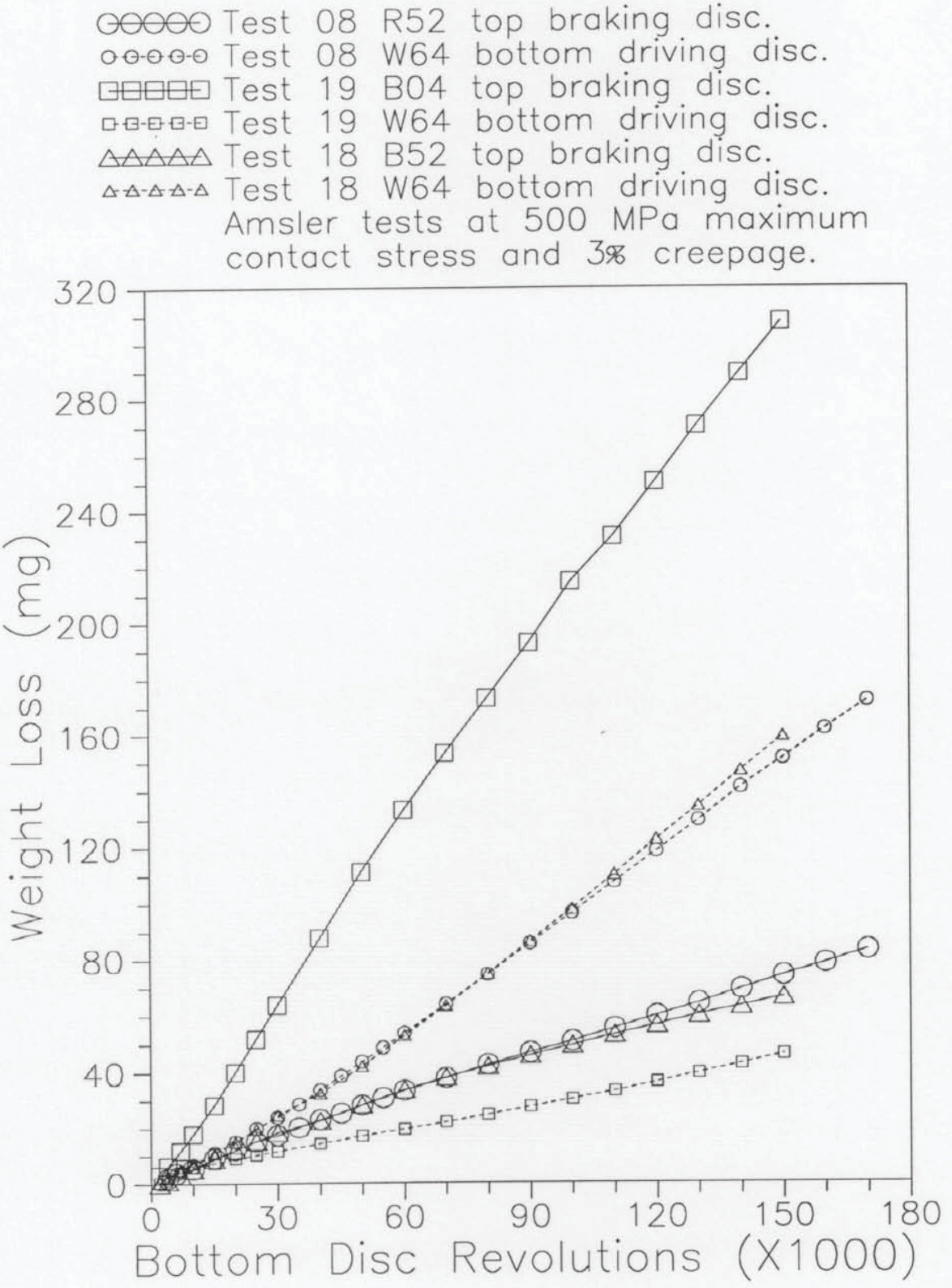

Figure 8.12 Top and bottom disc wear curves for mild* wear tests on the Amsler. [* Tests at 500 MPa p_o, 3% γ.]

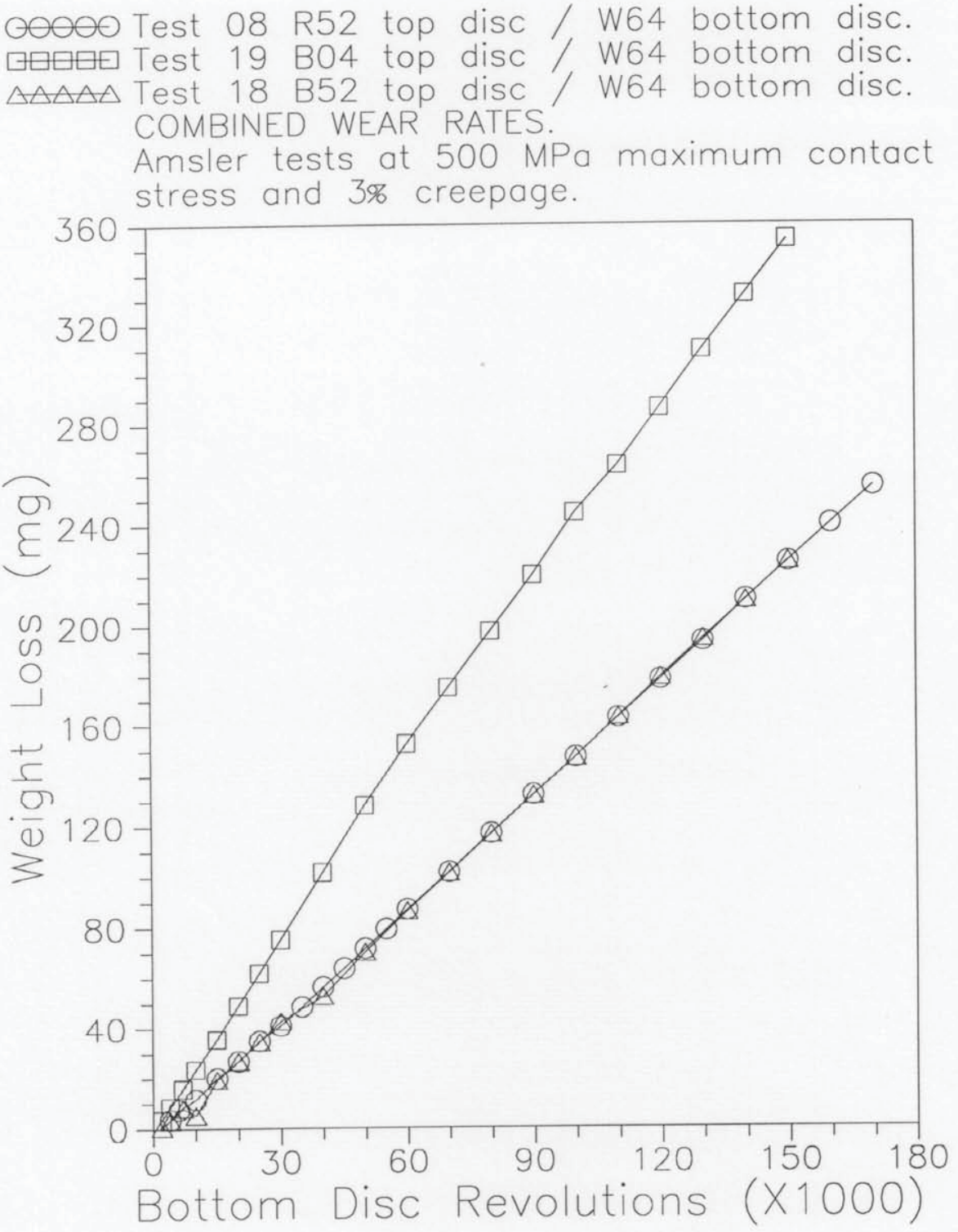

Figure 8.13 Combined top and bottom disc wear curves for mild wear tests on the Amsler.

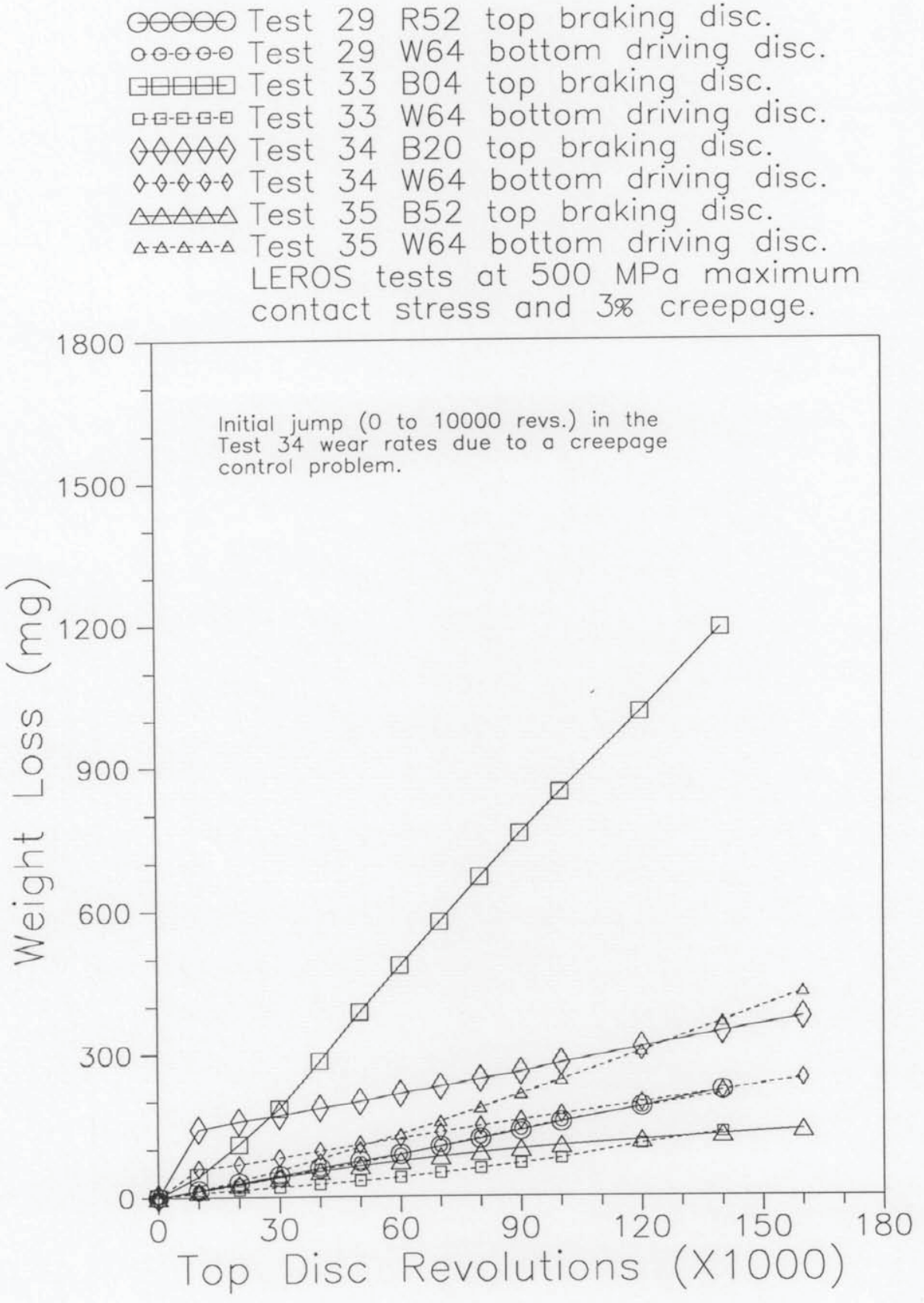

Figure 8.14 Top and bottom disc wear curves for mild wear test on LEROS.

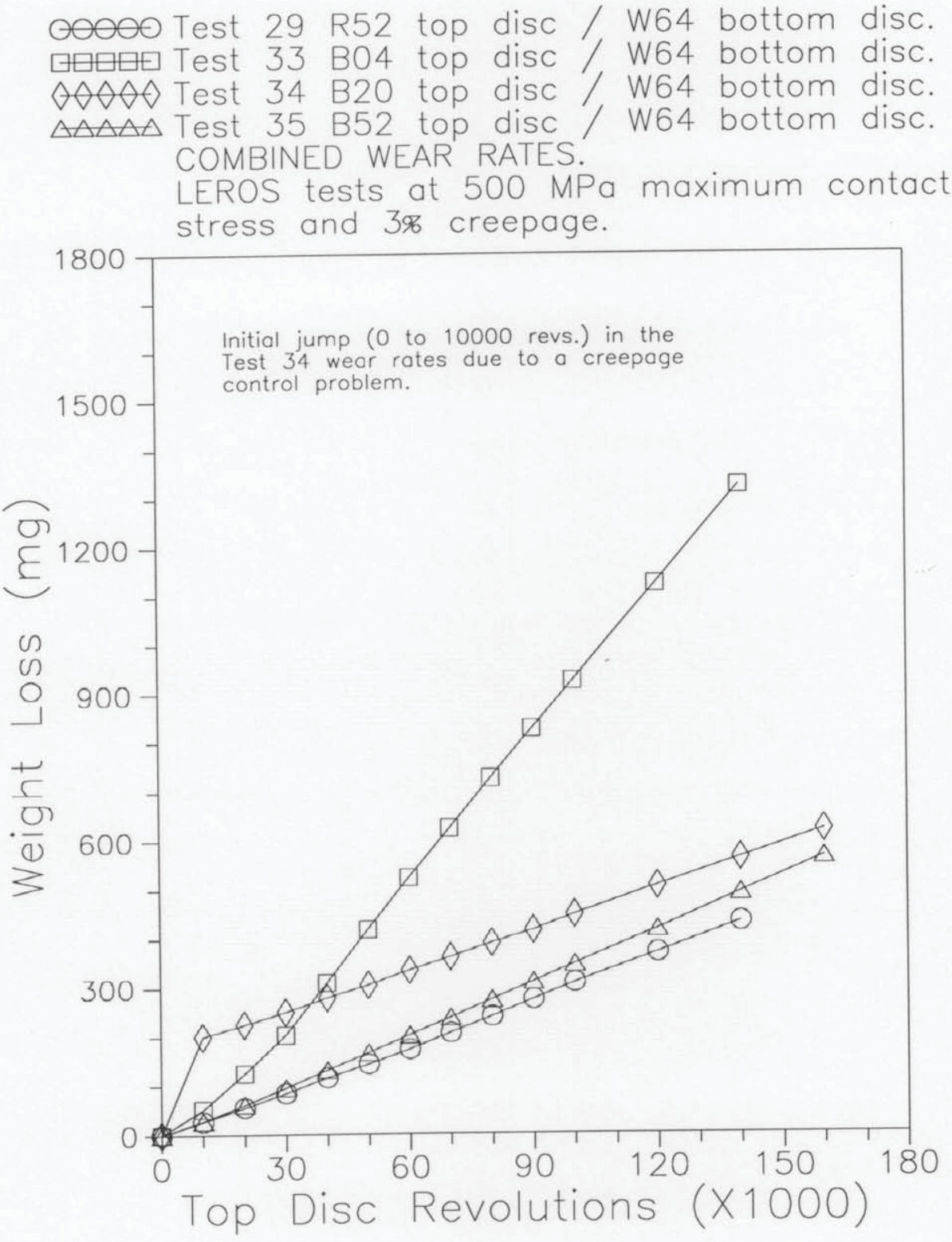

Figure 8.15 Combined top and bottom disc wear curves for mild wear tests on LEROS.

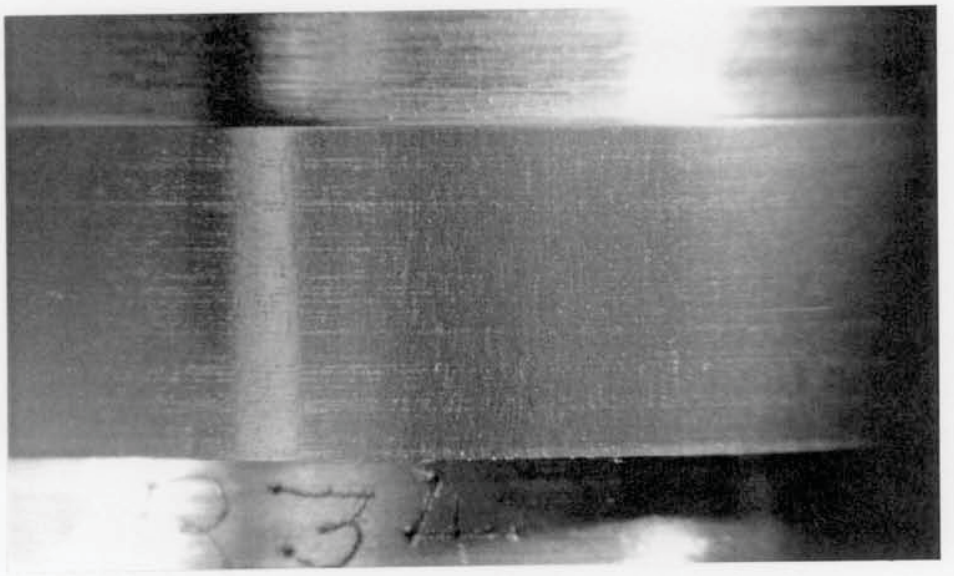

a (x4.6 mag.)

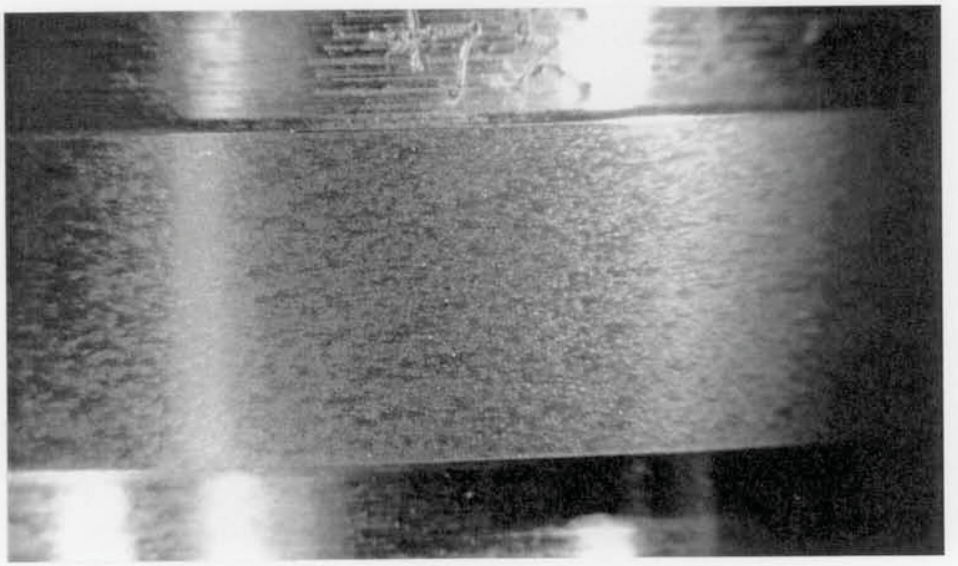

b (x4.6 mag.)

Figure 8.16 LEROS disc track surfaces after a mild wear test. (a) B04 top disc. (b) W64 bottom disc. [Test 34, 500 MPa p_o, 3% γ.]

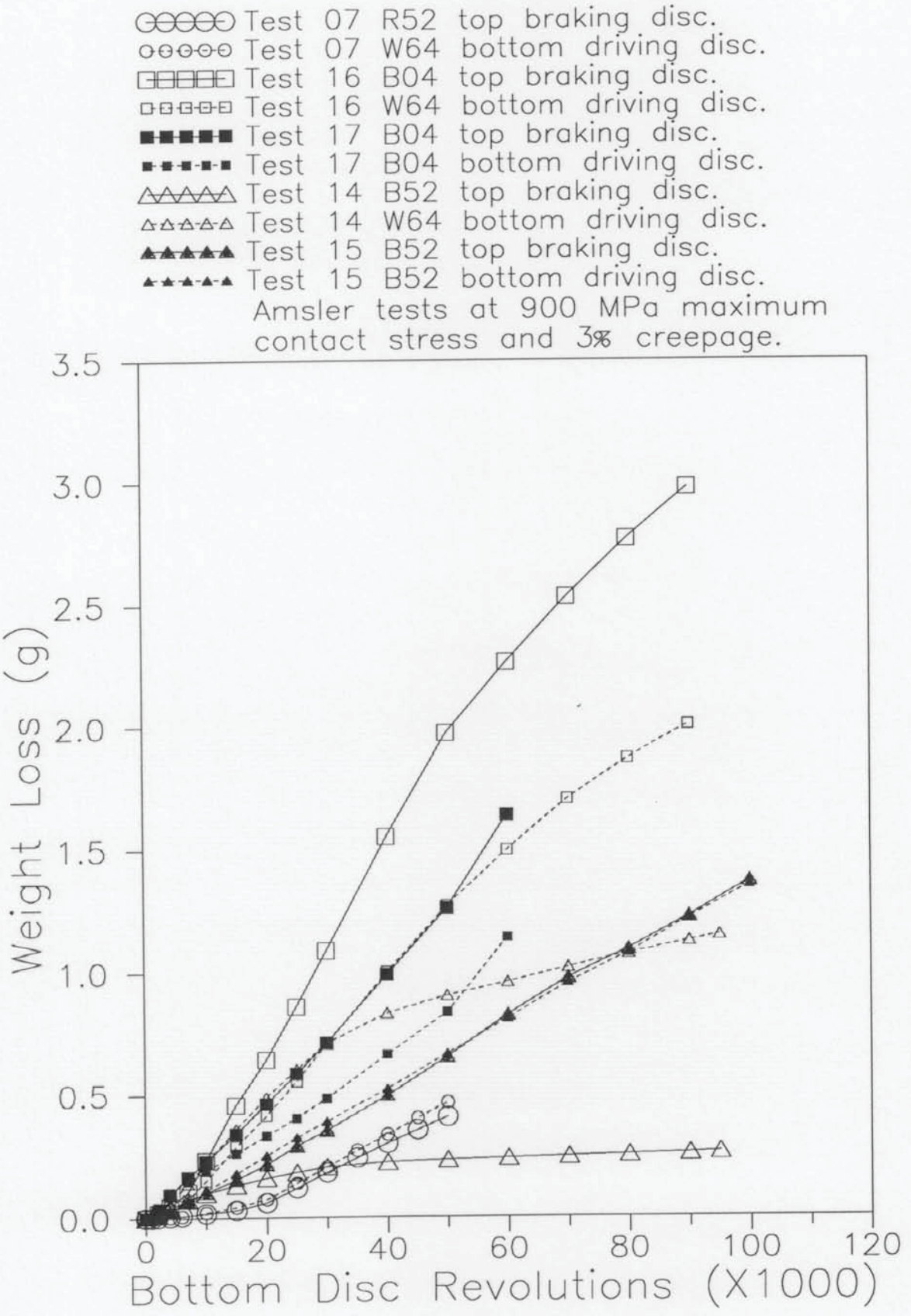

Figure 8.17 Top and bottom disc wear curves for Amsler tests at 900 MPa p_o, 3% γ. [Tests 15 and 17, bainite on bainite tests.]

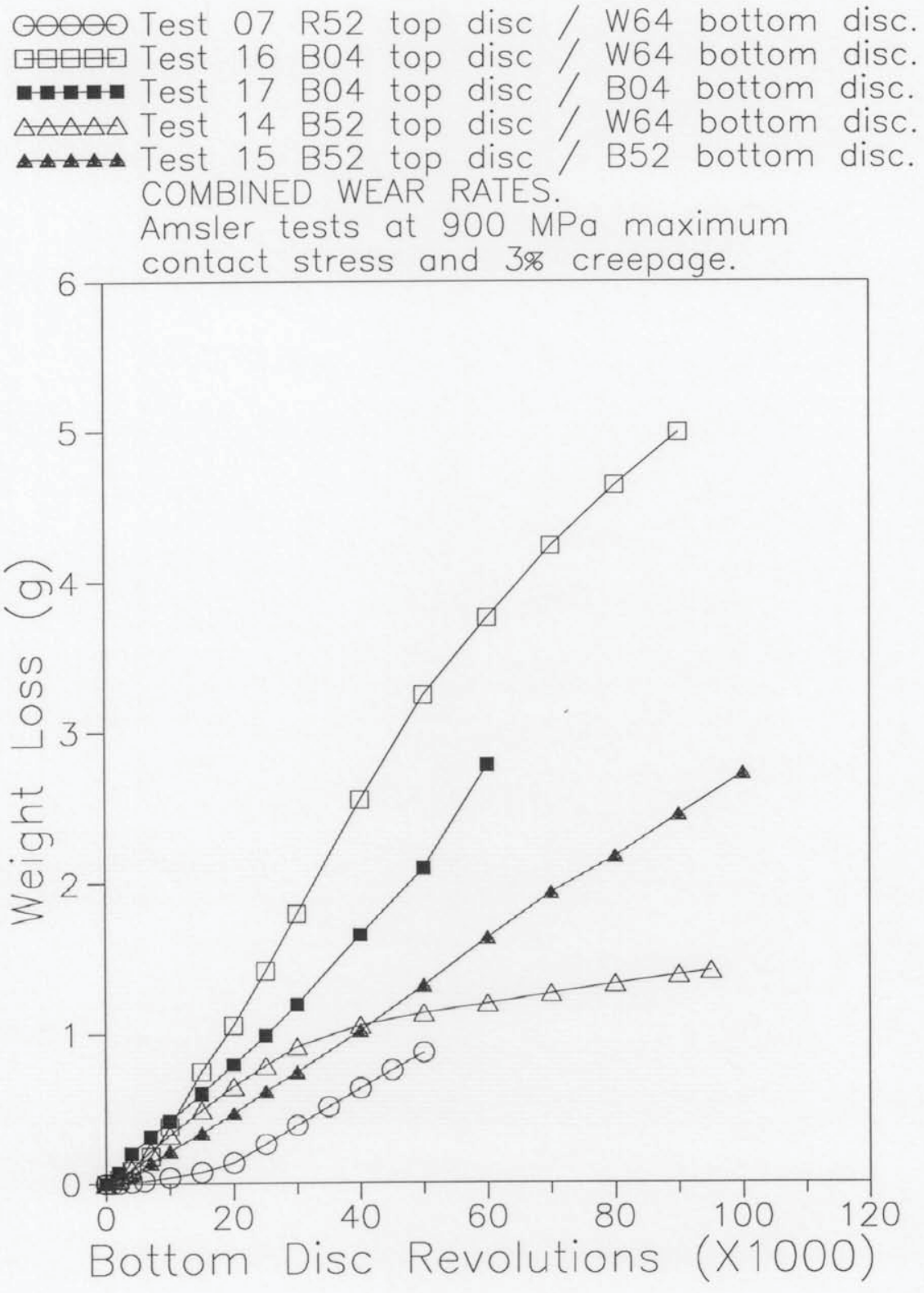

Figure 8.18 Combined top and bottom disc wear curves for Amsler tests at 900 MPa p_o, 3% γ. [Tests 15 and 17, bainite on bainite tests.]

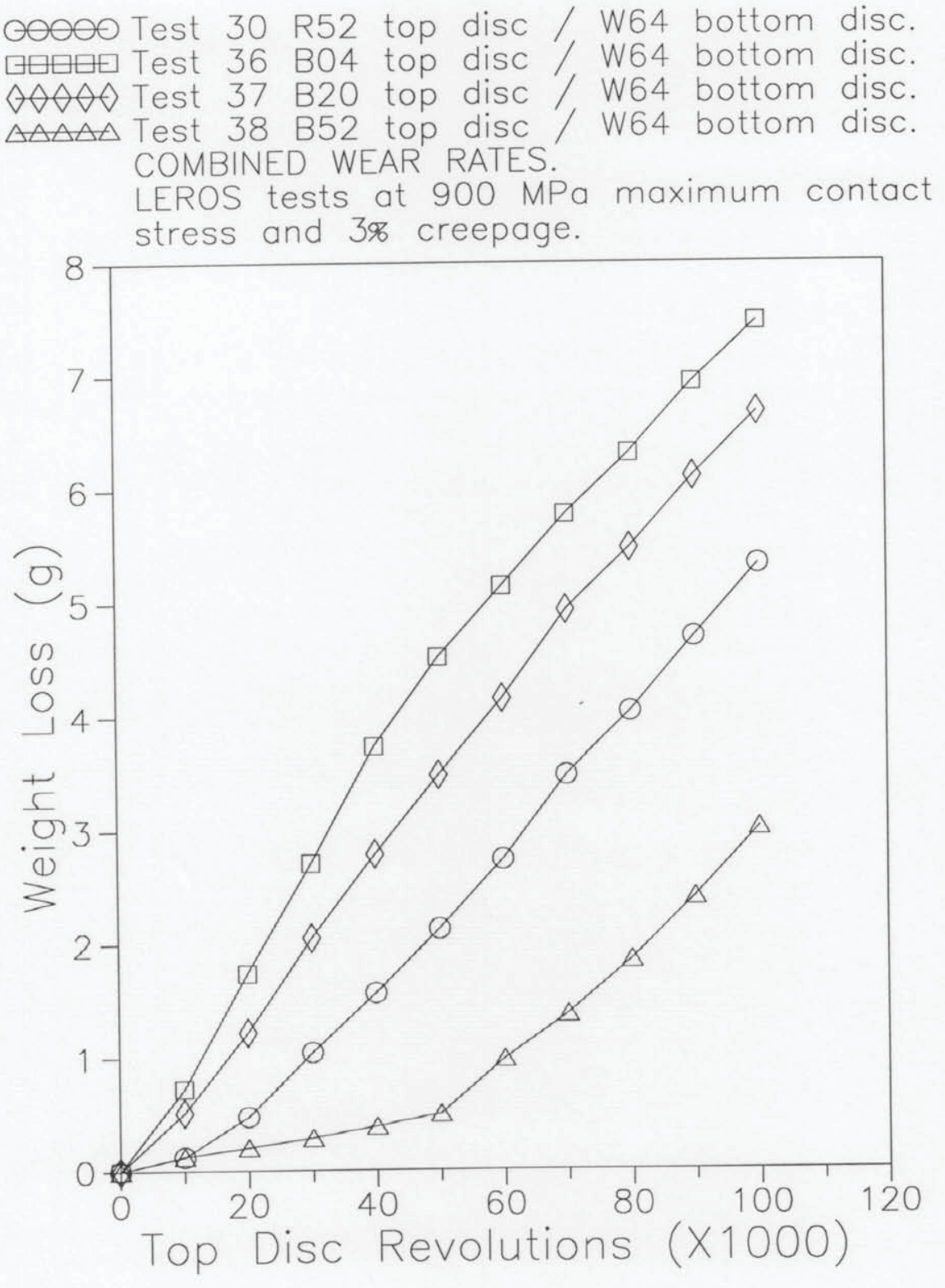

Figure 8.19 Combined top and bottom disc wear curves for LEROS tests at 900 MPa p_o, 3% γ. [Individual LEROS disc wear curves are shown in Figure 8.10.]

Test 10B Top disc.
Test 10B Bottom disc.
Test 11A Top disc.
Test 11A Bottom disc.
Test 10C Top disc.
Test 10C Bottom disc.

Standard test on modified Leicester Amsler.
Test on standard Amsler at British Rail Research, Derby.
Leicester Amsler test with a change to low speed at 60000 revs.

All tests, with R52 top braking discs and W64 bottom driving discs, at 1100 MPa maximum contact stress and 3% creepage.

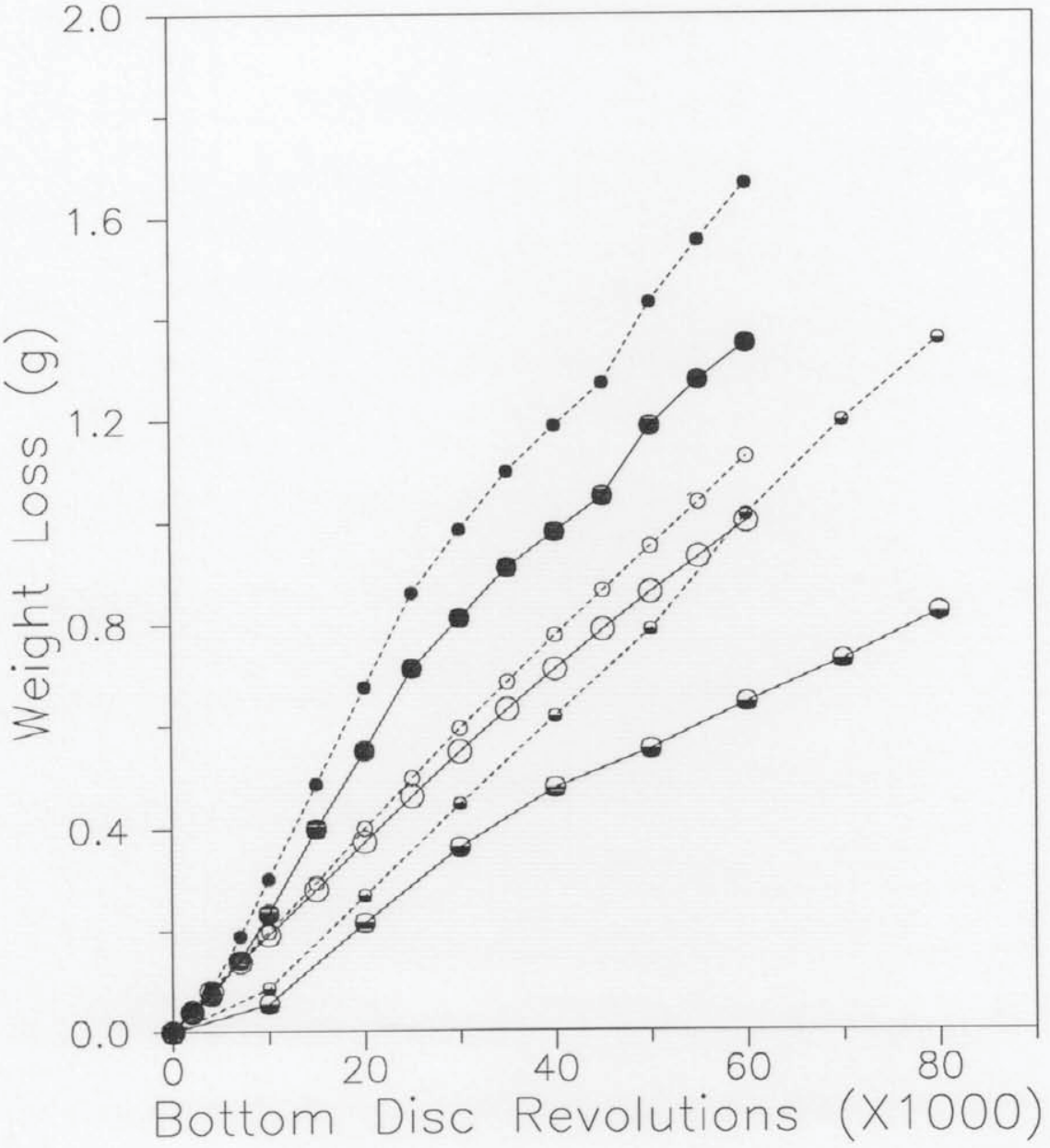

Figure 8.20 Top and bottom, R52/W64 disc wear curves for comparative Amsler tests. One set on the Leicester Amsler, another on a standard Amsler at British Rail Reseach and the third set on the Leicester Amsler with a speed change during the test. [Tests at 1100 MPa p_o, 3% γ.]

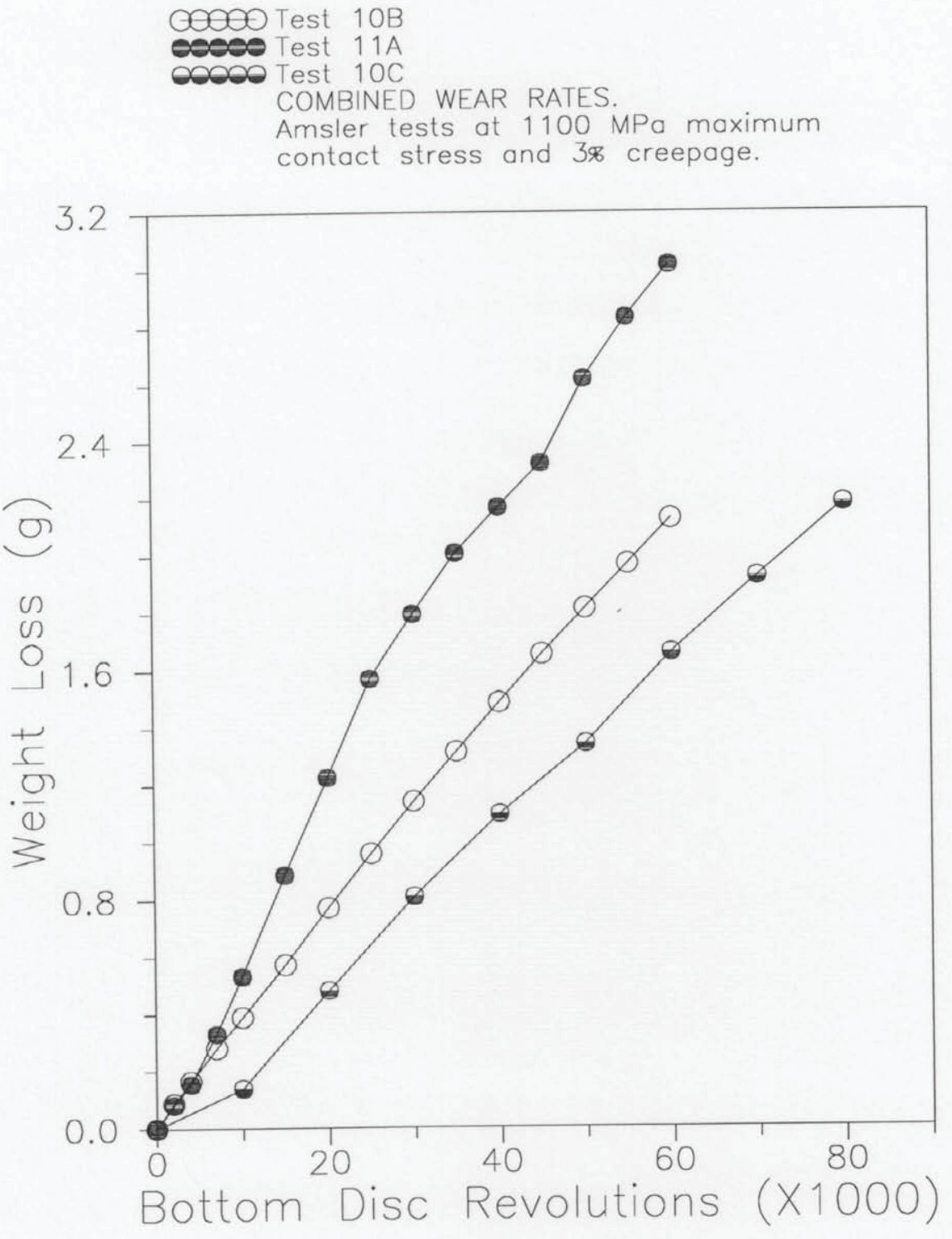

Figure 8.21 Combined top and bottom disc wear curves for the comparative tests shown in Figure 8.20.

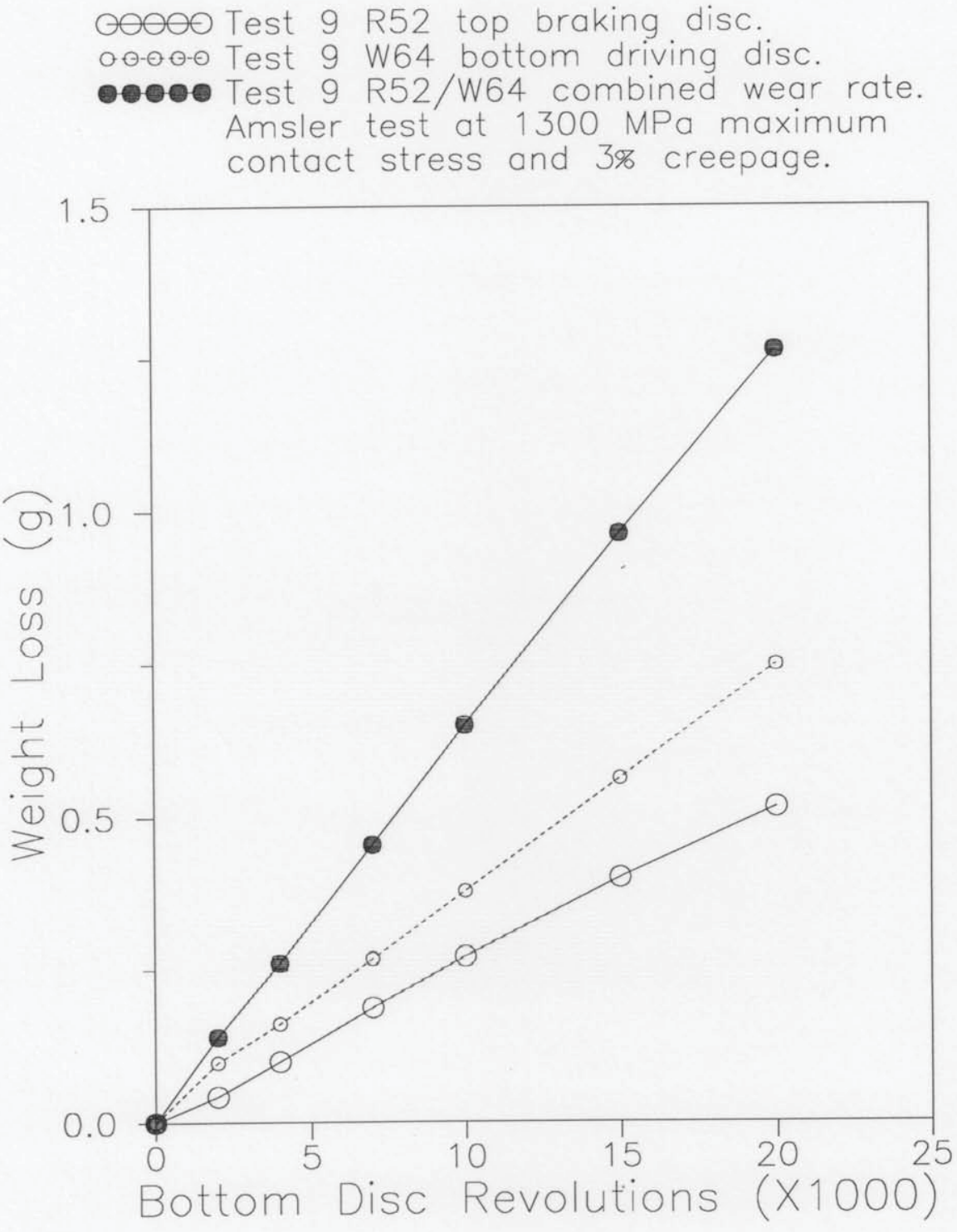

Figure 8.22 Top, bottom and combined disc wear curves for an Amsler test at 1300 MPa p_o, 3% γ.

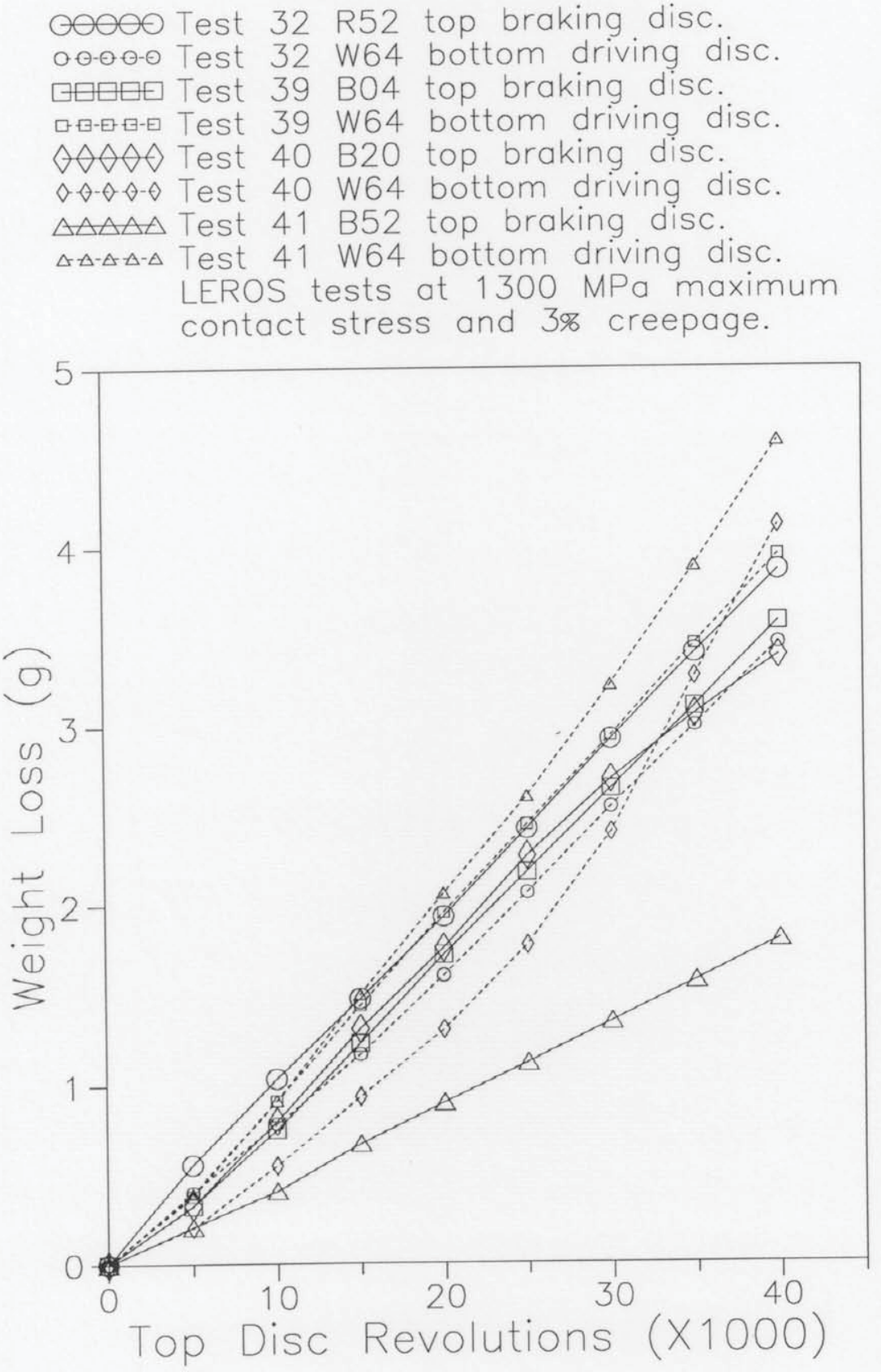

Figure 8.23 Top and bottom disc wear curves for LEROS tests at 1300 MPa p_o, 3% γ.

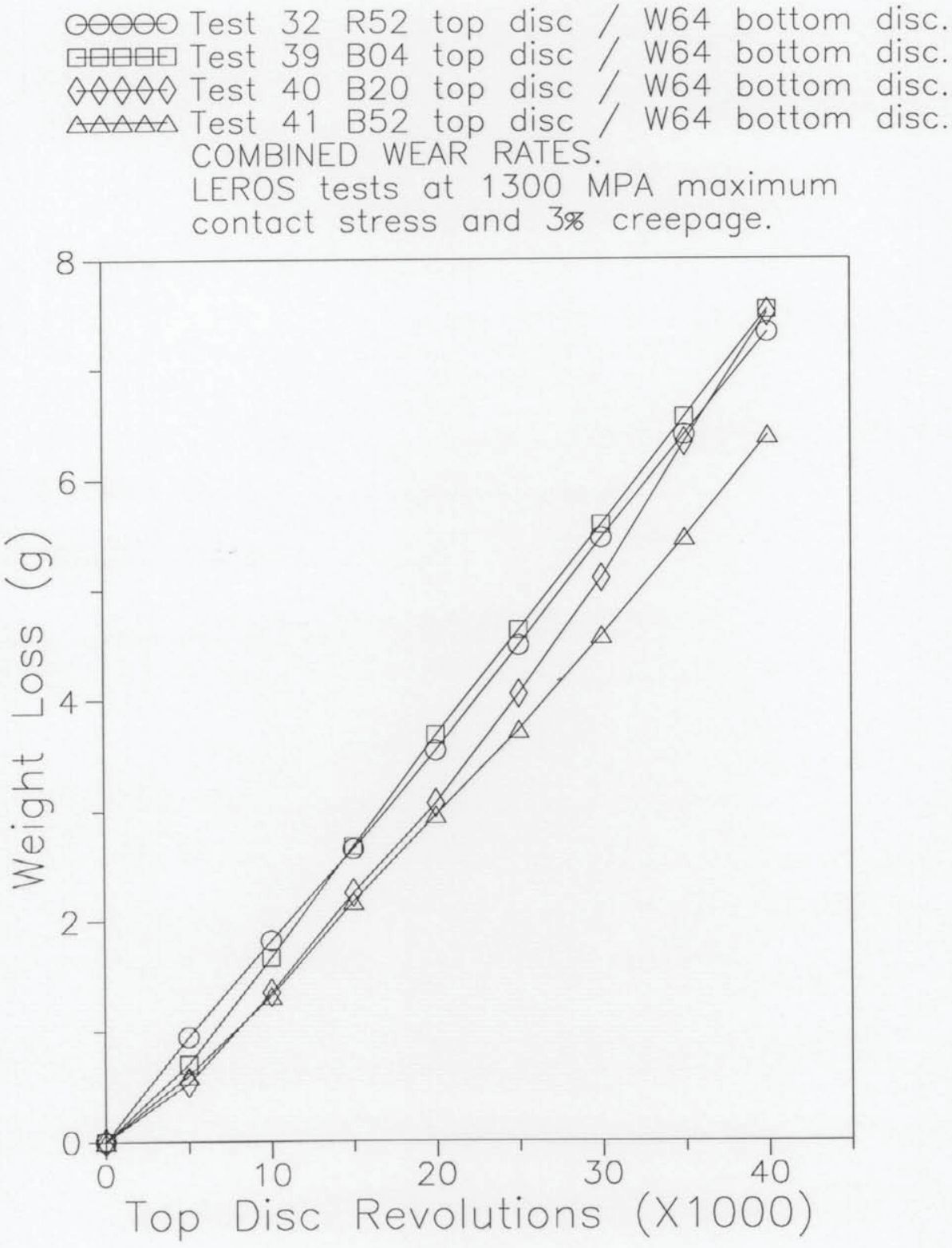

Figure 8.24 Combined top and bottom disc wear curves for LEROS tests at 1300 MPa p_o, 3% γ.

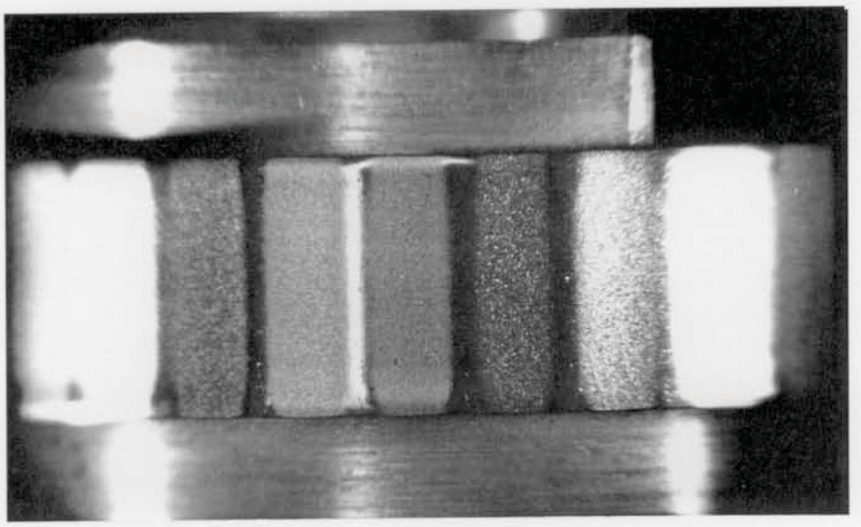

a (x3.4 mag.)

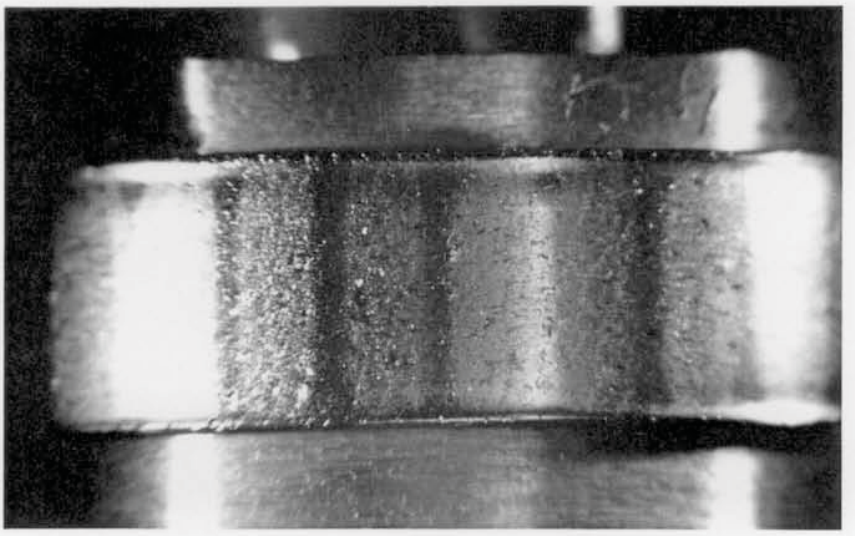

b (x 3.4 mag.)

Figure 8.25 With reference to Figures 8.23 and 8.24, the surface appearance of the Test 40 discs after 25000 top disc revolutions. (a) B20 top disc. (b) W64 bottom disc.

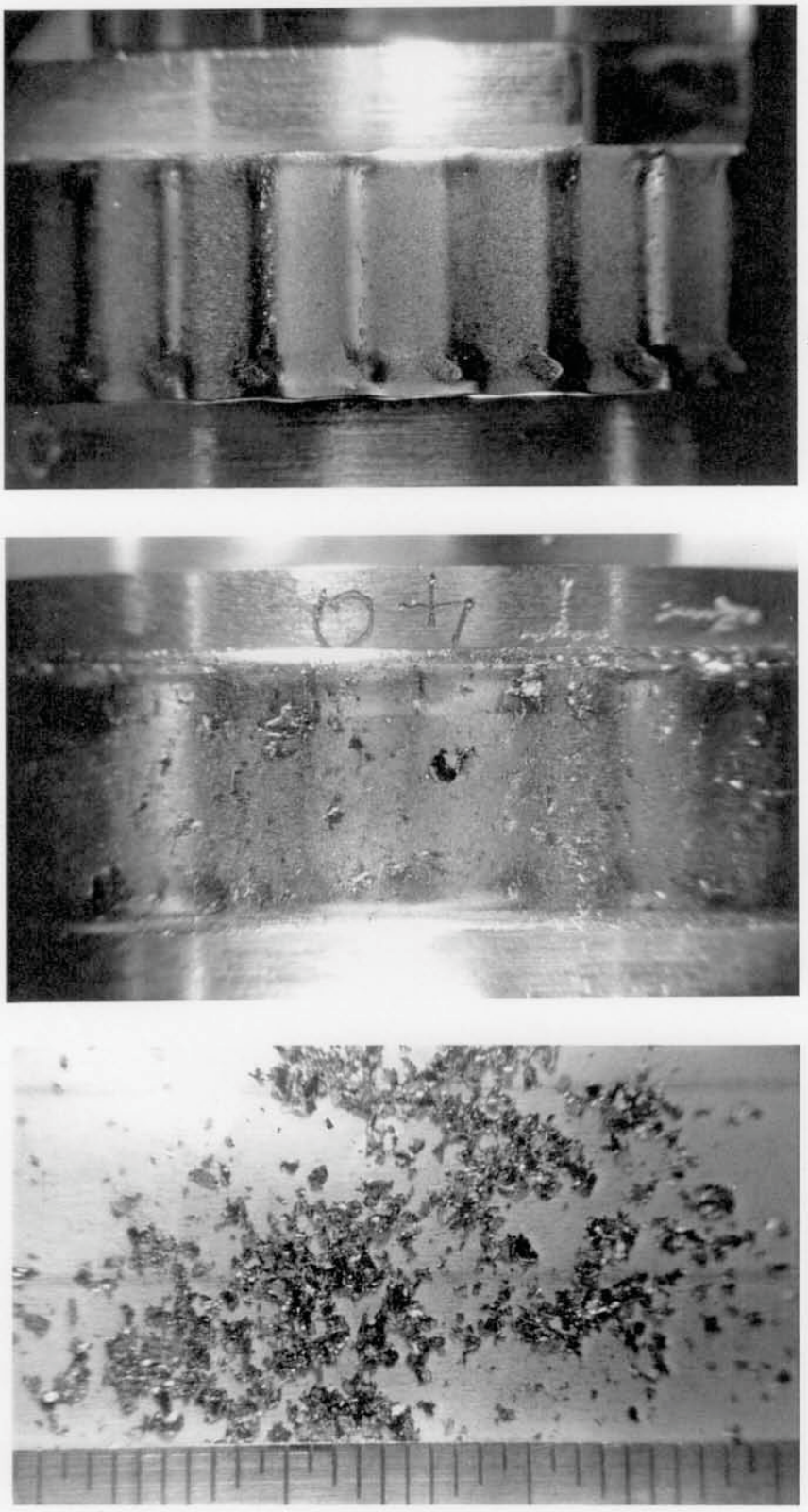

a (x3.5 mag.)

b (x 4.3 mag.)

c (x 3.5 mag.)

Figure 8.26 With reference to Figure 8.25, the changed surface appearance of the Test 40 discs after 40000 top disc revolutions. (a) B20 top disc. (b) W64 bottom disc. (c) 0.4mm grid filtered debris from the last 5000 revolutions.

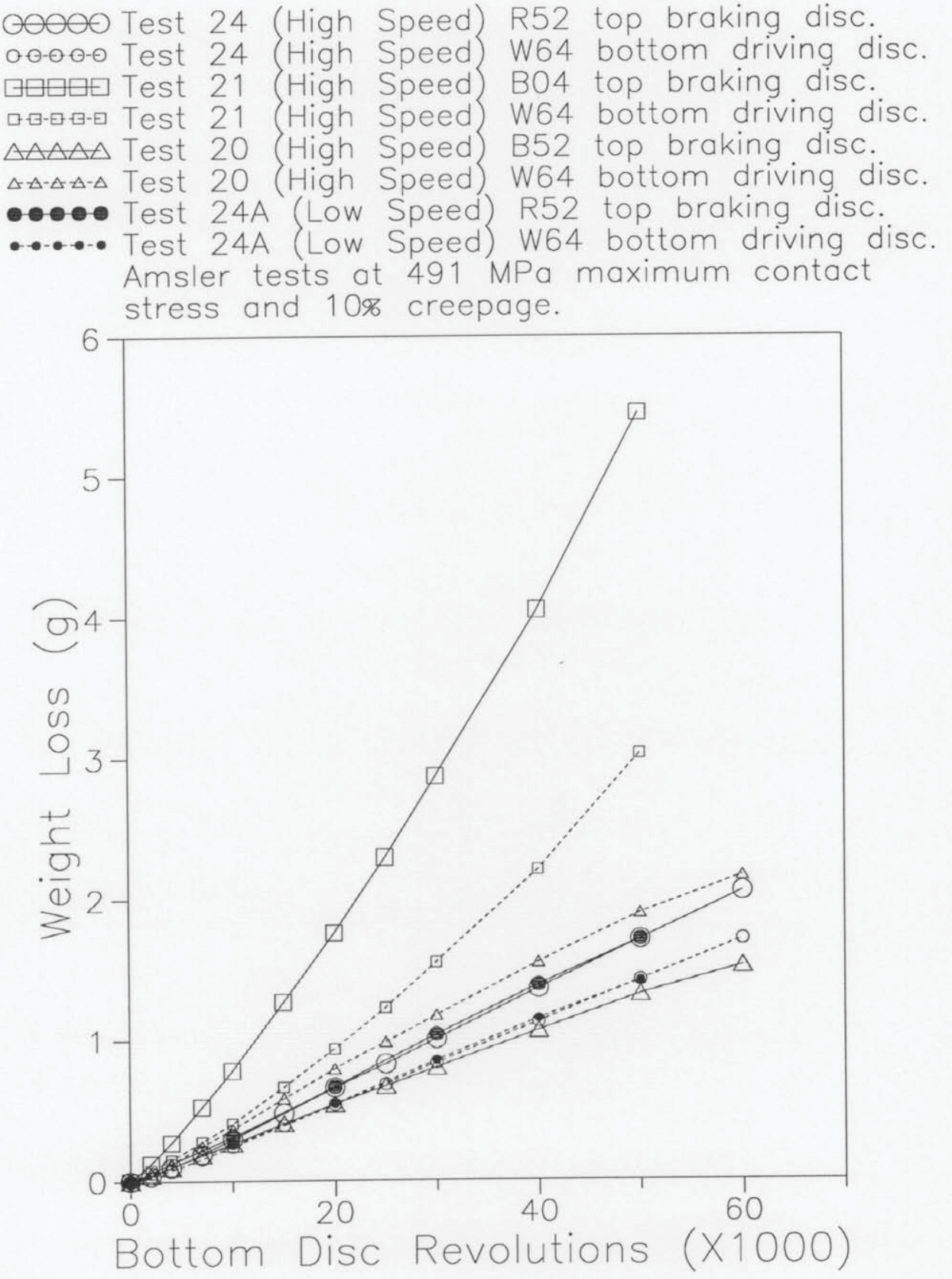

Figure 8.27 Top and bottom disc wear curves for Amsler tests at 491 MPa p_o, 10% γ. Results at two test speeds are shown.

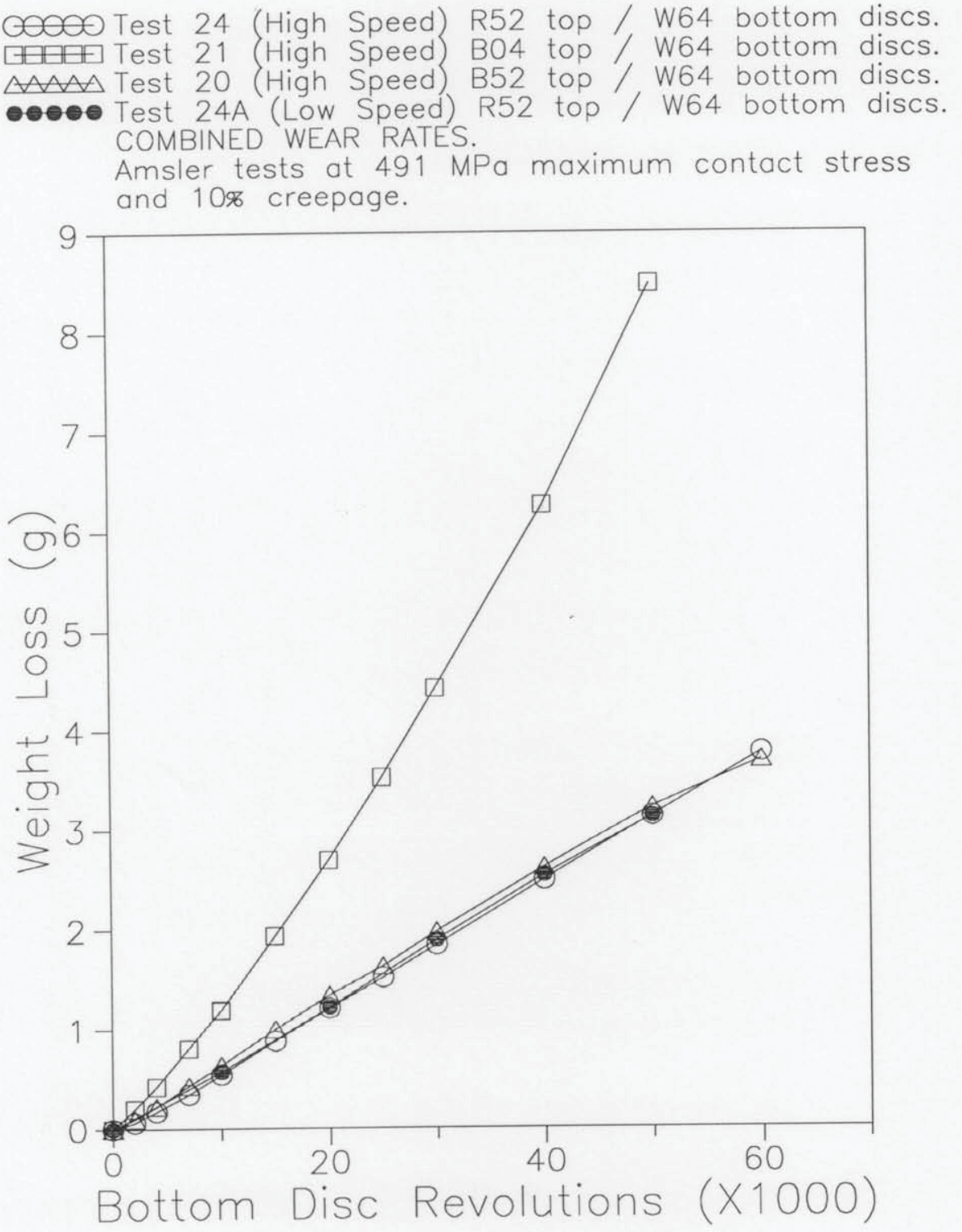

Figure 8.28 Combined top and bottom disc wear curves for Amsler tests at 491 MPa p_o, 10% γ. Results at two test speeds are shown.

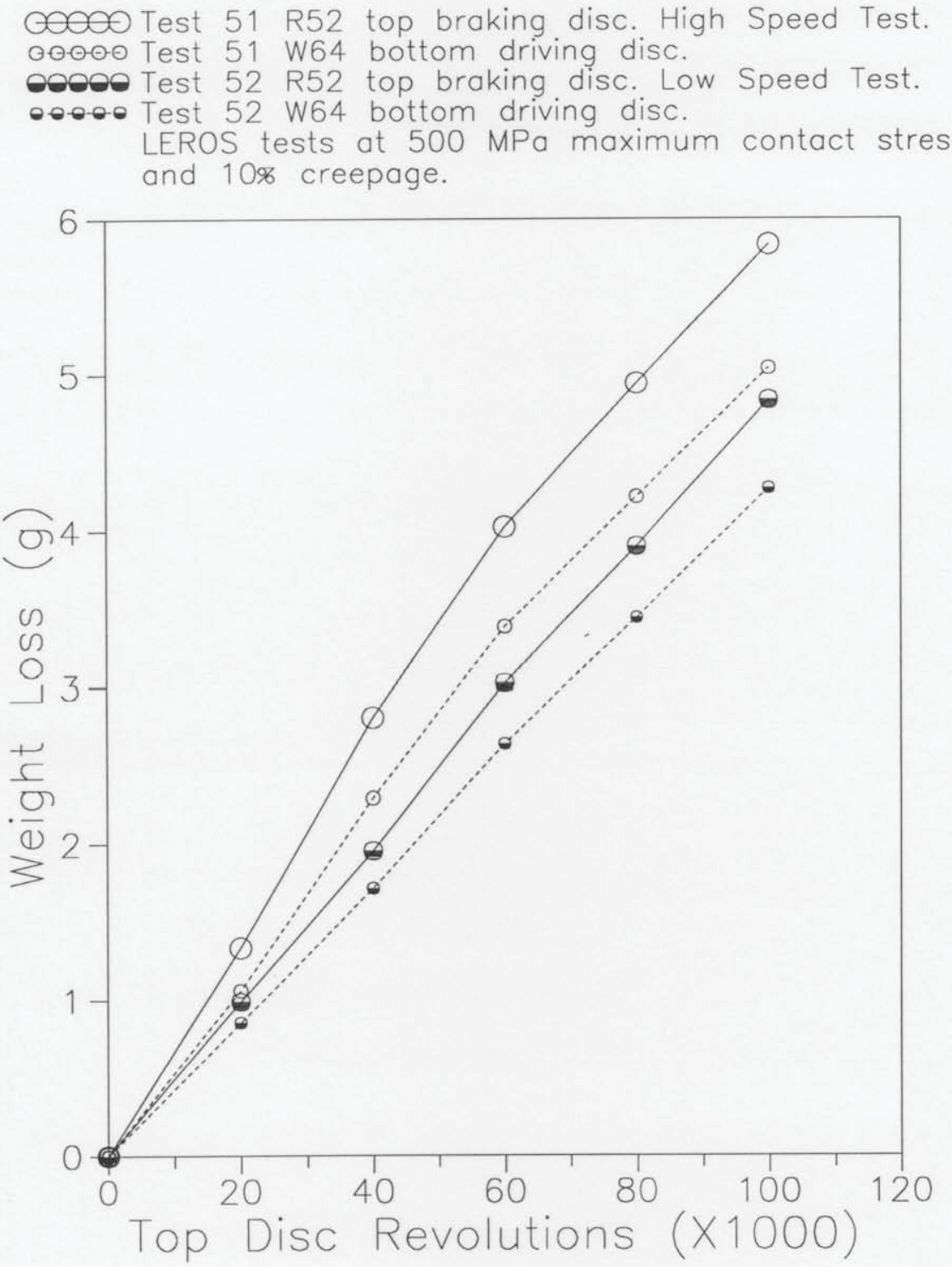

Figure 8.29 Top and bottom disc wear curves for LEROS tests at 500 MPa p_o, 10% γ.

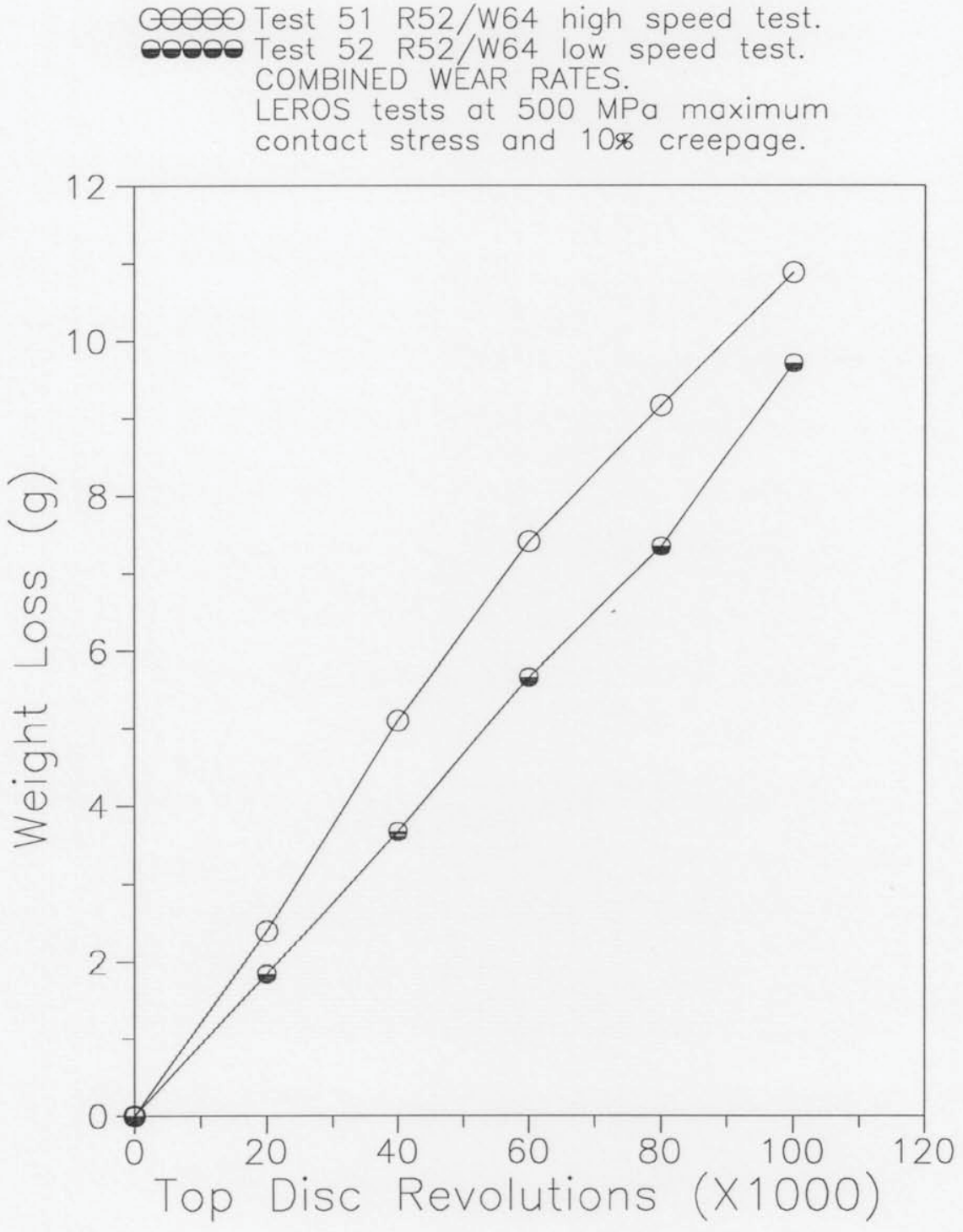

Figure 8.30 Combined top and bottom disc wear curves for LEROS tests at 500 MPa p_o, 10% γ.

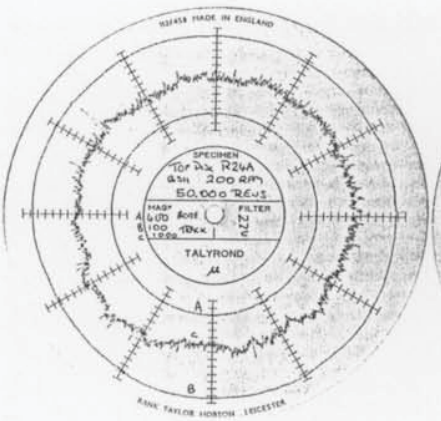

a

c

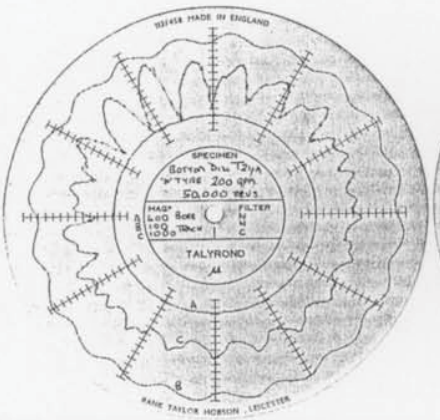

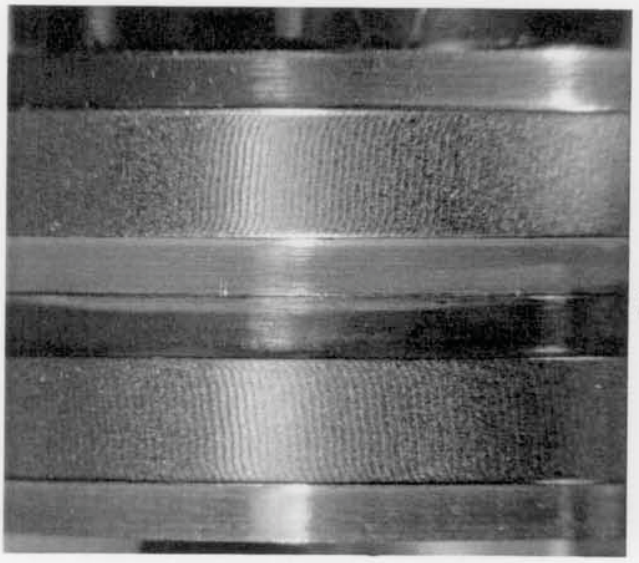

b (x3.5 mag.)

Figure 8.31 Comparative top and bottom, R52/W64, disc Talyrond profiles for Amsler tests at 500 MPa p_o, 10% γ, with (a) low speed test profiles, (b) corrugated surfaces of low speed discs and (c) high speed test profiles. The corrugations can be seen super-imposed on the facet profiles.

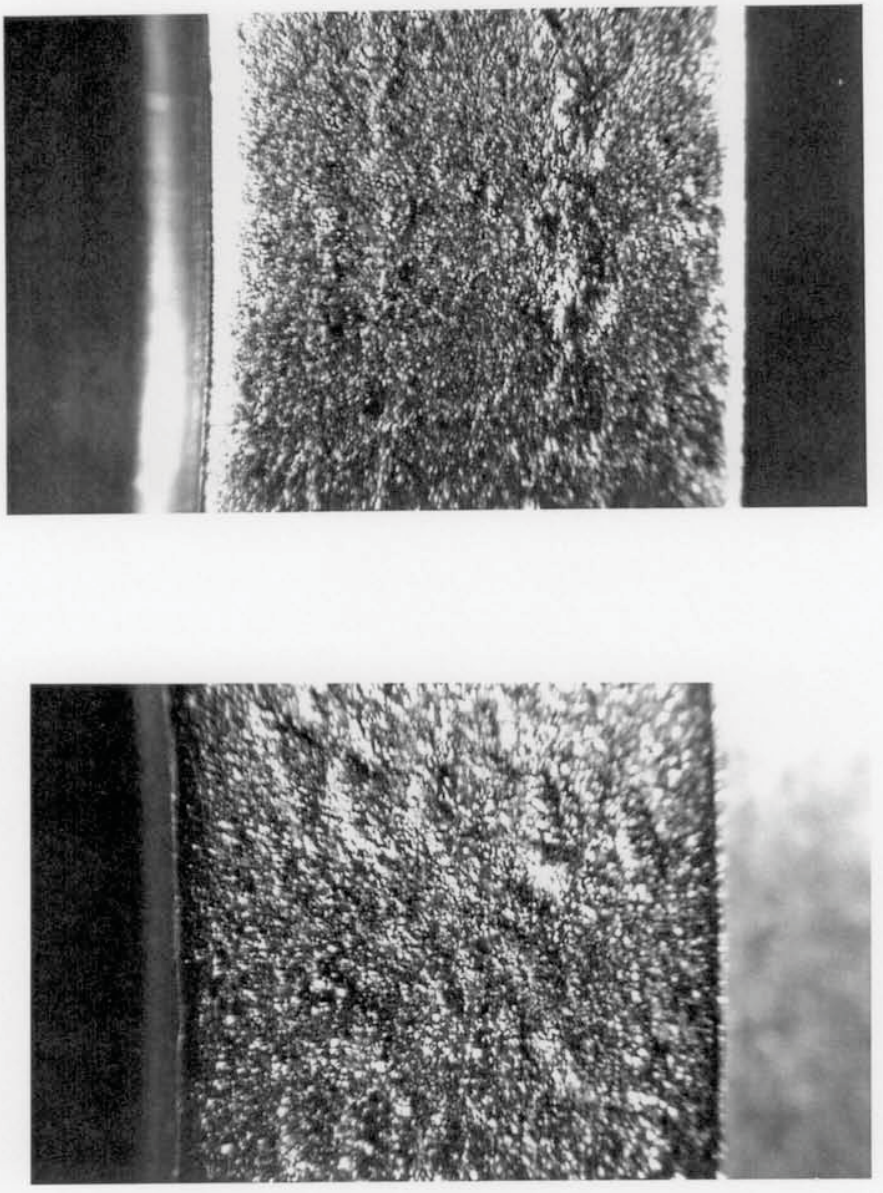

Figure 8.32 Severer wear surface appearance of top and bottom, B04/W64 discs tested at 500 MPa p_o, 10% γ.

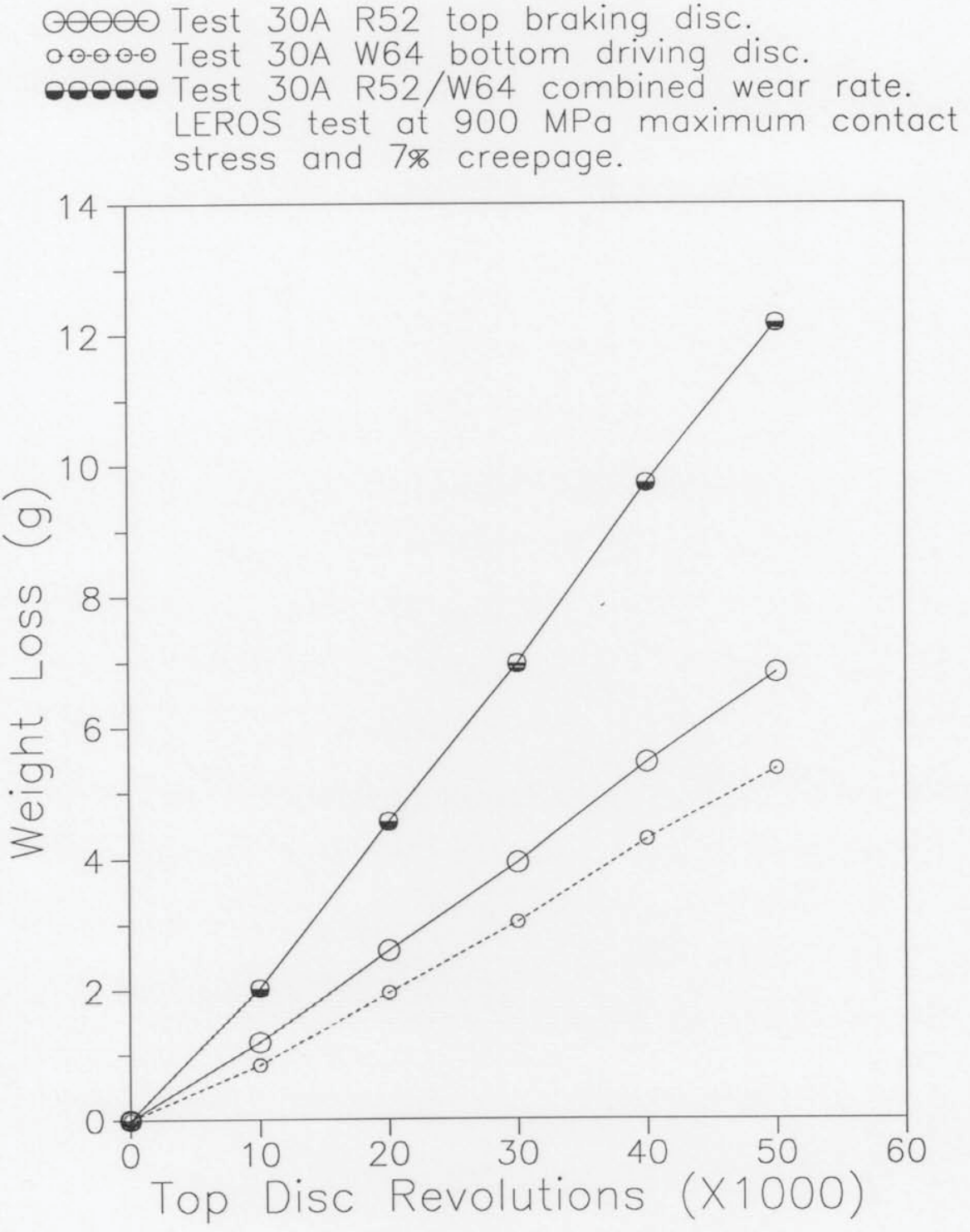

Figure 8.33 Top, bottom and combined wear curves for R52/W64 discs tested on LEROS at 900 MPa p_o, 7% γ.

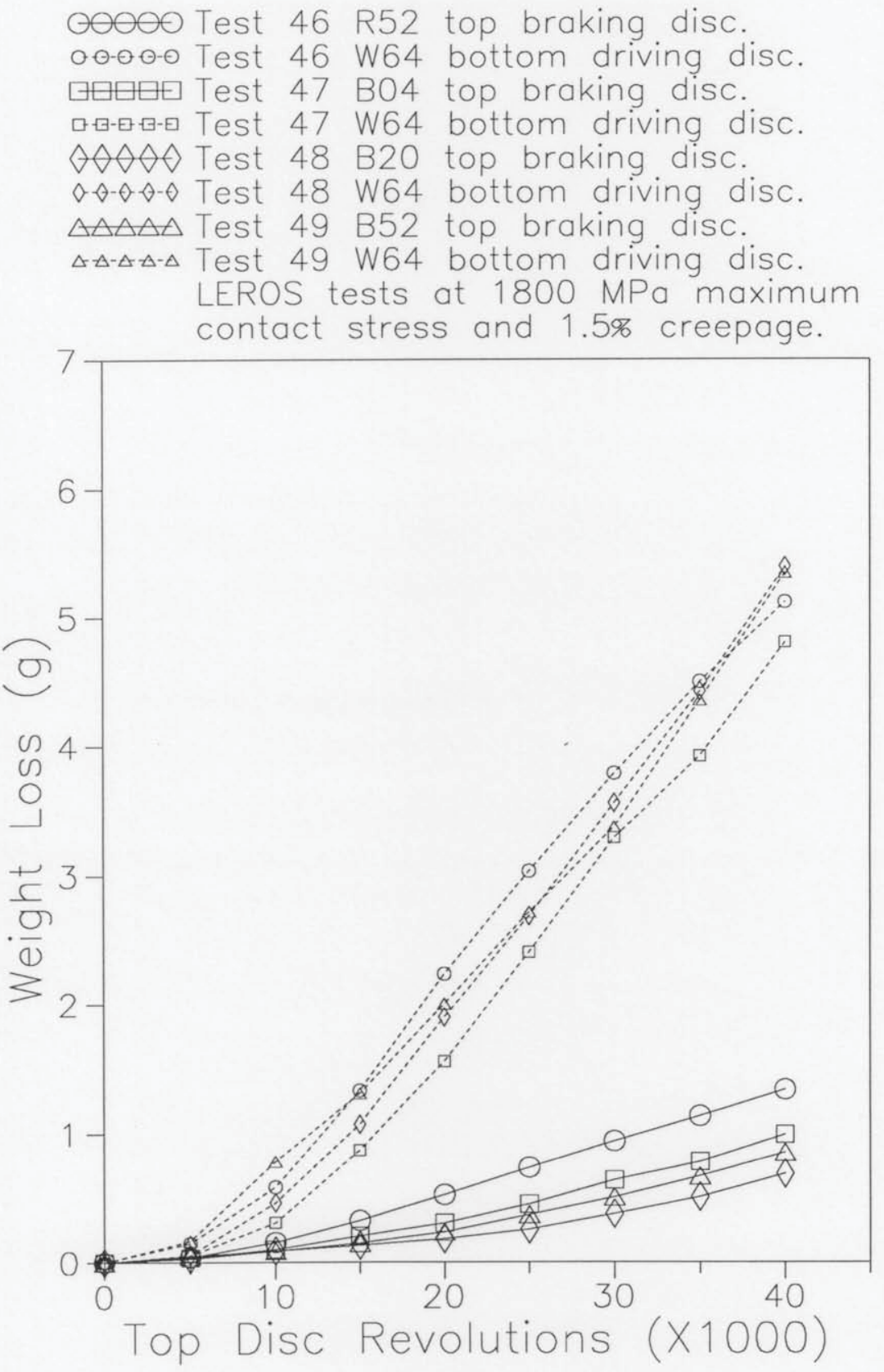

Figure 8.34 Diverging top and bottom disc wear curves for LEROS tests at 1800 MPa p_o, 1.5% γ.

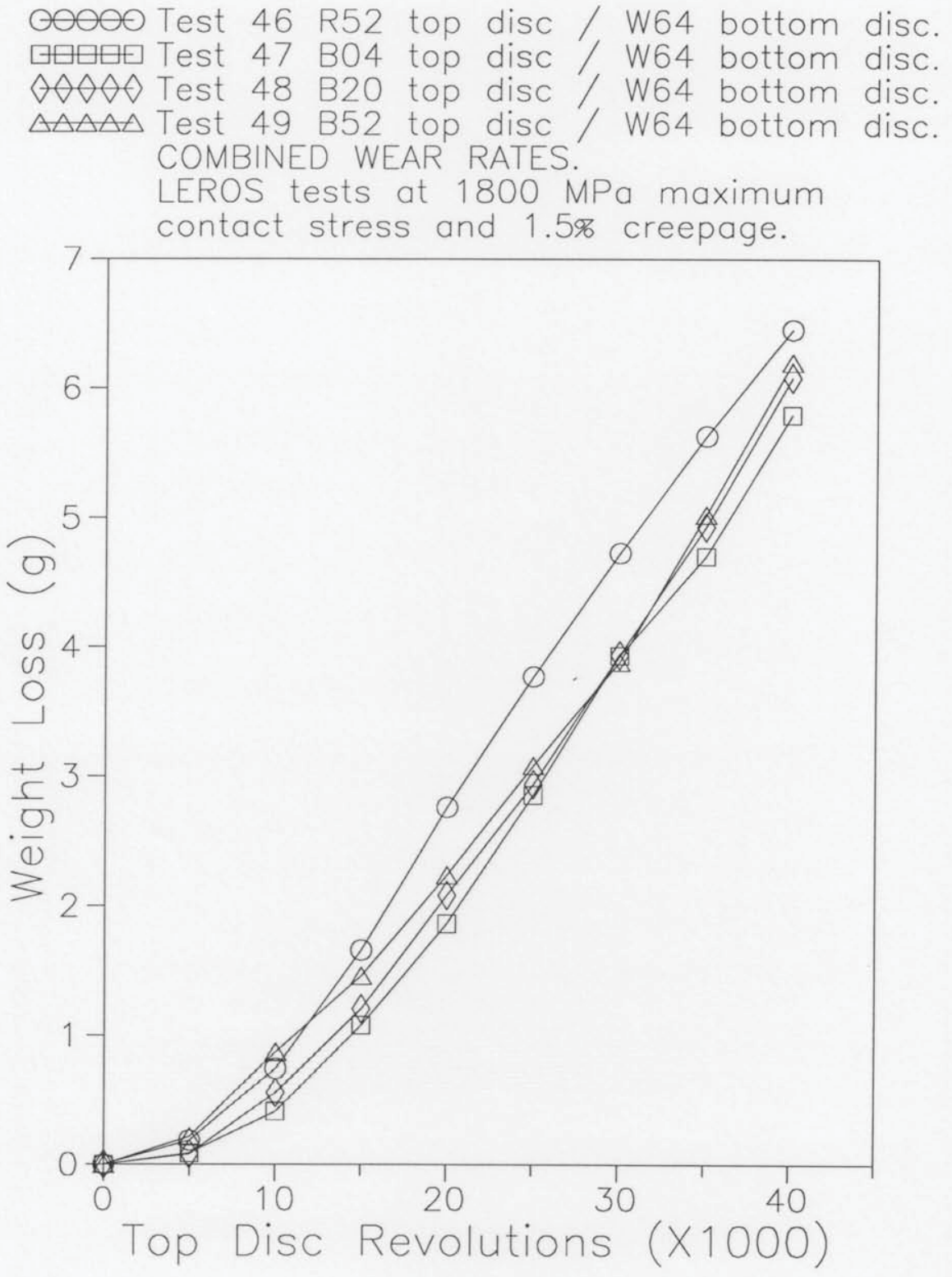

Figure 8.35 Combined top and bottom disc wear curves for LEROS tests at 1800 MPa p_o, 1.5% γ.

a (x8 mag.)

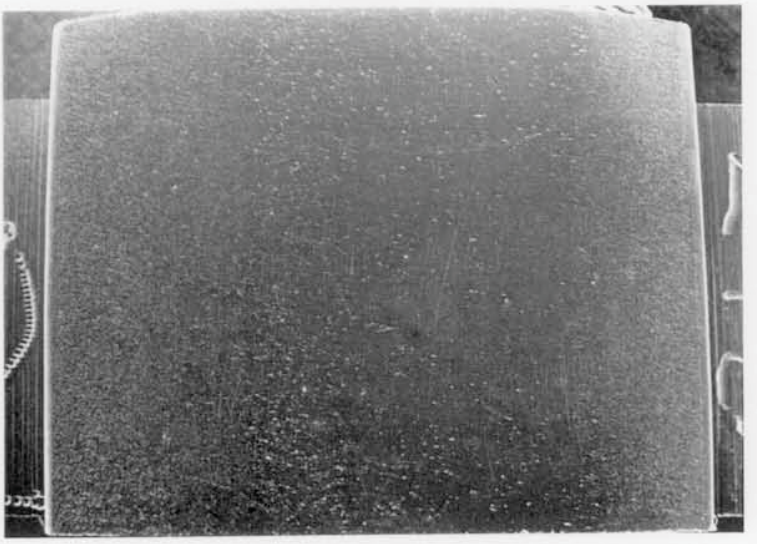

b (x1800 mag.)

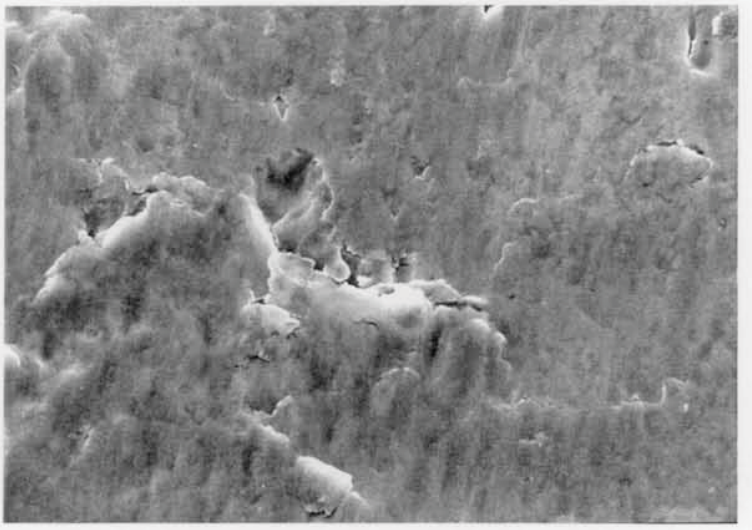

Figure 8.36 SEM photographs showing the surface appearance of the B04 top disc tested on LEROS at 1800 MPa p_o, 1.5% γ. Although the surface is smooth debris analysis indicated that flakes were generated and sheared within a cycle.

a (x8 mag.)

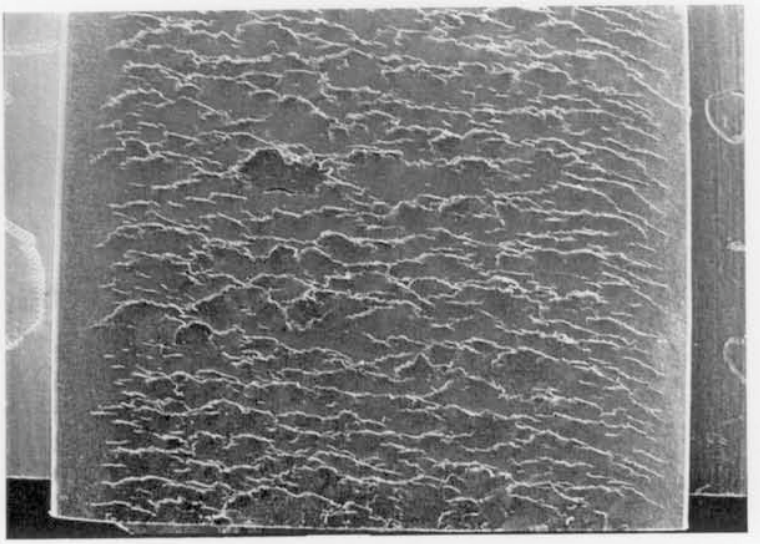

b (x8 mag.)

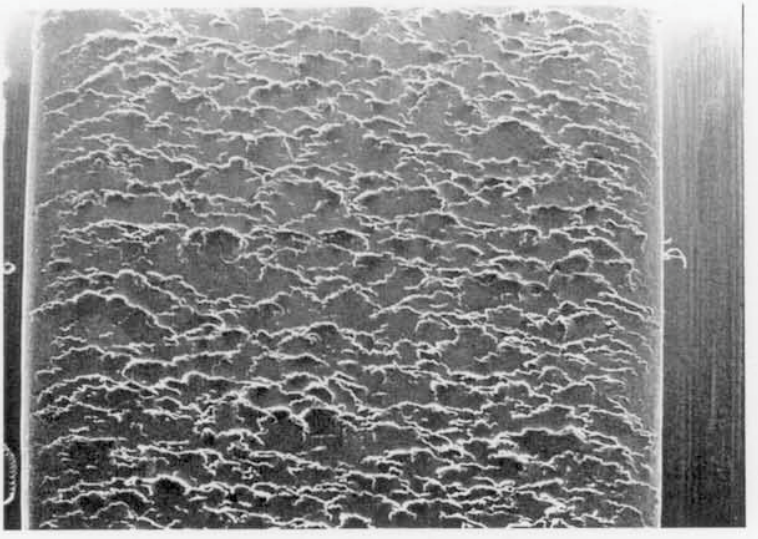

Figure 8.37 SEM photographs showing the surface appearance of the (a) B20 and (b) B52 top discs tested on LEROS at 1800 MPa p_o, 1.5% γ. This flaked surface was also typical of the R52 disc.

a (x11 mag.)

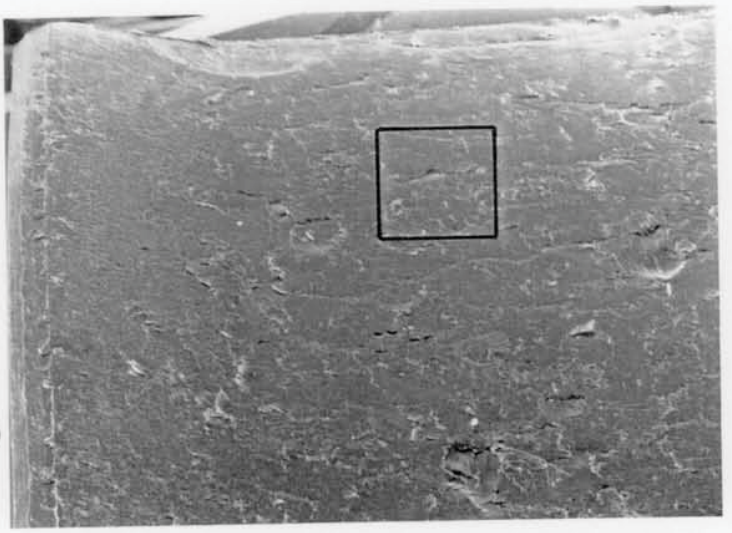

b (x65 mag.)

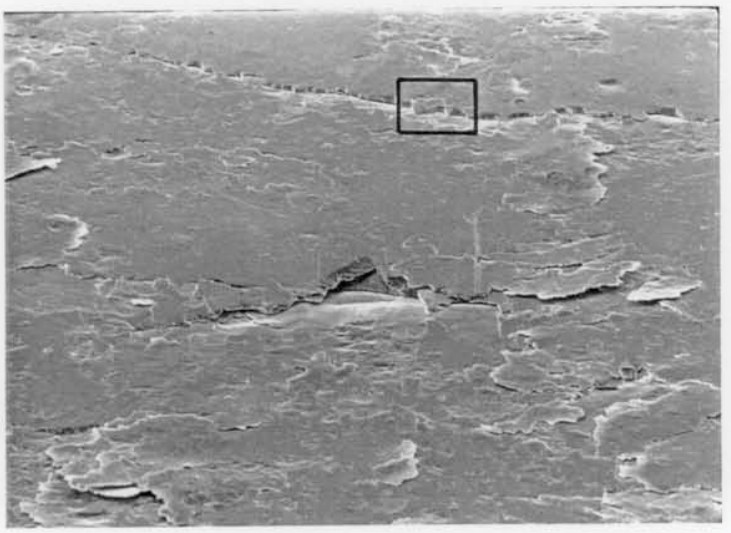

c (x860 mag.)

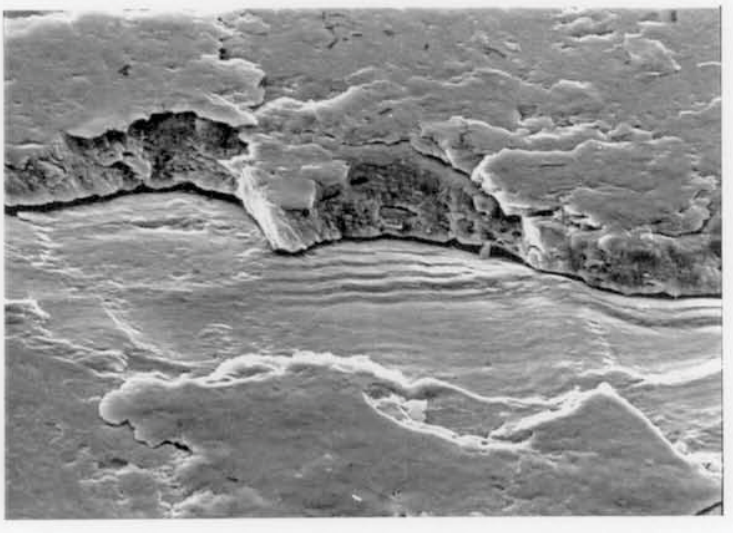

Figure 8.38 SEM photographs showing the surface appearance of the W64 disc, tested on LEROS against B04 at 1800 MPa p_o, 1.5% γ. (a) An overview of most of the track width, showing the track erosion within the original track width and not at the deformed edges. (b and c) Zooming in to show evidence of low cycle fatigue fracture of thick flakes.

a (x8 mag.)

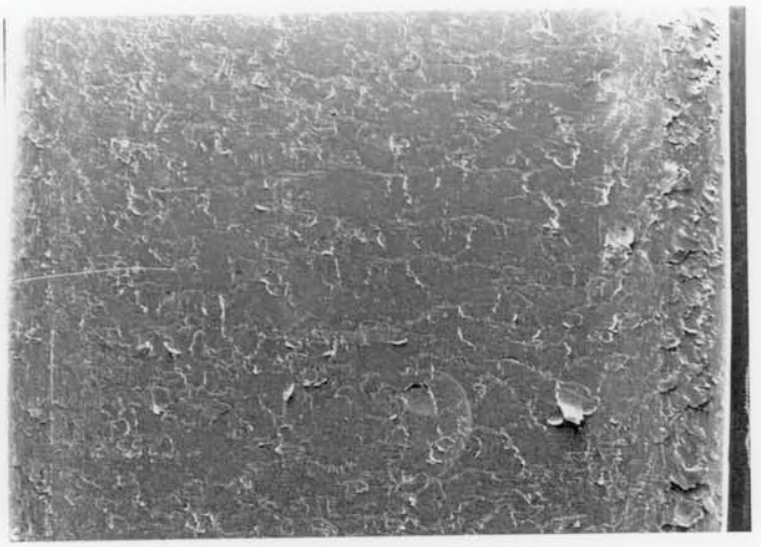

b (x90 mag.)

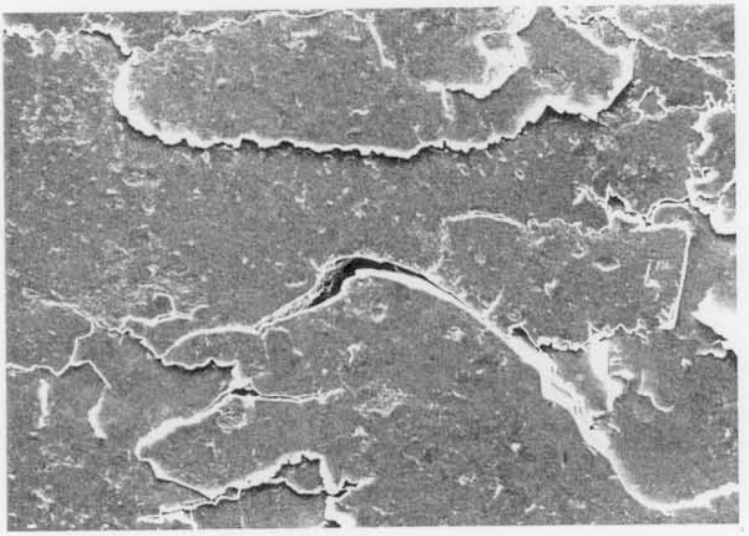

c (x450 mag.)

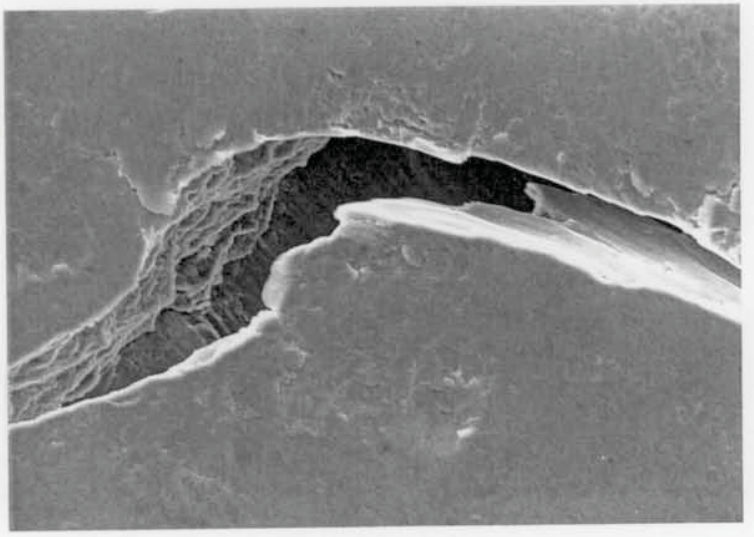

Figure 8.39 SEM photographs showing the surface appearance of the W64 disc, tested on LEROS against B20 at 1800 MPa p_o, 1.5% γ. (a) Eroded and flaking track centre. (b and c) Zooming in to show evidence of low cycle fatigue fracture and the shear plane below.

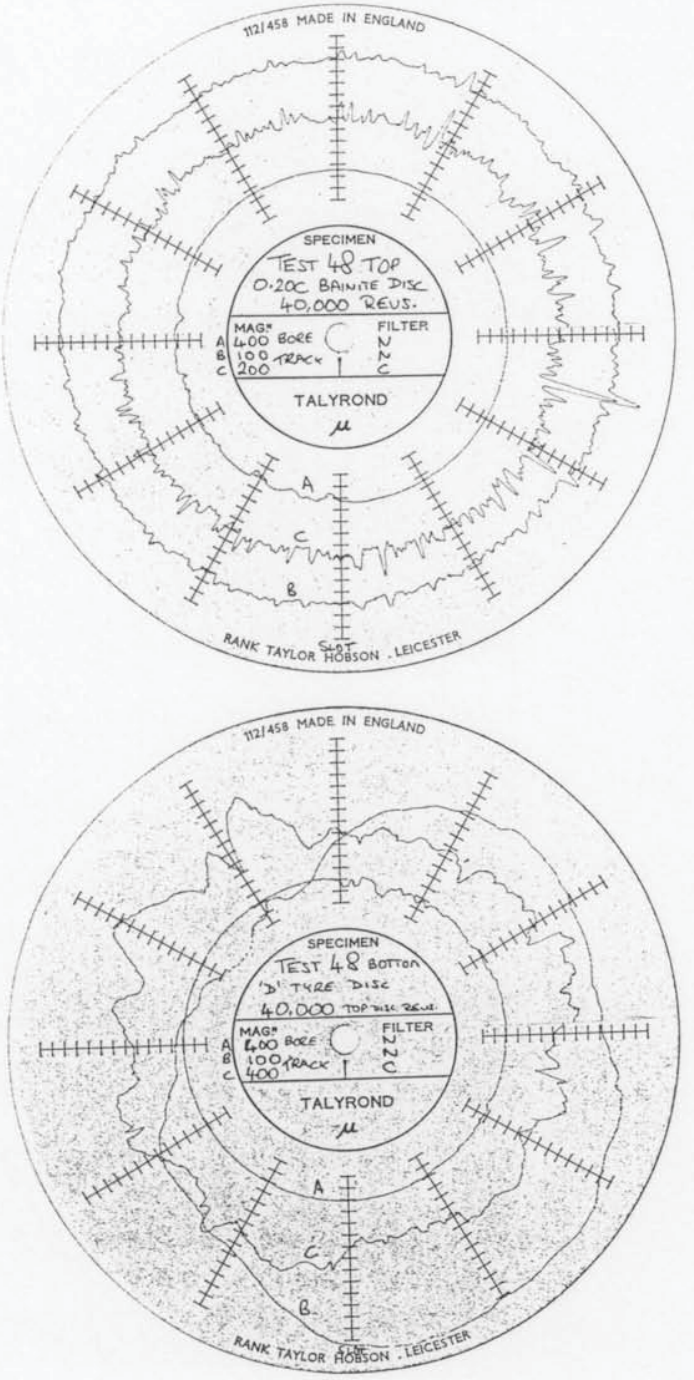

Figure 8.40 Test end Talyrond profiles of (top) B20 and (bottom) W64 disks tested on LEROS at 1800 MPa p_o, 1.5% γ.

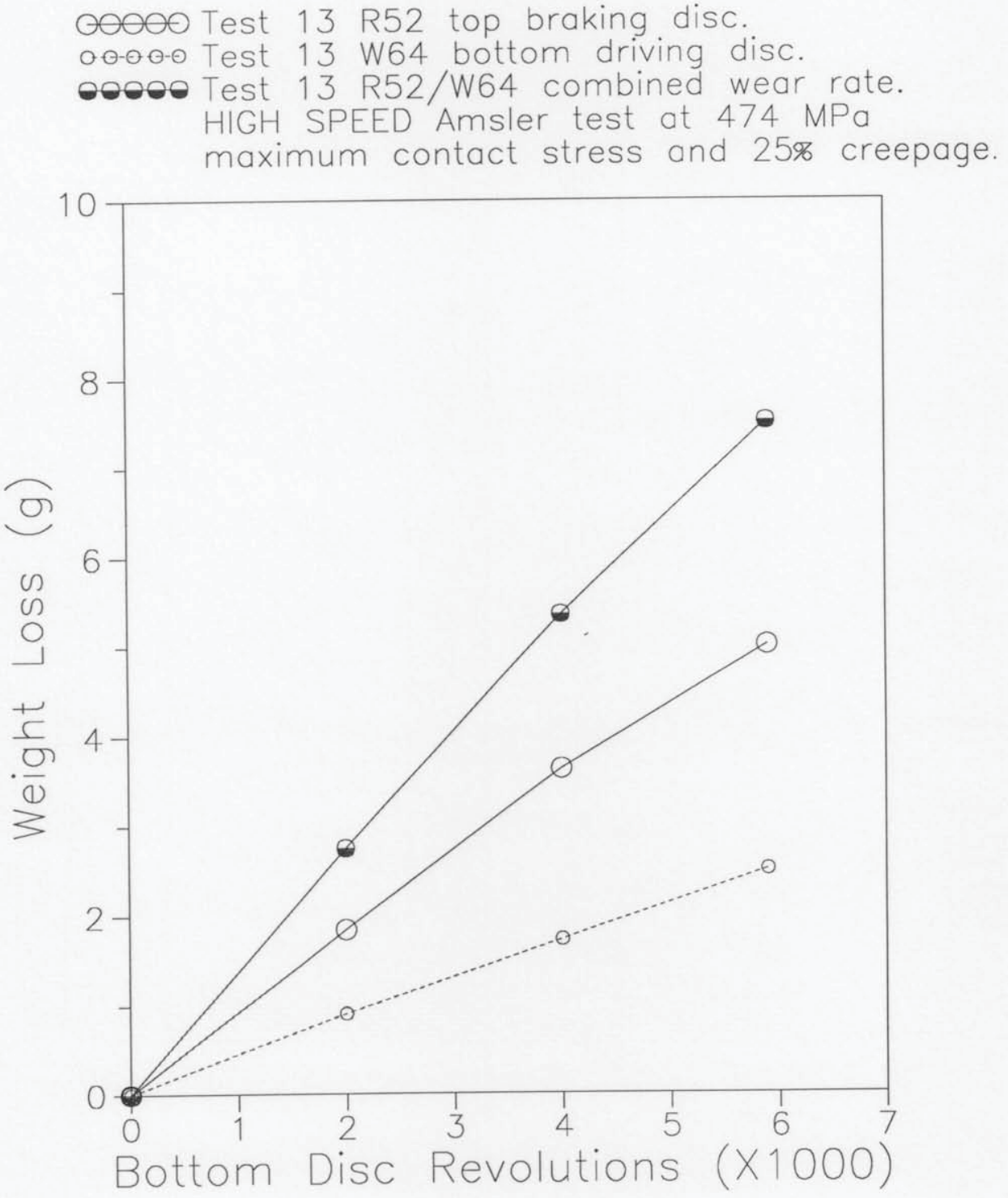

Figure 8.41 Top, bottom and combined R52/W64 disc wear curves for Amsler tests at 474 MPa p_o, 25% γ.

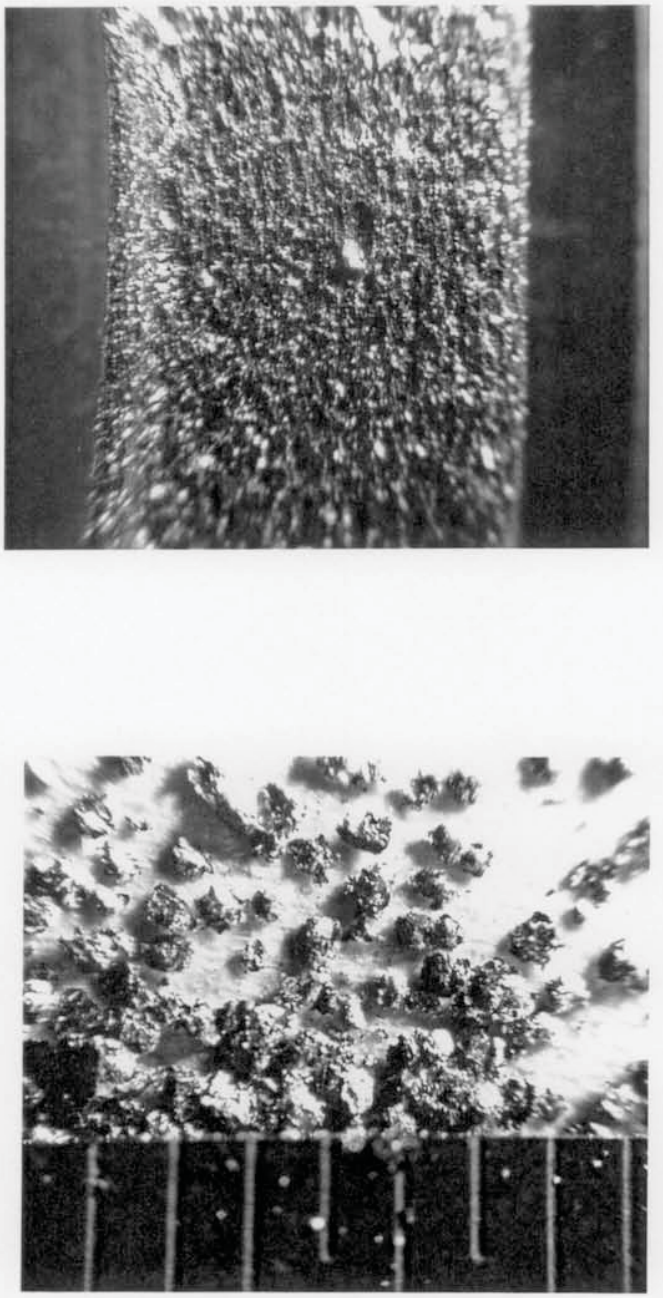

Figure 8.42 Severely worn R52 Amsler disc surface, with "scooped" depressions and the "scooped" coarse wear debris, after testing at 474 MPa p_o, 25% γ (cf. Figure 8.41).

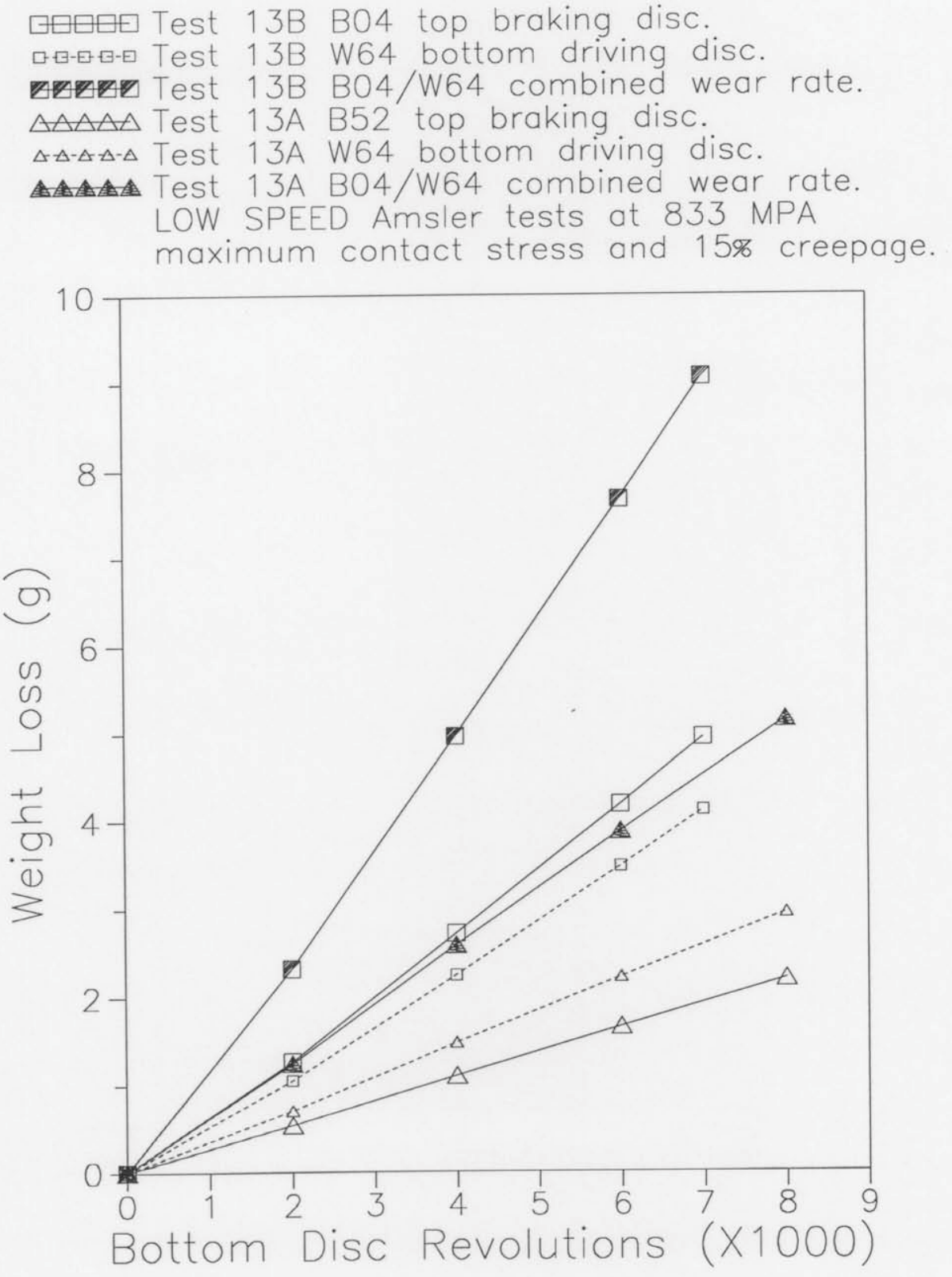

Figure 8.43 Top, bottom and combined disc wear curves for slow speed Amsler tests at 833 MPa p_o, 15% γ.

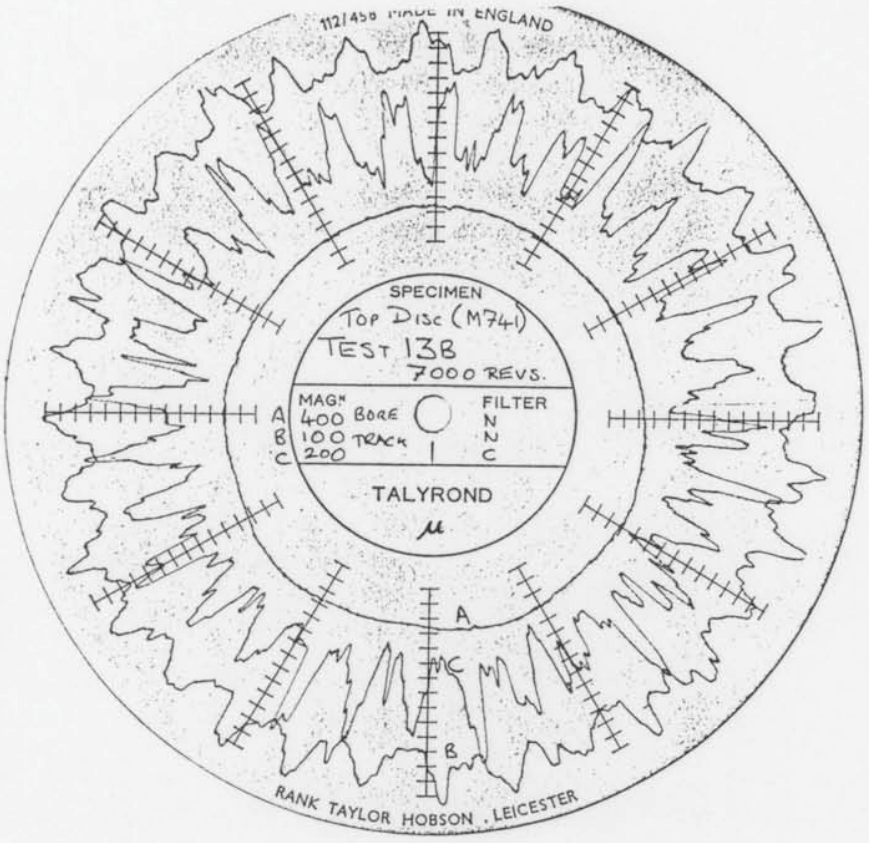

Figure 8.44 Test end Talyrond profile of the B04 Amsler disc tested at 833 MPa p_o, 15% γ, showing periodicy of rippled surface.

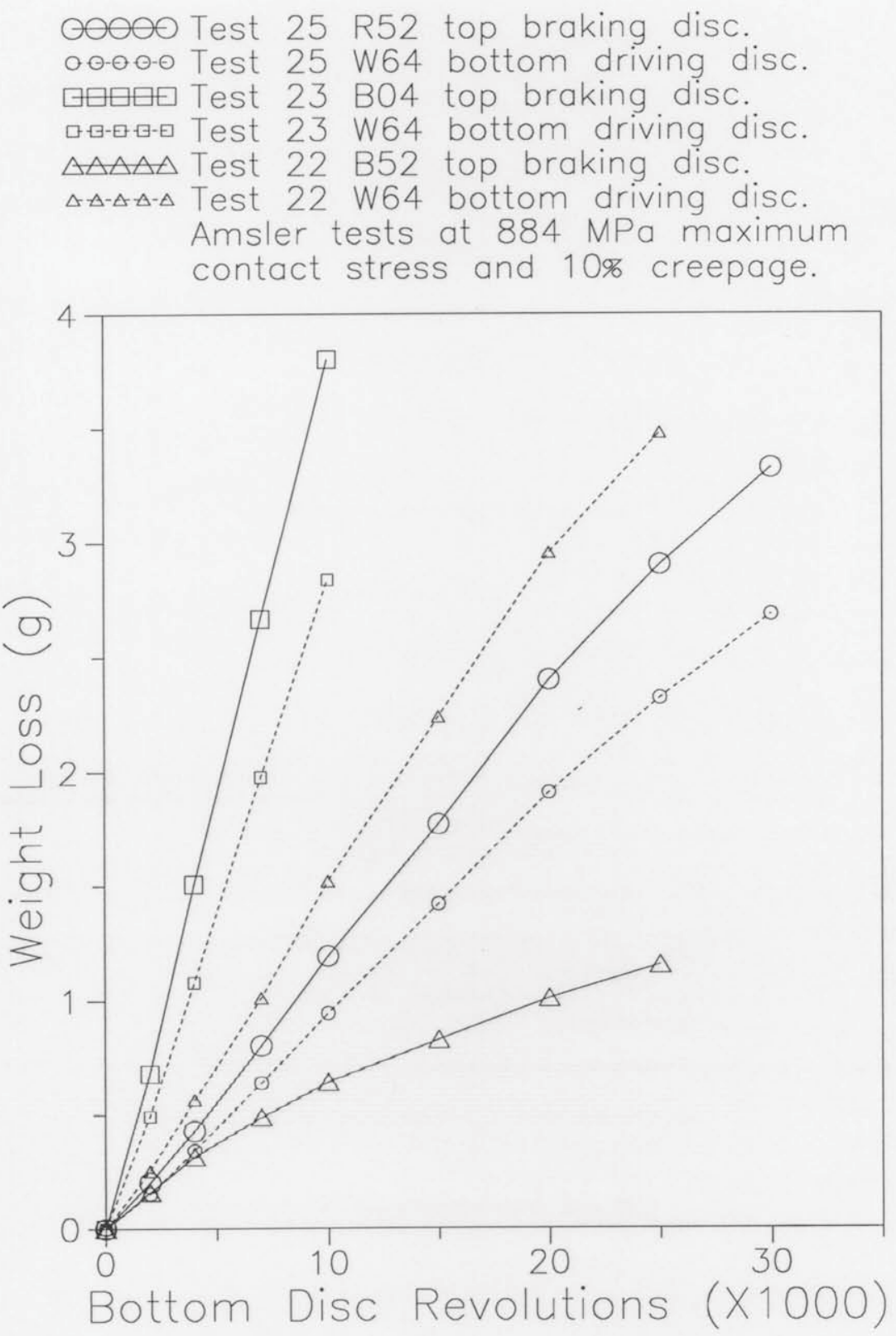

Figure 8.45 Top and bottom disc wear curves for Amsler tests at 884 MPa p_o, 10% γ.

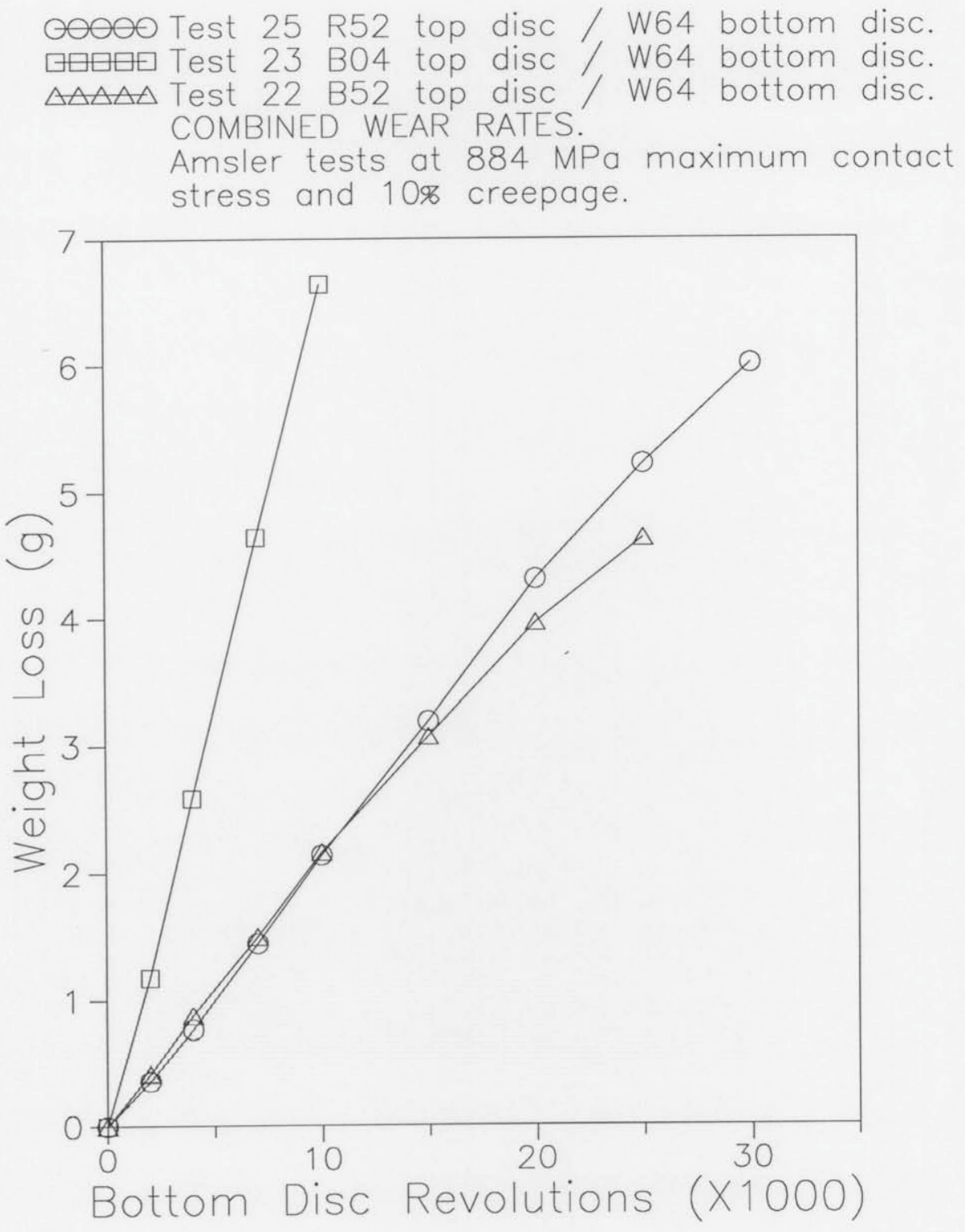

Figure 8.46 Combined top and bottom disc wear curves for Amsler tests at 884 MPa p_o, 10% γ.

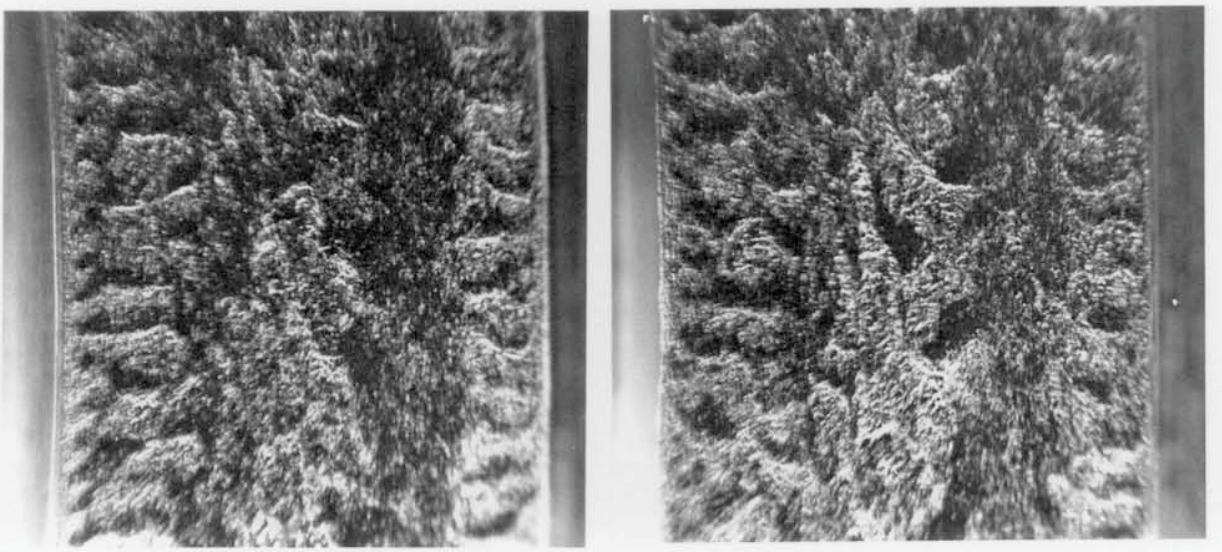

a (x13 mag.)

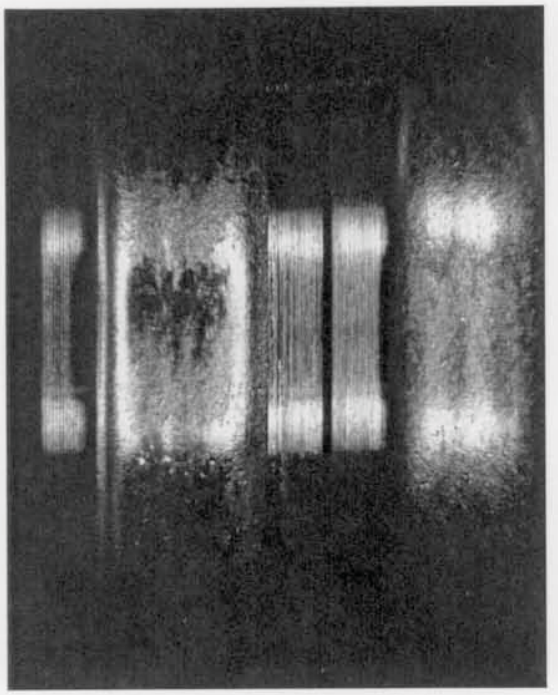

b (x4.2 mag.)

Figure 8.47 Changing surface appearance of R52/W64 discs tested on the Amsler at 884 MPa p_o, 10% γ (top disc to the left). (a) After 4000 revolutions. (b) After 30000 revolutions.

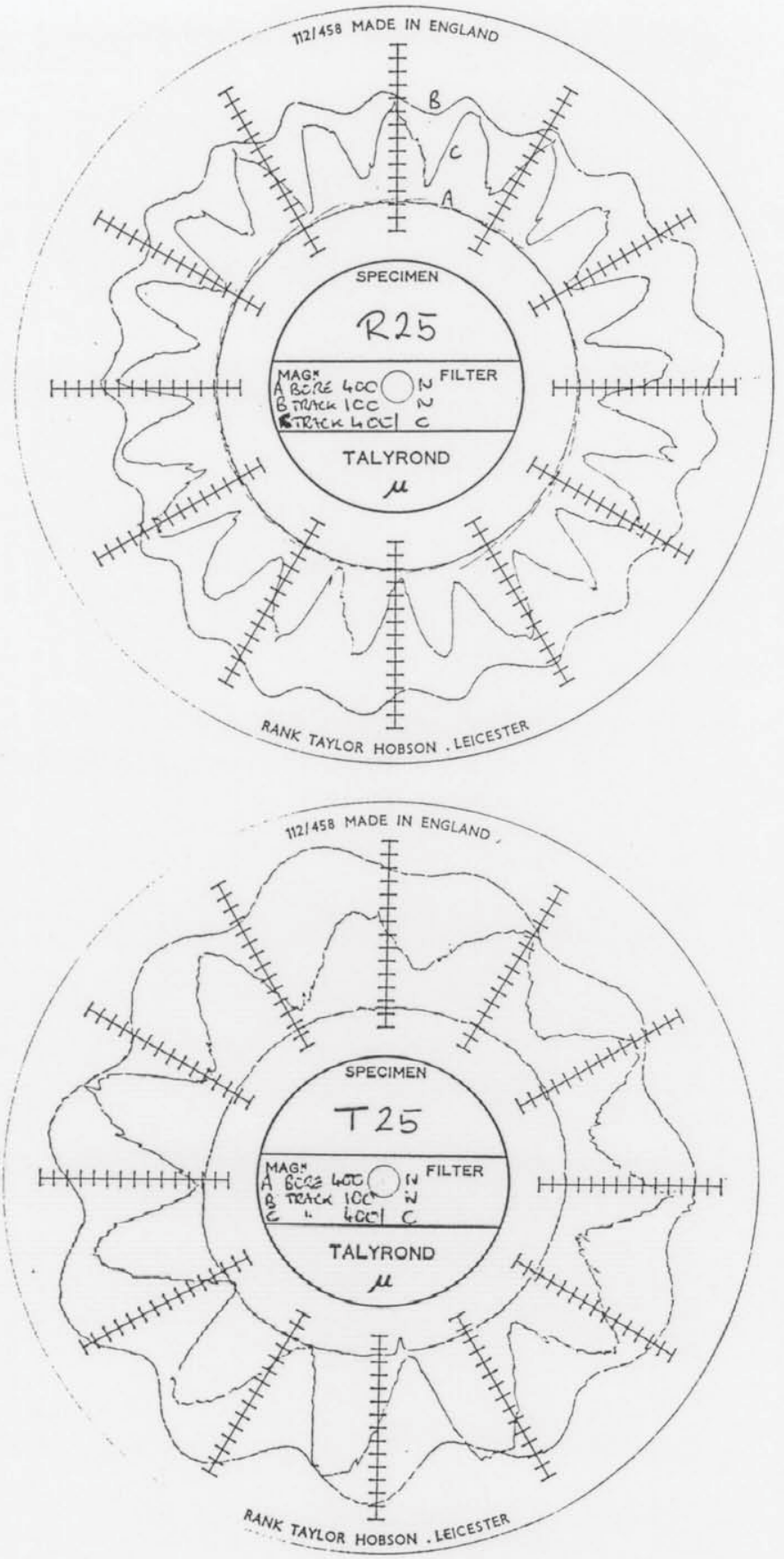

Figure 8.48 Talyrond profiles of the R52/W64 discs shown in Figure 8.47b. The distinct bottom disc facets were not visually apparent.

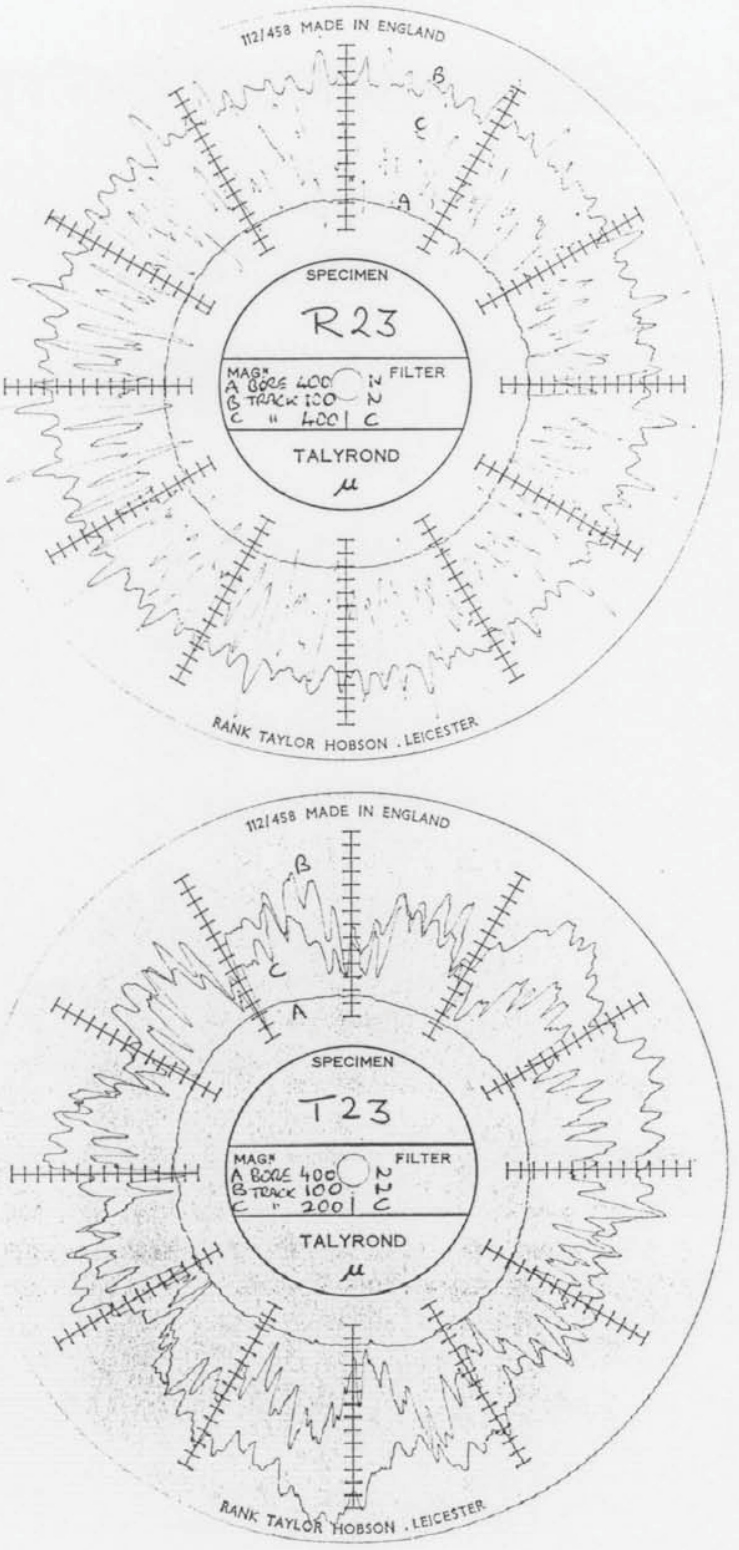

Figure 8.49 Talyrond profiles of B04/W64 discs tested for 10000 revolutions on the Amsler at 884 MPa p_o, 10% γ. Rippling on both discs is reflected in the profiles; on the bottom disc this is superimposed on a facet pattern.

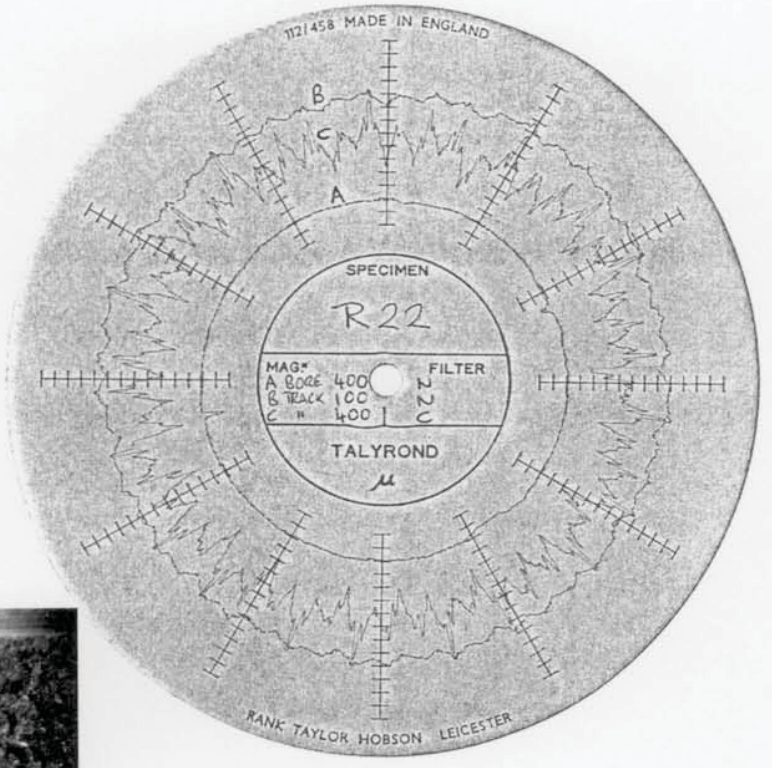

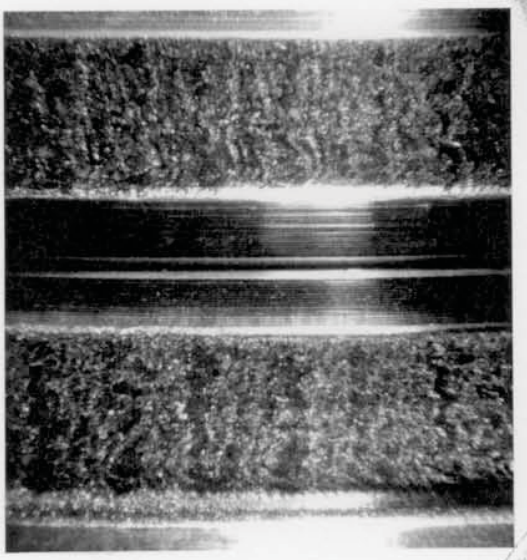

(x4.2 mag.)

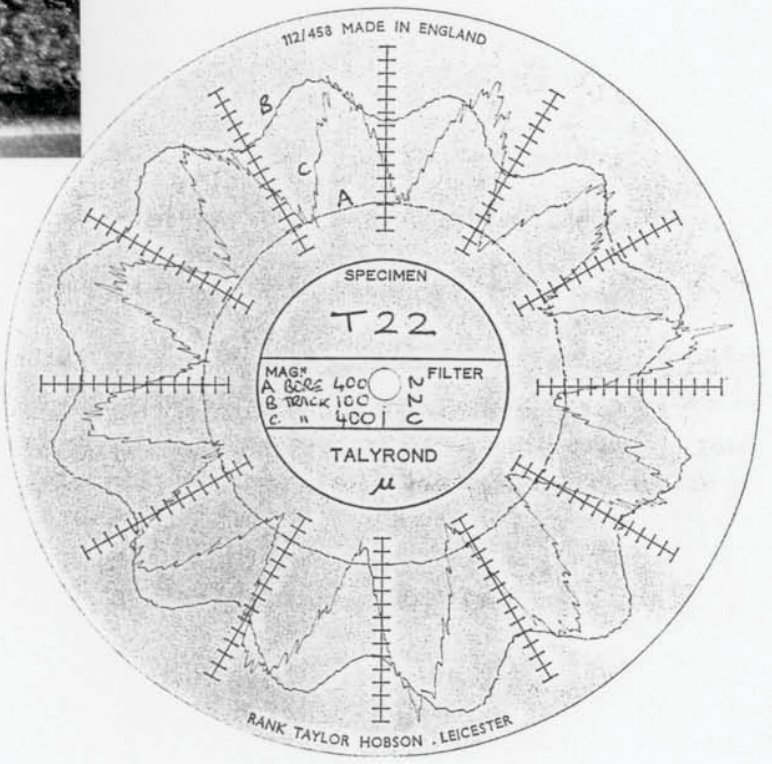

Figure 8.50 Talyrond profiles and surface appearance of B52/W64 discs tested for 25000 revolutions on the Amsler at 884 MPa p_o, 10% γ. On both (B52 top disc, upper photograph and profile; W64, bottom), periodic undulations have formed that were not clearly visually apparent.

a (x440 mag.)

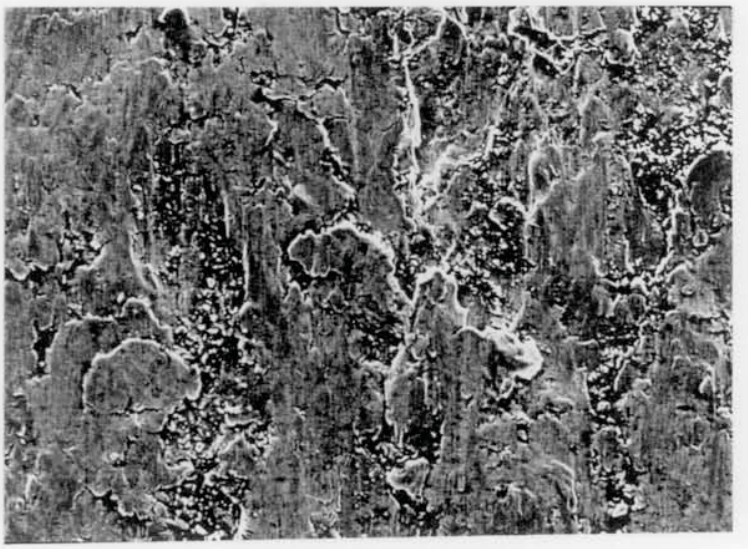

b (x440 mag.)

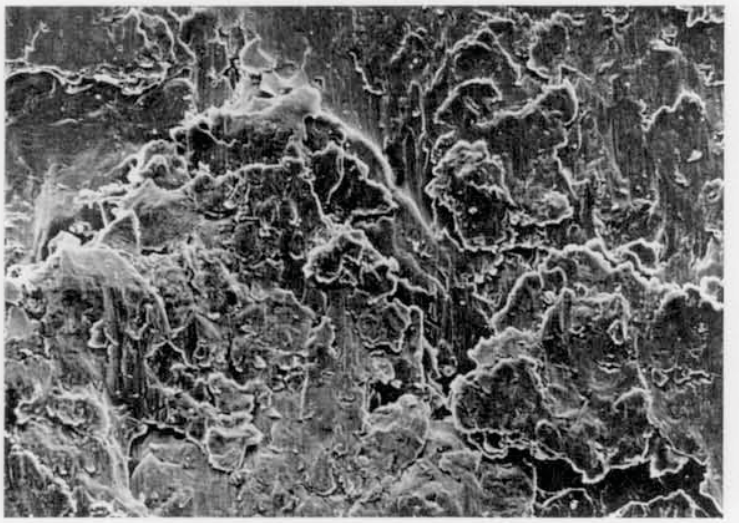

c (x440 mag.)

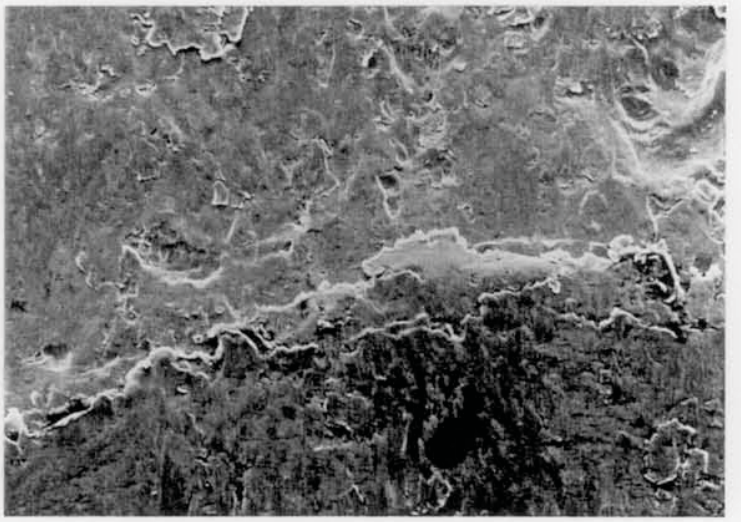

Figure 8.51 SEM photographs of the surface condition of top driven Amsler discs tested at 884 MPa p_o, 10% γ. (a) R52 disc. (b) B04 disc. (c) B52 disc.

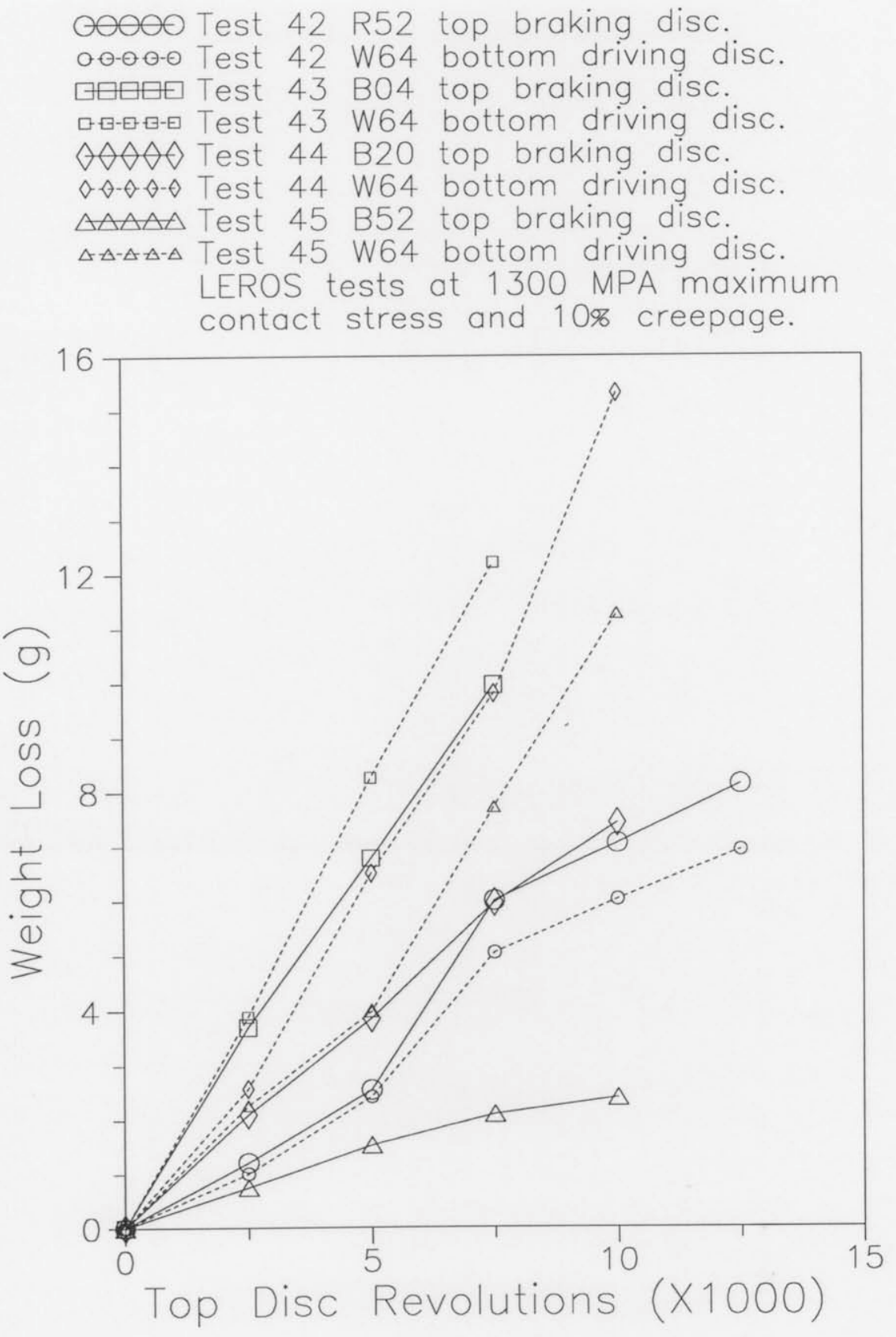

Figure 8.52 Top and bottom disc wear curves for severe LEROS tests at 1300 MPa p_o, 10% γ.

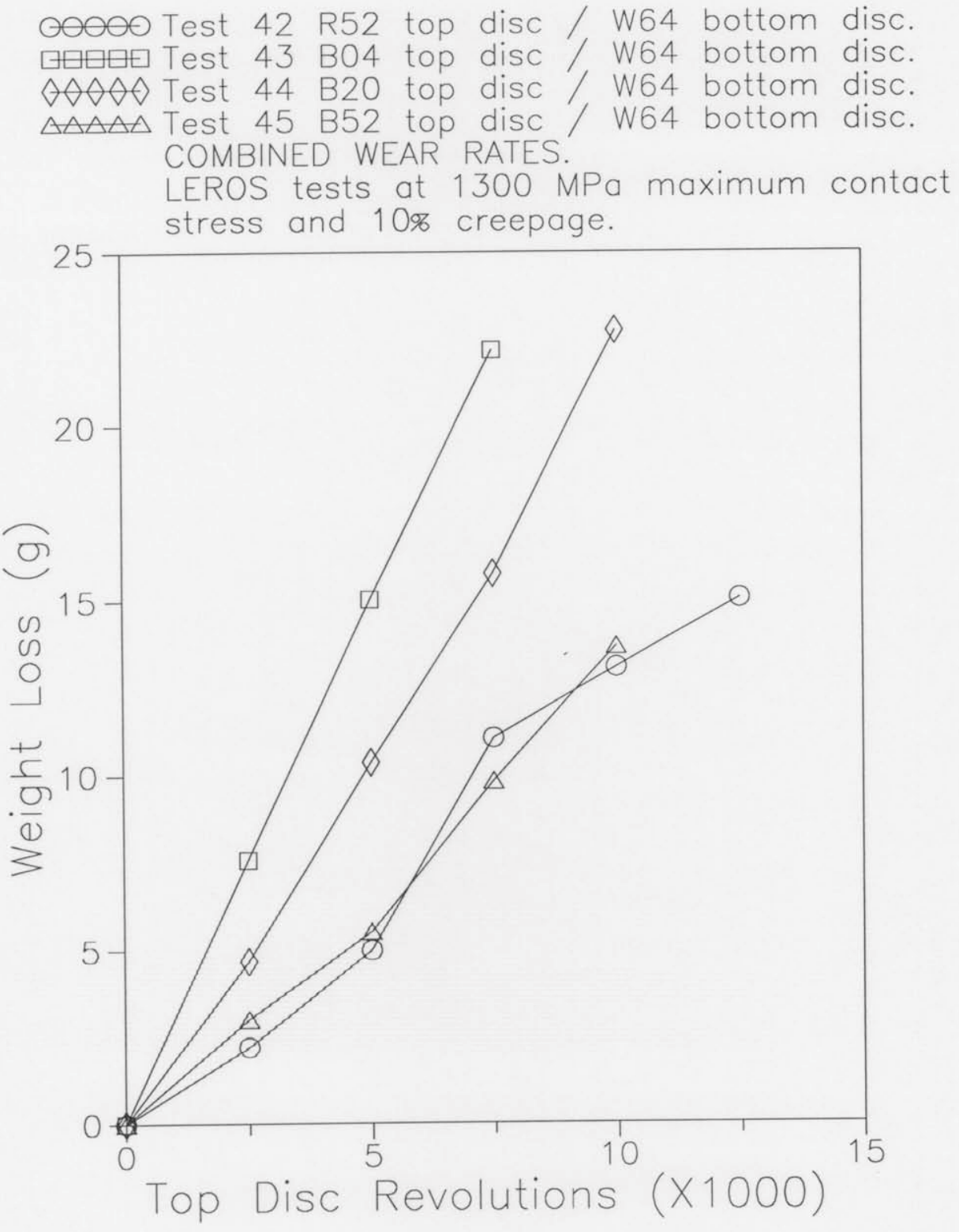

Figure 8.53 Combined top and bottom disc wear curves for severe LEROS tests at 1300 MPa p_o, 10% γ.

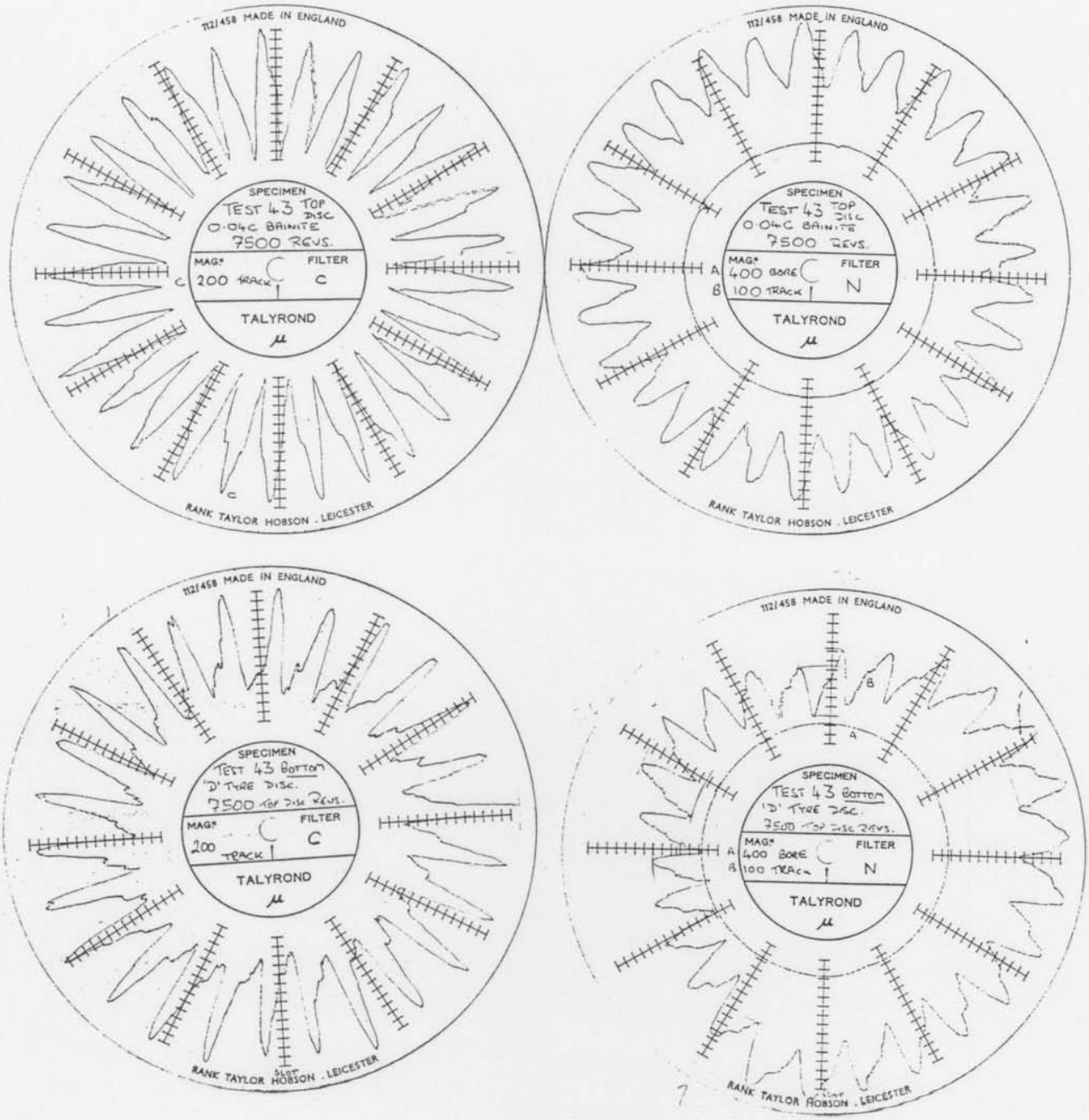

Figure 8.54 Test end Talyrond disc profiles, B04 top disc upper set and W64 bottom disc lower set, after testing on LEROS at 1300 MPa p_o, 10% γ. There is strong undulation periodicy of the rippled disc surfaces. The bottom disc was unevenly worn (bottom right). Use of the "C" filter to centre the profiles shows the patterns more clearly (leftside profiles).

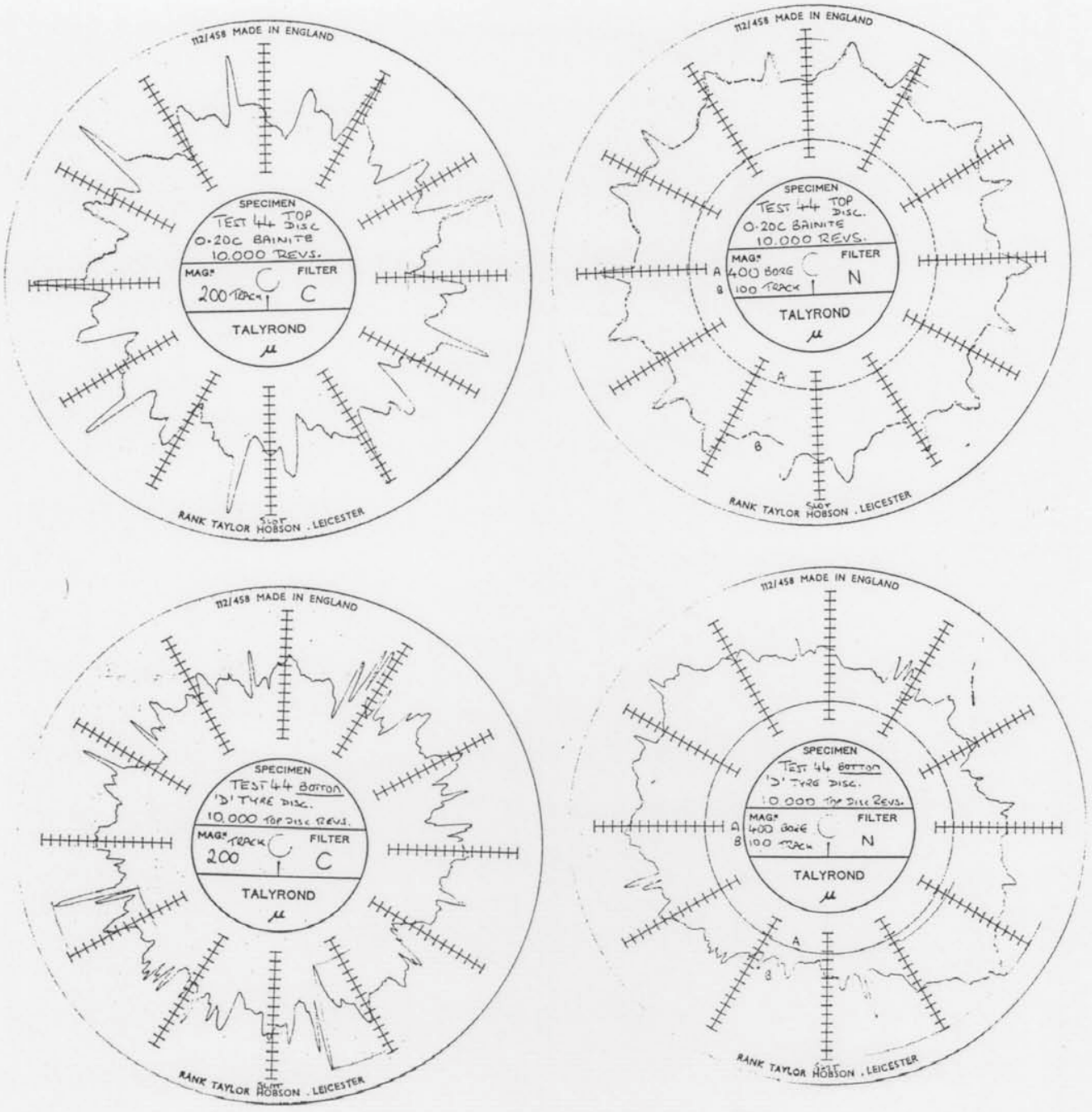

Figure 8.55 Test end Talyrond disc profiles, B20 top disc upper set and W64 bottom disc lower set, after testing on LEROS at 1300 MPa p_o, 10% γ. There is less undulation periodicy on these rippled disc surfaces, but it is still present. The bottom disc was highly and unevenly worn (bottom right). Use of the "C" filter to centre the profiles shows the patterns more clearly (leftside profiles).

a
(x4.73 mag.)

b
(SEM x8 mag.)

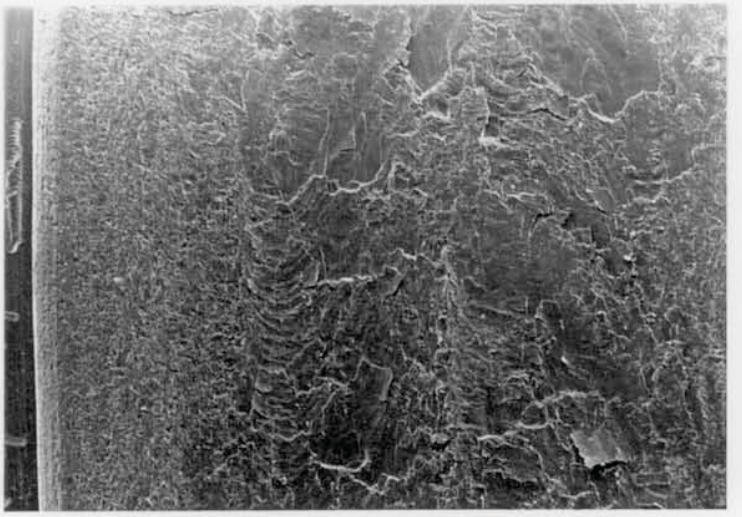

c
(SEM x32 mag.)

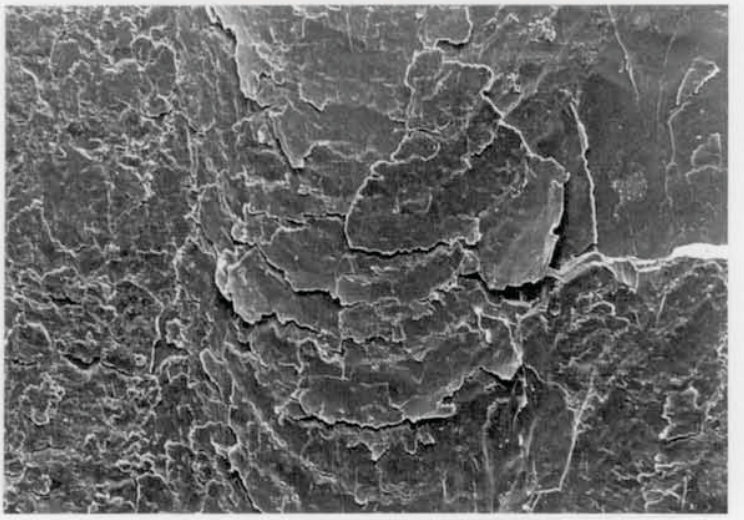

Figure 8.56 Surface appearance of the worn W64 bottom disc tested against B20 on LEROS at 1300 MPa p_o, 10% γ. The surface has zones of low cycle fatigue damage throught due to impacts from top disc ripple peaks (shown in the following Figure and Figure 7.17c).

a
(x7.4 mag.)

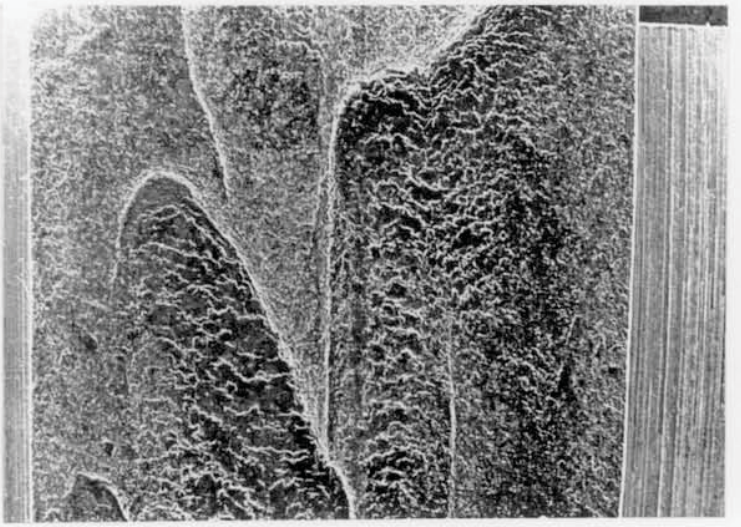

b
(SEM x34 mag.)

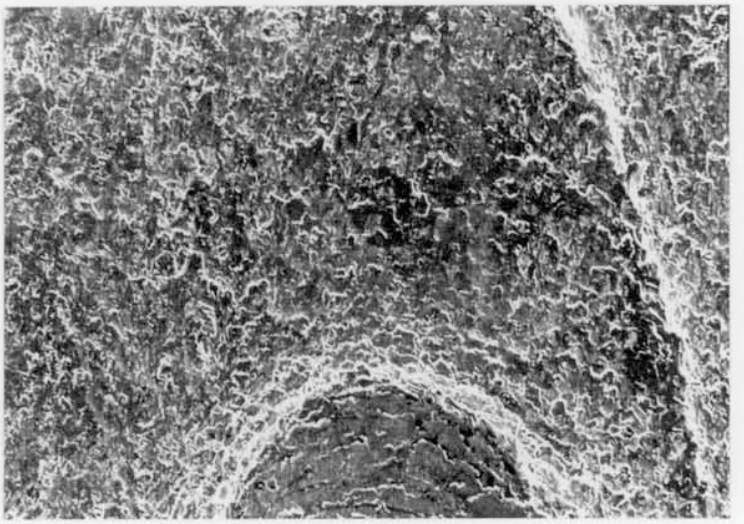

c
(SEM x33 mag.)

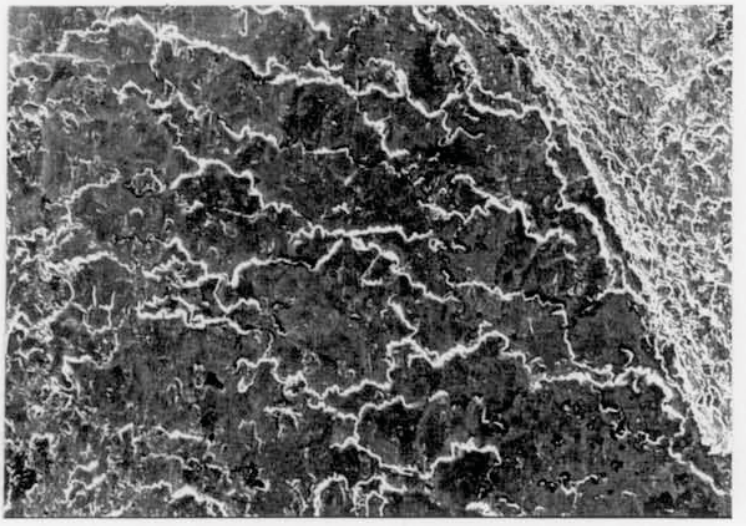

Figure 8.57 Surface appearance of worn B20 top disc tested on LEROS at 1300 MPa p_o, 10% γ (also shown in Figure 7.17c). A fine flaking wear mechanism can be seen distributed over the coarser rippled surface.